AWARD NUMBER: W81XWH-13-1-0158

TITLE: Targeting the Immune System's Natural Response to Cell Death to Improve Therapeutic Response in Breast Cancers

PRINCIPAL INVESTIGATOR: Rebecca S. Cook

CONTRACTING ORGANIZATION: Vanderbilt University
Nashville, TN 37240

REPORT DATE: September 2016

TYPE OF REPORT: Final

PREPARED FOR: U.S. Army Medical Research and Materiel Command
Fort Detrick, Maryland 21702-5012

REPORT DOCUMENTATION PAGE

Form Approved
OMB No. 0704-0188

1. REPORT DATE	2. REPORT TYPE	3. DATES COVERED
September 2016	Final Report (Year 3)	07/01/2013 - 06/30/2016

Targeting the Immune System's Natural Response to Cell Death to Improve Therapeutic Response in Breast Cancers

5a. CONTRACT NUMBER
W81XWH-13-1-0158

5b. GRANT NUMBER

5c. PROGRAM ELEMENT NUMBER

6. AUTHOR(S)

Rebecca S. Cook

E-Mail: Rebecca.cook@vanderbilt.edu

5d. PROJECT NUMBER

5e. TASK NUMBER

5f. WORK UNIT NUMBER

7. PERFORMING ORGANIZATION NAME(S) AND ADDRESS(ES)

Vanderbilt University
Nashville, TN 37232

8. PERFORMING ORGANIZATION REPORT NUMBER

9. SPONSORING / MONITORING AGENCY NAME(S) AND ADDRESS(ES)

U.S. Army Medical Research and Materiel Command
Fort Detrick. Marvland 21702-5012

10. SPONSOR/MONITOR'S ACRONYM(S)

11. SPONSOR/MONITOR'S REPORT NUMBER(S)

12. DISTRIBUTION / AVAILABILITY STATEMENT

Approved for Public Release; Distribution Unlimited

13. SUPPLEMENTARY NOTES

14. ABSTRACT

Purpose. We have proposed experiments to test the hypothesis that MerTK-mediated efferocytosis by tumor associated macrophages (TAMs) is a major limitation to effective therapeutic responses, because efferocytosis of dying tumor cells drives production of wound-healing/Th2-like cytokines, limits anti-tumor immunity, and promotes tumor growth. **Scope:** Two Aims were proposed to test this hypothesis. The goal of **Aim 1** was to determine if MerTK-directed efferocytosis modulates cytokine expression, leukocyte infiltration, and growth of mouse mammary tumors, specifically testing the hypothesis that loss of MerTK would impair efferocytosis of dying tumor cells by TAMs, thus limiting production of Th2/WH cytokines in the tumor microenvironment (TME), resulting in decreased tumor growth and metastasis. The goal of **Aim 2** was to measure the impact of MerTK-directed efferocytosis on tumor re-emergence in therapeutically treated breast cancers, specifically testing the hypothesis that loss of MerTK-directed efferocytosis in the TME will limit Th2/WH cytokines, thereby preventing immune tolerance and tumor regrowth. **Major Findings.** We have found and reported that MerTK inhibition promotes tumor rejection by the immune system (Cook et al., 2013). We found that MerTK signaling, primarily in tumor associated macrophages, limits expansion of CD8+ T-lymphocytes in the tumor microenvironment (Cook et al., 2013). We also found that efferocytosis within post-partum breast tumors increased tumor metastasis 17-fold, explaining the lethality associated with post-partum breast cancers (Stanford et al., 2014). We also found that MerTK inhibition could block the exaggerated metastasis associated with post-partum breast cancer (Stanford et al., 2014). Further, we showed that MerTK-mediated efferocytosis following therapeutic tumor cell death increases tumor wound healing and metastasis, but that blockade of MerTK can prevent efferocytosis and partially block tumor wound healing (Cook, 2015).

15. SUBJECT TERMS

efferocytosis, breast cancer, MerTK, therapeutic response, lapatinib, wound healing, cytokines, leukocytes, tumor associated macrophages

16. SECURITY CLASSIFICATION OF:			17. LIMITATION OF ABSTRACT	18. NUMBER OF PAGES	19a. NAME OF RESPONSIBLE PERSON
a. REPORT	b. ABSTRACT	c. THIS PAGE			19b. TELEPHONE NUMBER *(include area code)*
Unclassified	Unclassified	Unclassified	Unclassified	70	USAMRMC

Table of Contents

Page

1. INTRODUCTION.

We have proposed experiments to test the hypothesis that MerTK-mediated efferocytosis by tumor associated macrophages (TAMs) is a major limitation to effective therapeutic responses, because efferocytosis of dying tumor cells drives production of wound-healing/Th2-likecytokines, limits anti-tumor immunity, and promotes tumor growth. Two Aims were proposed to test this hypothesis. The goal of **Aim 1** was to determine if MerTK-directed efferocytosis modulates cytokine expression, leukocyte infiltration, and growth of mouse mammary tumors, specifically testing the hypothesis that loss of MerTK would impair efferocytosis of dying tumor cells by TAMs, thus limiting production of Th2/WH cytokines in the tumor microenvironment (TME), resulting in decreased tumor growth and metastasis. This Aim relies on the use of an immune competent mouse mammary tumor model with systemic loss of MerTK, measuring intra-tumoral leukocytes and tumor epithelial cell signaling using flow cytometry. This Aim also proposed using a novel cell co-culture model to assess MerTK-mediated efferocytosis by time-lapse microscopy. The goal of **Aim 2** was to measure the impact of MerTK-directed efferocytosis on tumor re-emergence in therapeutically treated breast cancers, specifically testing the hypothesis that loss of MerTK-directed efferocytosis in the TME will limit Th2/WH cytokines, thereby preventing immune tolerance and tumor regrowth. Like experiments proposed in Aim 1, those proposed in Aim 2 use an immune competent mouse mammary tumor model with systemic loss of MerTK or with pharmacological MerTK inhibition, measuring intra-tumoral leukocytes and tumor epithelial cell signaling in the post-therapeutic setting using flow cytometry and monitoring post-treatment tumor progression.

2. Keywords

efferocytosis
breast cancer
MerTK
therapeutic response
lapatinib
wound healing
cytokines
leukocytes
tumor associated macrophages

3. Accomplishments

I. Overview.

We have proposed experiments to test the hypothesis that MerTK-mediated efferocytosis by tumor associated macrophages (TAMs) is a major limitation to effective therapeutic responses, because efferocytosis of dying tumor cells drives production of wound-healing/Th2-like cytokines, limits anti-tumor immunity, and promotes tumor growth. **Scope:** Two Aims were proposed to test this hypothesis.

II. **What were the major goals of the project?**

The goal of **Aim 1** was to determine if MerTK directed efferocytosis modulates cytokine expression, leukocyte infiltration, and growth of mouse mammary tumors, specifically testing the hypothesis that loss of MerTK would impair efferocytosis of dying tumor cells by TAMs, thus limiting production of Th2/WH cytokines in the tumor microenvironment (TME), resulting in decreased tumor growth and metastasis. The goal of **Aim 2** was to measure the impact of MerTK-directed efferocytosis on tumor reemergence in therapeutically treated breast cancers, specifically testing the hypothesis that loss of MerTK directed efferocytosis in the TME will limit Th2/WH cytokines, thereby preventing immune tolerance and tumor regrowth.

III. **What was accomplished under these goals?**

Table 7. Statement of Work Timeline

		Year	Year1				Year2				Year3			
		Quarter	Q1	Q2	Q3	Q4	Q5	Q6	Q7	Q8	Q9	Q10	Q11	Q12
Aim 1	Task 1	Generate tumor-bearing mice												
	Task 2	Tumor formation &progression												
	Task 3	Tumor and tissue analysis												
	Task 4	Imaging of efferocytosis												
Aim 2	Task 5	Generate tumor-bearing mice												
	Task 6	Tumor formation												
	Task 7	Tumor treatment and growth												
	Task 8	Tumor and tissue analysis												

Year 1 (Quarters 1-4)

i. Task 1. Generate tumor-bearing mice. [Task1 was completed, in accordance with the scheduled timeline, in Year 1, Quarters 1-4.] We used three rounds of breeding (as shown in Statement of Work Table 5, below) to generate 12 female MerTK$^{+/+}$NIC^{Cherry} mice and 12 female MerTK$^{-/-}$NIC^{Cherry} mice. These studies were completed in early Quarter 4 (March, 2014), resulting in a complete cohort (controls and experimentals) of age-matched siblings born between March 1, 2014 and March 20, 2014.

Year 1-2 (Quarters 1-7)

ii. Task 2. Tumor formation and progression. (Quarters 1-7). The average tumor latency for the MMTV-NIC mouse model is 6.5 months. Thus, mice generated in Task1 developed tumors arising between late Quarter 5 and early Quarter 7. We palpated mouse mammary glands twice weekly to detect tumors beginning when mice were 3 weeks of age to detect tumors.

Year 2 (Quarters 5-8)

iii. Task 3. Tumor and tissue analysis. [Task 3 was completed, in accordance with the scheduled timeline, Year 2, Quarters 5-8] Our major findings are shown below, and are published in *Journal of Clinical Investigation* (Cook et al., 2013; published manuscript is enclosed as Appendix 1) and published in *Journal of Clinical Investigation* (Stanford et al., 2014, enclosed as Appendix 2)

A. Loss of MerTK does not affect the rate of mammary tumor formation (i.e., tumor latency) in nulliparous female mice. (**See Appendix 2, Supplemental Figure S5B**)
B. Loss of MerTK does not affect the rate of mammary tumor growth (tumor volume) or proliferation (PCNA+ cells) in nulliparous female mice. (**See Appendix 2, Supplemental Figure S5D**)
C. Loss of MerTK does not affect the number of CD45+ leukocytes in the tumor microenvironment. (**Appendix 2, Supplemental Figure S5C**).
D. Loss of MerTK increases macrophages and dendritic cells in the tumor microenvironment (**Appendix 1, Figure 3A-3B**).
E. Loss of MerTK increases tumor-induced lymphocyte proliferation (**Appendix 1, Figure 3D**)
F. Loss of MerTK does not affect the number of TUNEL+ cells in mammary tumors from nulliparous mice. (**Appendix 2, Supplemental Figure S5E**)
G. Widespread cell death during post-partum involution induces M2 macrophage polarization, but this is blocked by MerTK loss. (**Appendix 2, Figure 6C-E and Figure 6H-J**).
H. Loss of MerTK does not affect the number of nulliparous female tumor-bearing mice harboring lung metastases or the average number of lung metastases per mouse. (Appendix 2, Figure 3B). However, in the context post-partum involution, when efferocytosis increases causing increased tumor metastasis, loss of MerTK blocks the post-partum increase in the number of lung metastases (**Appendix 2, Figure 3C**).
I. Loss of MerTK causes an accumulation of dying tumor cell bodies (carcasses) in the context of post-partum involution, but not in tumors from nulliparous mice. (**Appendix 2, Figure 2A-B**).
J. Loss of MerTK does not profoundly affect expression of TGFβ, IL-10, or IL-4 in tumors harvested from nulliparous mice, but MerTK loss prevents the induction of tumor TGFβ, IL-10, and IL-4 during post-partum involution. (**Appendix 2, Figure 4A-G, and Appendix 1, Figure 3C-D**).
K. Targeted inhibition of TGFβ using the antibody 1D11 does not affect tumor metastasis in nulliparous mice, but blocks the post-partum induction of metastasis (**Appendix 2, Figure 7D-J**), revealing a key role for TGFβ signaling in MerTK-directed enhancement of metastasis during post-partum involution.

Year 2 (Quarters 5-8)

iv. Task 4. Imaging of efferocytosis. [Task 4 is complete, in accordance with the scheduled timeline, Year2 Quarters 5-8.] Our major findings are listed below, and are published in the *Journal of Clinical Investigation* (**Appendix 2**).

A. Co-culture of live breast cancer cells with macrophages does not induce the engulfment of tumor cells by macrophages. In contrast, co-culture of dying breast cancer cells with macrophages induces the engulfment of the dying tumor cell by macrophages. (**Appendix 2, Figure 5D**-E)

B. Engulfment of the dying cell (i.e., efferocytosis) is blocked upon inhibition of MerTK using anti-MerTK antibodies or small molecular tyrosine kinase inhibitors of MerTK. (**Appendix 2, Figure 5D-F**)
C. Efferocytosis of dying cancer cells by macrophages induces expression changes in macrophages that support the production of Th2-like/wound healing cytokines, including IL-4, IL-10, and TGFbeta. (**Appendix 2, Figure 5H-I**)
D. Blockade of MerTK (i.e., blockade of efferocytosis) blocks induction of wound healing cytokines. (**Appendix 2, Figure 5H-I**)

Year 3 (Quarters 9-12)

v. Task 5. Generate tumor-bearing mice. [Task 5 is completed, in accordance with the scheduled timeline, Quarters 9-12]. While this task was not experimental in nature, it was a necessary step for enabling the experiments outlined below in Task 7. Thus, our major findings for Task 5 are that tumor-bearing mice were generated as expected, and we able to move on to Task6 (another necessary but non-experimental task that enabled progression to Task7 experimentation).

vi. Task 6. Tumor formation and progression. [Task 6 is completed, in accordance with the scheduled timeline, Quarters 9-12.] While this task was not experimental in nature, it was a necessary step for enabling the experiments outlined below in Task 7. Thus, our major findings for Task 6 are that tumor generation occurred as expected, and we able to move on to Task 7.

vii. Task 7. Tumor treatment and growth. [Task 7 is completed, in accordance with the C. scheduled timeline, Quarters 9-12.]

A. Apoptosis in response to therapeutic treatment of breast cancer increases tumor collagen accumulation (Figure 1A-1B). We used the MMTV-HER2 transgenic mouse model of HER2-amplified breast cancer. These tumors develop in the FVB mouse background, which is a fully immune-competent model. These tumors express human HER2, which drives tumor formation. Previous studies confirmed that these tumors are lapatinib-sensitive, and that lapatinib-treated tumor cells undergo apoptosis. Therefore, when MMTV-HER2 mammary tumors reached a volume of 100 mm^3, mice were randomized into two treatment groups (**Figure 1A**), the first receiving a single treatment with vehicle (50 µl of 0.5% methyl cellulose and 0.1% tween-80 in sterile water), and the other receiving a single treatment with lapatinib (100 mg/kg, emulsified in 50 µl vehicle). TUNEL analysis of tumors collected 1 day after treatment with lapatinib confirmed lapatinib-mediated induction of apoptosis in MMTV-HER2 tumors (**Figure 1B**, upper panel, N = 3 per condition). To examine potential wound healing in tumors in the post-treatment setting, we harvested tumors 7 days after the single treatment with lapatinib, and assessed tumors histologically (**Figure 1B,** lower panels). Analysis of formalin-fixed paraffin embedded (FFPE) tumor sections stained with hematoxylin and eosin (H&E) revealed extracellular matrix (ECM) deposition throughout lapatinib-treated tumors, while vehicle-treated tumors did not display ECM accumulation.

B. Apoptosis in response to therapeutic treatment of breast cancer increases immune suppressive leukocytes in tumors (Figure 1). We assessed additional molecular markers of wound healing, including wound healing-associated T_{Reg}s and M2-like macrophages/MDSCs, in lapatinib-treated tumors. Immunohistochemical staining for FoxP3, a molecular marker of T_{Reg}s, was

markedly increased in lapatinib-treated tumors, as was staining for Arginase 1, a marker of M2-like macrophages and MDSCs.

C. Apoptosis in response to therapeutic treatment of breast cancer increases immune suppressive cytokines in tumors (Figure 1C). RT-qPCR analysis of tumors harvested 7 days after treatment revealed increased expression of genes encoding wound healing-associated cytokines *Il10*, *Il13*, and *Tgfb1* (**Figure 1C,** N = 3), which collectively dampen cytotoxic immune responses. Importantly, we saw upregulation of *Mertk* in lapatinib-treated tumors, consistent with the hypothesis that increased MerTK-mediated efferocytosis is upregulated in the context of widespread tumor cell death.

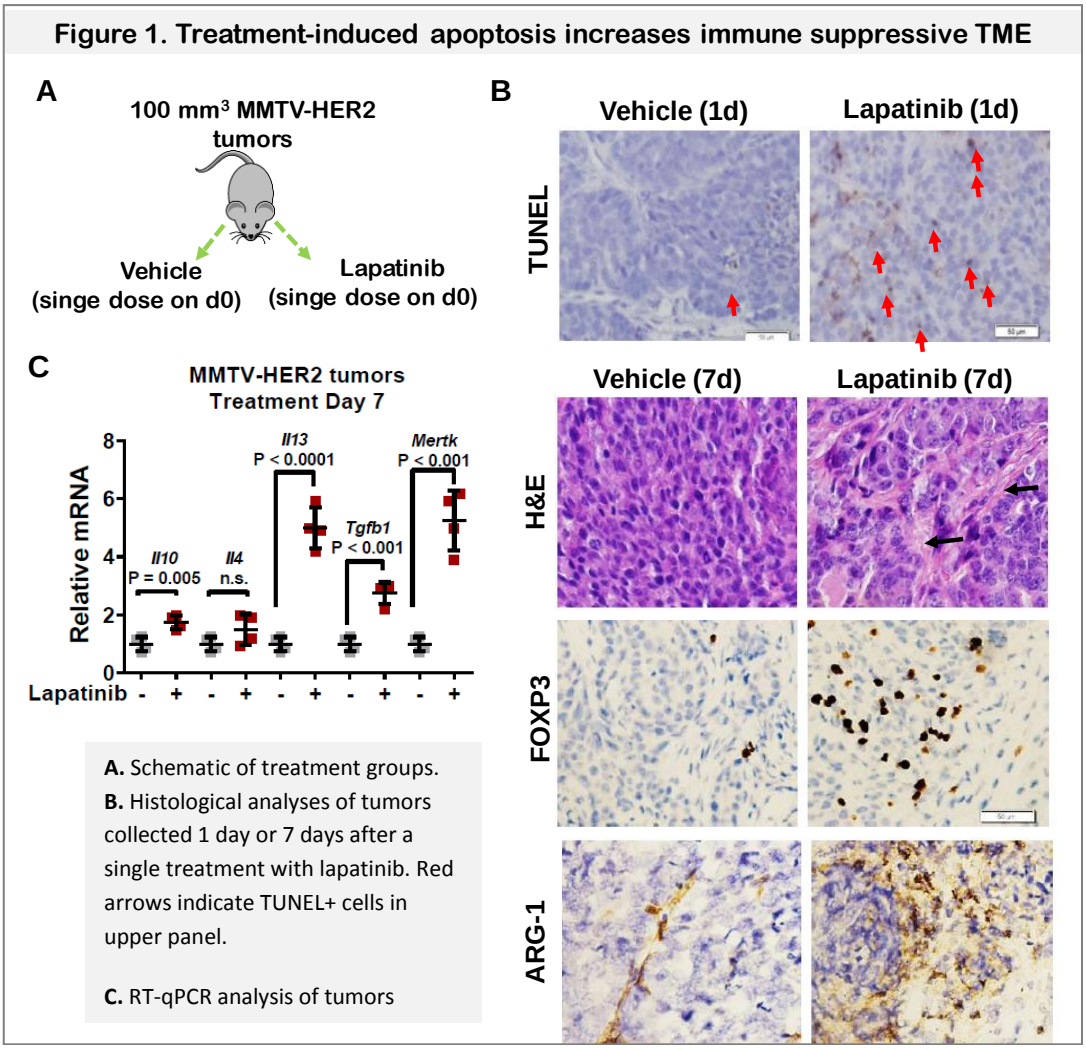

D. Inhibition of MerTK-mediated efferocytosis in lapatinib-treated MMTV-HER2 tumors (Figure 2A-2B). We administered a single dose of vehicle or lapatinib to MMTV-HER2 tumor-bearing mice when tumors reached 100 mm^3, then further randomized these into two additional groups for daily treatment with vehicle (50 µl of 0.5% methyl cellulose and 0.1% tween-80 in sterile water), or daily treatment with the MerTK inhibitor BMS-777607 (20 mg/kg, emulsified in 50 µl vehicle). It should be noted that BMS-777607 also inhibits the receptor tyrosine kinases Met, Ron, Axl, and Tyro-3. Western analysis of tumors harvested 1 day after initial treatment confirmed lapatinib-mediated inhibition of HER2 tyrosine phosphorylation, and lapatinib-mediated blocked of Akt phosphorylation (**Figure 2B**), consistent with the known role of HER2 in driving PI3K/Akt

pathway. Western analysis confirmed that lapatinib treatment did not alter MerTK tyrosine phosphorylation, but that BMS-777607 potently blocked MerTK tyrosine phosphorylation. Further, these studies revealed that BMS-777607 did not alter P-Akt levels, either as a single agent or in combination with lapatinib.

E. Blockade of MerTK-mediated efferocytosis fails to inhibit IL-10 induction in the therapeutic setting (Figure 2C). To examine the impact of MerTK-mediated efferocytosis on establishing a wound healing phenotype following lapatinib treatment, we harvested tumors 7 days after initial treatment, using RT-qPCR to measure relative expression of wound healing-associated cytokines IL-13, IL-4, and IL-10 (**Figure 2C**). Although we expected that MerTK inhibition would have blocked the lapatinib-induced elevation of wound healing cytokines, this occurred only for IL-13, and not for IL-4 or for IL-10.

Figure 2. BMS-777607 blocks efferocytosis but not immune suppressive wound healing features in lapatinib-treated tumors

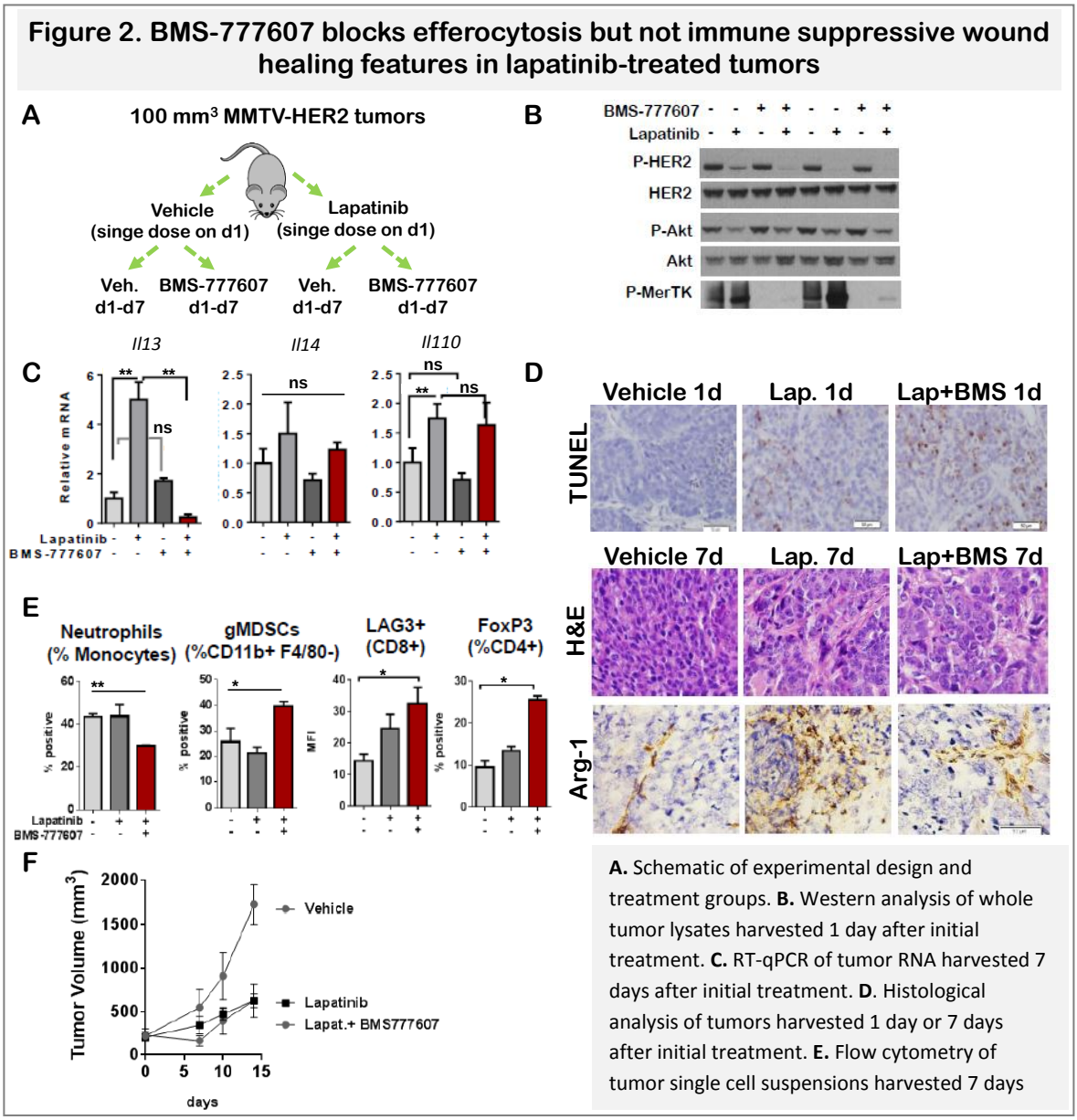

A. Schematic of experimental design and treatment groups. **B.** Western analysis of whole tumor lysates harvested 1 day after initial treatment. **C.** RT-qPCR of tumor RNA harvested 7 days after initial treatment. **D**. Histological analysis of tumors harvested 1 day or 7 days after initial treatment. **E.** Flow cytometry of tumor single cell suspensions harvested 7 days

F. **Blockade of MerTK-mediated efferocytosis fails to block collagen deposition and immune suppressive leuukocyte accumulation (Figure 2D-2E).** TUNEL analysis of FFPE sections from tumors harvested 1 day after initial treatment revealed that MerTK inhibition using BMS-777607 increased the number of TUNEL+ cells in lapatinib-treated tumors (**Figure 2D**). Although this could be interpreted as an increase in total tumor cell death, this scenario is unlikely given that MMTV-

HER2 tumor cells do not inherently express MerTK (data not shown), and given that BMS-777607 did not affect P-Akt levels when used alone or in combination with lapatinib (**Figure 2B**). Therefore, we tentatively conclude that the increased content of TUNEL+ cells in samples treated with lapatinib + BMS-777607 is due to the blockade of efferocytosis, resulting in an accumulation of dead cell bodies. Analysis of FFPE tumor sections harvested on treatment day 7 revealed that BMS-777607 had little impact on ECM deposition, as seen in H&E-stained sections, or the presence of Arg-1 cells, as measured by immunohistochemistry (**Figure 2D**). Flow cytometry of tumors harvested 7 days after treatment revealed that tumors treated with the combination of lapatinib + BMS-777607 harbored an increased content of MDSCs ($CD45^+CD11b^+F4/80^{neg}Ly6G^{hi}$) and T_{Reg}s ($CD45^+CD3^+CD4^+CD8^{neg}FoxP3^+$) over what was seen in tumors treated with lapatinib alone (**Figure 2E**). Additionally, the mean fluorescence intensity (MFI) of LAG3 in CD8+ T-cells was robustly increased in tumors treated with the combination of lapatinib + BMS-777607, suggesting that, rather than increased cytotoxicity of CD8+ T-cells as we might have anticipated, we found increased anergy and/or exhaustion of CD8+ T-cells upon inhibition of efferocytosis. These data have not yet been published.

G. Blockade of MerTK-mediated efferocytosis will increase necrosis (Figure3A). In sterile wounds of untransformed tissues, blockade of efferocytosis causes apoptotic cells to undergo a secondary necrosis (**Figure 3A**), which is known to cause IFNγ induction and a pro-inflammatory response. Interestingly, IFNγ also induces expression of an enzyme called IDO-1, a potently immune suppressive enzyme (**Figure 3A**), which converts tryptophan (Trp) to kynurenine (Kyn), thus supporting expansion of T_{Reg}s and MDSCs, preventing expansion of effector T-cells, and blocking maturation of NK, DC, and macrophages, collectively dampening inflammation to promote wound healing in post-necrotic sterile wounds.

H. *IFNG* directly correlates with *IDO1* expression in invasive breast cancers, which correlates with a worse outcome for patients (Figure 3B). We examined the correlation between *IFNG* and *IDO1* mRNA levels in clinical breast tumor specimens using an expression dataset generated from invasive breast cancers curated by The Cancer Genome Atlas (TCGA), confirming a direct correlation between *IFNG* and *IDO1*(**Figure 3B**, left panel). The potential importance of IDO-1 in breast tumors was illustrated in this same dataset, revealing that overall survival (OS) of patients whose tumors over-expressed *IDO1* (defined as levels 2.0 S.D. greater than the median levels of all samples combined) was substantially diminished as compared to the remaining patients (**Figure 3B**, right panel), underscoring the key role of IDO-1 in tumor progression.

I. Blockade of MerTK-mediated efferocytosis increased *Ifng* and *Ido1* levels and IDO-1 activity in therapeutically-treated tumors in vivo (Figure 3C-3E). We measured *Ifng* and *Ido1* levels in MMTV-HER2 tumors treated with a single dose of lapatinib (or vehicle) on day 0, followed by 7 daily treatments with BMS-777607 (or vehicle) as described in Figure 2A. We found increased levels of both *Ifng* and *Ido1* in tumors treated with the combination of lapatinib and BMS-777607 as compared to those treated with lapatinib alone (**Figure 3C**, **left two panels**). Further, ELISA-based measurements of Kyn and Trp in plasma harvested from tumor-bearing mice revealed a large increase in the Kyn:Trp ratio, consistent with increased IDO-1 activity (**Figure 3C**, right panel)

Because numerous factors within the complex TME might cause upregulation of IDO-1 activity, we used a cell culture-based model to understand how blockade of MerTK-mediated efferocytosis might affect *Ido1* and *Ifng* expression by RT-qPCR. MMTV-HER2-derived primary mouse mammary tumor cells were treated with lapatinib (1 μM) and the Bcl-2/Bcl-xL inhibitor ABT-263 (1 μM) in suspension for 2 hours to induce the intrinsic apoptosis pathway. These cells were washed in serum-free media 5 times to remove the inhibitors, then plated at a ratio of 5:1 with the mouse macrophage-like cell line, RAW264.7, in 1% heat-inactivated serum. Parallel monocultures of RAW264.7 cells were maintained for comparison. Mono- and co-cultures were treated with a neutralizing anti-MerTK monoclonal antibody, or with a control antibody (goat IgG2a). After 4 hours, the cultured media was

Fig.3. MerTK inhibition following tumor cell death increases IDO-1 expression and activity

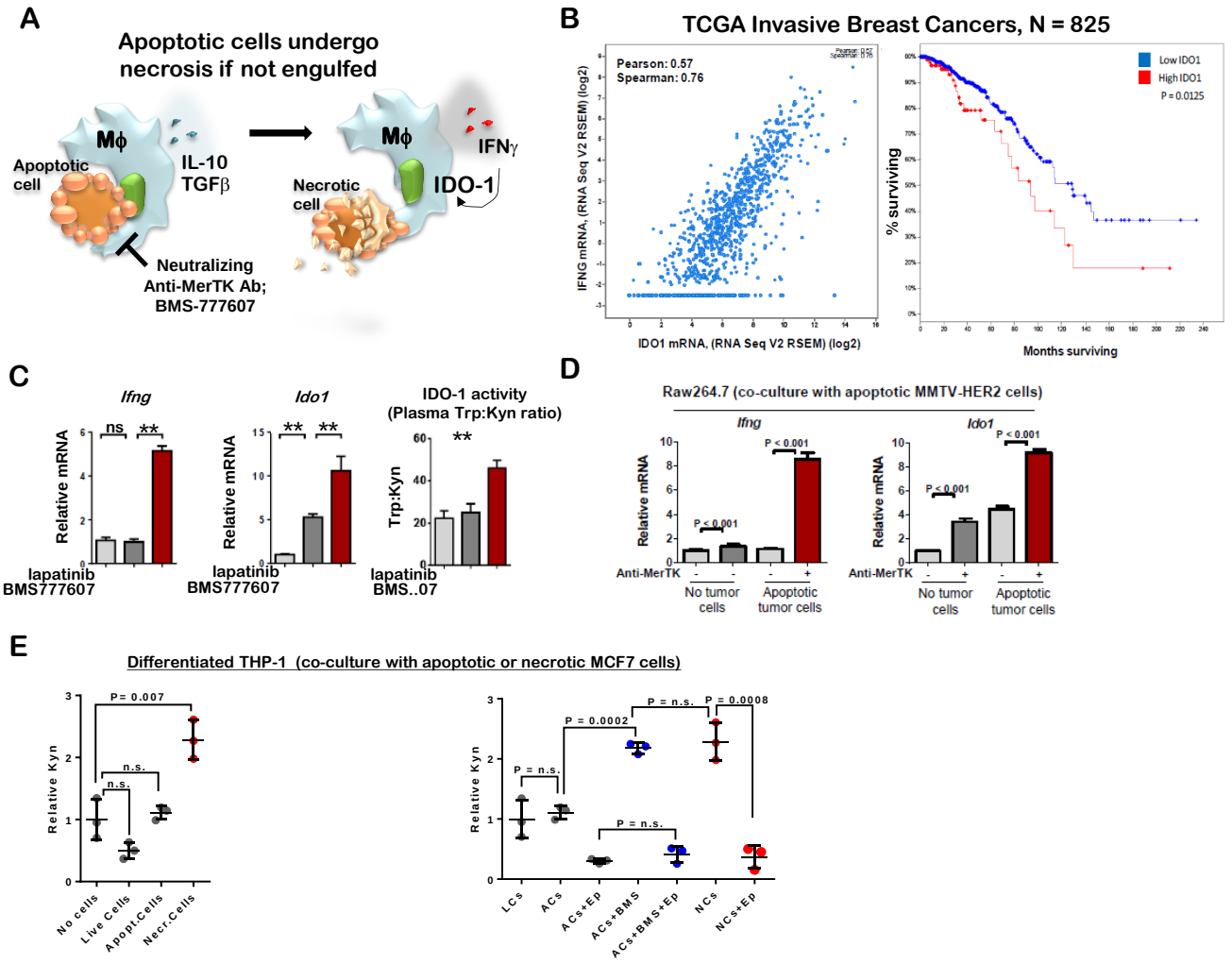

A. Schematic of how blockade of efferocytosis using antibodies or compounds against MerTK would cause secondary necrosis of apoptotic tumor cells, causing IFN-mediated induction of IDO-1. **B**. Analysis of TCGA-curated invasive breast cancer datasets for expression of IDO1 and IFNG, and assessing how IDO1 might correlate with outcome. C. MMTV-HER2 tumors treated with lapatinib ± BMS777607 were assessed by RT-qPCR; plasma of tumor bearing mice was assessed by Kyn and Trp ELISAs**. D.** Raw264.7 cells co-cultured ± apoptotic MMTV-HER2 and ± a neutralizing MerTK antibody for 4 hours were assessed by RT-qPCR for *Ifng* and *Ido1*. **E**. Differentiated THP-1 cells were co-cultured with live, apoptotic, or necrotic MCF7 cells, in the presence or absence of BMS-777607 and/or epacadostat. ELISA was used to measure Kyn in the

collected and filtered. The adherent Raw264.7 were washed to remove apoptotic (non-adherent) MMTV-HER2 cells, then the filtered media was replaced onto the respective well. Cells were then cultured for an additional 18 hours. This approach revealed that the presence of apoptotic MMTV-HER2 cells had no impact on *Ifng* expression by Raw264.7 cells, but caused a 4-fold induction of Ido1 levels (**Figure 3D**). Interestingly, the neutralizing MerTK antibody induced *Ifng* and *Ido1* expression in mono-cultured Raw264.7 cells, even in the absence of apoptotic tumor cells. However, blockade of MerTK in the context of co-culture with apoptotic tumor cells increased *Ifng* levels nearly 8-fold, and *Ido1* levels nearly 10-fold.

A similar approach was used in the human monocyte-like cell line THP-1, which was differentiated to macrophages using GM-CSF for 3 days. Non-adherent (undifferentiated) cells were removed prior to co-culture with apoptotic tumor cells. In this case, we used the human breast cancer cell line MCF7 for co-culture with THP-1 cells. We tested live MCF7 cells, apoptotic MCF7 cells [inducing the intrinsic apoptotic pathway with a combination of the PI3K/mTOR dual kinase inhibitor BEZ-235

(1μM) and ABT-263 as described above] and necrotic MCF7 cells (one cycle of rapid freeze/rapid thaw in serum-free DMEM). Mono- and co-cultures were incubated 4 hours (a time point to prevent the secondary necrosis of apoptotic tumor cells in the presence of the THP-1 cells). Differentiated THP-1 cells were washed, then cultured for an additional 48 hours. (It is possible that the co-cultures with live MCF7 cells retained some of the MCF7 cells after washing.) Cultured media was collected and assessed by ELISA for Kyn, revealing increased Kyn accumulation in co-cultures with necrotic MCF7 cells, but not in co-cultures with live or apoptotic MCF7 cells (**Figure 3E, left panel**).

Importantly, we found that the Incyte IDO-1 inhibitor epacadostat (500 nM) blocked Kyn accumulation in the media from THP-1 co-cultured with necrotic cells (**Figure 3E, right panel**), confirming that necrotic tumor cells, like necrotic cells in untransformed tissues, increases IDO-1 activity. While apoptotic MCF7 cells did not induce Kyn production from THP-1 cells, inhibition of MerTK-mediated efferocytosis using BMS-777607 in co-cultures resulted in robust Kyn production, which was blocked upon treatment with epacadostat. These results support the idea that blockade of MerTK-mediated efferocytosis results in secondary necrosis of dying tumor cells, IFNg induction, and IDO1 activation. These results are not published.

IV. What opportunities for training and professional development has the project provided?

This project has provided me the opportunity to develop my research program, my scientific network, and my scientific communication skills.

V. How were the results disseminated to communities of interest?

A. These results were published in **three research articles and one book chapter**.

a. Cook et al., 2013, ***J Clin Invest***. 123(8):3231-42;
b. Stanford et al., ***J Clin Invest***. 2014 Nov;124(11):4737-52; ,
c. Vaught and Cook, ***Oncotarget.*** 2015 Sept. 22; 6(28): 24590-2459),
d. Vaught, Stanford, and Cook, ***Cancer Cell and Microenvironment.*** 2015. NIHMSID:689387

B. These results were also presented at internationally attended scientific conferences:

1. **Innate immune response to cell death in the post-partum mammary gland increases malignancy of parity associated tumors.**
   Stanford JC, Fingleton B, Owen P, and ***Cook RS***.
   2013 AACR Special Conference Advances in Breast Cancer, San Diego CA.
   Published in ***Molecular Cancer Research*** 2013. 11(10 Supplement):B097.

2. **Cell death and efferocytosis generate a pro-metastatic landscape during mammary gland involution that increases disseminatioin of post-partum breast cancers.**
   Cook RS, Earp HS, and Stanford JC.
   2014 San Antonio Breast Cancer Symposium.
   Published in ***Cancer Research*** 2015. 75(9 Supplement):P-04-02.

3. **Tumor wound healing response to treatment-induced tumor cell death increases tumor metastasis**
   Cook RS.
   2015 AACR Inaugural Conference on Cancer Immunotherapy, New York, NY
   Published in ***Cancer Research*** 2015. 75(15 Supplement): 2916

C. These results were presented at invited presentations at three medical schools

1. **"Wound healing in the tumor microenvironment" presented by Rebecca S. Cook**
   New Horizons in Breast Cancer Research, the 14th Annual Meharry Medical College-Vanderbilt University- Tennessee State University U54 Cancer Partnership. Meharry Medical College, Nashville, TN. April 10, 2015.

2. **"Efferocytosis accelerates malignant tumor progression" presented by Rebecca S. Cook**
   Gordon Research Conference on Apoptotic Cell Clearance. University of New England, Biddeford, ME. June 24, 2015.

VI. **What do you plan to do during the next reporting period to accomplish the goals?**

Nothing to report.

4. IMPACT:

I. What was the impact on the development of the principal discipline(s) of the project?

We have discovered and reported that MerTK-expressing tumor leukocytes support tumor tolerance, a process that involves decreased expansion of CD8+ T-lymphocytes in the tumor and in the tumor draining lymph node (Cook et al., 2013). Further, we report that macrophages support efferocytosis in the tumor microenvironment, resulting in a robust induction of tumor wound healing, characterized by macrophage-mediated expression of TGFbeta, IL-10, and IL-4 (Stanford et al., 2014). TGFbeta induction drove enhanced metastasis following widespread efferocytosis. Inhibition of MerTK or TGFbeta, but not IL-4, blocked the induction of metastasis following widespread tumor cell death (Stanford et al., 2014). We reported that MerTK inhibition in combination with lapatinib modestly decreased metastatic dissemination of HER2-overexpressing mouse mammary tumors as compared to either inhibitor used alone [conference abstract published in ***Cancer Research*** 2015. 75(15 Supplement): 2916]. However, immune suppressive tumor leukocytes were upregulated in lapatinib-treated tumors treated with MerTK inhibitor (Figure 3, final report).

It should be said that, although metastatic dissemination was reduced upon inhibition of efferocytosis, not all metastatic dissemination was eliminated. Further, not all immune-suppressive cytokines that are normally upregulated in response to efferocytosis were blocked when efferocytosis was inhibited. This suggests that other mechanisms operate to resolve immune responses in the tumor microenvironment when efferocytosis is impaired. Because blockade of efferocytosis leads to a secondary necrosis, our current hypothesis is that necrosis initially induces potent type I immunity in tumors, this is followed by resolution of inflammation. In support of this idea, models of necrosis that occur in non-transformed tissue, such as in the case of ischemia, for example, reveal that necrosis induces a 'sterile inflammation' response, that is followed by a coordinated upregulation of pro-resolving factors aimed at limiting immune-mediated damage in surrounding healthy tissues. For example, the tryptophan metabolizing enzyme IDO-1 is often upregulated in cases of ischemia, and in other examples of necrosis. Interestingly, IDO-1 is a known suppressor of anti-tumor immunity. Our future directions will focus on analysis of IDO-1 in response to secondary necrosis within the tumor microenvironment.

References.

MerTK inhibition in tumor leukocytes decreases tumor growth and metastasis.
Cook RS, Jacobsen KM, Woffard AM, DeRyckere D, Stanford JC, Prieto AL, Redente E, Sandahl M, Hunter DM, Strunk KE, Graham DK, and Earp HS.
J Clin Invest. 2013 123(8):3231-42.

Efferocytosis produces a prometastatic landscape during postpartum mammary gland involution.
Stanford JC, Young C, Hicks D, Owens P, Williams A, Vaught DB, Morrison MM, Lim J, Williams M, Brantley-Sieders DM, Balko JM, Tonetti D, Earp HS 3rd, ***Cook RS***.
J Clin Invest. 2014 Nov;124(11):4737-52.

Tumor wound healing response to treatment-induced tumor cell death increases tumor metastasis
Cook RS.
2015 AACR Inaugural Conference on Cancer Immunotherapy, New York, NY
Published in ***Cancer Research*** 2015. 75(15 Supplement): 2916

II. What was the impact on other disciplines?

Nothing to report

III. What was the impact on technology transfer?

Nothing to report

IV. **What was the impact on society beyond science and technology?**

These studies will impact our understanding of the breast tumor microenvironment. Therapeutically-induced widespread cell death followed by efferocytosis, massive Th2-like cytokine production, immune tolerance and tumor 'wound healing' would suggest that current therapeutic strategies that induce tumor cell death are self-limiting based on the immune system's inherent response to cell death. However, targeted inhibition of efferocytosis in combination with current therapeutic inhibitors would impair Th2-like cytokine production, immune tolerance, and 'wound healing' in the treated tumor, allowing the full effect of the therapeutic inhibitor to be revealed, *vastly improving the response to **current** treatment strategies to decrease breast cancer mortality.*

5. CHANGES/PROBLEMS:

a. **Changes in approach and reasons for change**
    i. Nothing to report

b. **Actual or anticipated problems or delays and actions or plans to resolve them**
    i. Nothing to report

c. **Changes that had a significant impact on expenditures**
    i. Nothing to report

d. **Significant changes in use or care of human subjects, vertebrate animals, biohazards, and/or select agents**
    i. Nothing to report

e. **Significant changes in use or care of human subjects**
    i. Nothing to report

f. **Significant changes in use or care of vertebrate animals.**
    i. Nothing to report

g. **Significant changes in use of biohazards and/or select agents**
    i. Nothing to report

6. Products

a. Publications, conference papers, and presentations

MerTK inhibition in tumor leukocytes decreases tumor growth and metastasis.
Cook RS, Jacobsen KM, Woffard AM, DeRyckere D, Stanford JC, Prieto AL, Redente E, Sandahl M, Hunter DM, Strunk KE, Graham DK, and Earp HS.
J Clin Invest. 2013 123(8):3231-42.

Efferocytosis produces a prometastatic landscape during postpartum mammary gland involution.
Stanford JC, Young C, Hicks D, Owens P, Williams A, Vaught DB, Morrison MM, Lim J, Williams M, Brantley-Sieders DM, Balko JM, Tonetti D, Earp HS 3rd, ***Cook RS***.
J Clin Invest. 2014 Nov;124(11):4737-52.

Clearance of dying cells accelerates malignancy.
Vaught DB and ***Cook RS***.
Oncotarget. 2015 Sept. 22; 6(28): 24590-24591. Pubmed PMID:26387138.

Efferocytosis creates a tumor microenvironment supportive of tumor survival and metastasis.
Vaught DB, Stanford JC, and ***Cook RS***.
Cancer Cell and Microenvironment. 2015. NIHMSID:689387.

Innate immune response to cell death in the post-partum mammary gland increases malignancy of parity associated tumors.
Stanford JC, Fingleton B, Owen P, and ***Cook RS***.
2013 AACR Special Conference Advances in Breast Cancer, San Diego CA.
Published in ***Molecular Cancer Research*** 2013. 11(10 Supplement):B097.

Cell death and efferocytosis generate a pro-metastatic landscape during mammary gland involution that increases disseminatioin of post-partum breast cancers.
Cook RS, Earp HS, and Stanford JC.
2014 San Antonio Breast Cancer Symposium.
Published in ***Cancer Research*** 2015. 75(9 Supplement):P-04-02.

Tumor wound healing response to treatment-induced tumor cell death increases tumor metastasis
Cook RS.
2015 AACR Inaugural Conference on Cancer Immunotherapy, New York, NY
Published in ***Cancer Research*** 2015. 75(15 Supplement): 2916

"Wound healing in the tumor microenvironment" presented by Rebecca S. Cook
New Horizons in Breast Cancer Research, the 14th Annual Meharry Medical College-Vanderbilt University- Tennessee State University U54 Cancer Partnership. Meharry Medical College, Nashville, TN. April 10, 2015.

"Efferocytosis accelerates malignant tumor progression" presented by Rebecca S. Cook
Gordon Research Conference on Apoptotic Cell Clearance. University of New England, Biddeford, ME. June 24, 2015.

"Apoptotic cell clearance in the tumor microenvironment" presented by Rebecca S. Cook
Rigel Pharmaceuticals, Inc. South San Francisco, CA. June 8, 2015.

"Taking out the trash: The role of efferocytosis in breast cancer" presented by Rebecca S. Cook
Dartmouth University Giesel School of Medicine. Hanover, NH. November 23, 2013.

b. Books or other non-periodical, one-time publications

Efferocytosis creates a tumor microenvironment supportive of tumor survival and metastasis.
Vaught DB, Stanford JC, and ***Cook RS***.
Cancer Cell and Microenvironment. 2015. NIHMSID:689387.

c. Other publications, conference papers, and presentations.
Nothing to report

d. Website(s) or other Internet site(s)
Nothing to report

e. Technologies or techniques
1. Imaging of efferocytosis using fluorescent microscopy.
2. Controlled timing of apoptotic tumor cell death
3. Controlled necrotic tumor cell death

f. Inventions, patent applications, and/or licenses
1. Generated a cohort of mice that will form spontaneous mCherry+ tumors in efferocytosis-competent ($MerTK^{+/+}$) and efferocytosis-impaired ($MerTK^{-/-}$) backgrounds.

g. Other Products
Nothing to report

7. PARTICIPANTS & OTHER COLLABORATING ORGANIZATIONS

Name:	*Rebecca S. Cook*
Project Role:	*PI*
Researcher Identifier (e.g. ORCID ID):	*eRA login: COOKR1*
Nearest person month worked:	*12*
Contribution to Project:	*Intellectual contribution, experimental design, interpretation of data*
Funding Support:	*NIH* 5P50CA098131-13 (also this grant)
Name:	*Jamie C. Stanford*
Project Role:	*Post-doctoral Research Fellow*
Researcher Identifier (e.g. ORCID ID):	*unknown*
Nearest person month worked:	*12*
Contribution to Project:	*Experimental performance*
Funding Support:	T32 Training grant Molecular Influences in the Tumor Microenvironment, J. Chen, PI

Has there been a change in the active other support of the PD/PI(s) or senior/key personnel since the last reporting period?

Nothing to report.

What other organizations were involved as partners?

Nothing to report.

8. SPECIAL REPORTING REQUIREMENTS

h. COLLABORATIVE AWARDS

Nothing to report

i. **QUAD CHARTS:**

Nothing to report

9. APPENDICES:

Appendix 1.
MerTK inhibition in tumor leukocytes decreases tumor growth and metastasis.
Cook RS, Jacobsen KM, Woffard AM, DeRyckere D, Stanford JC, Prieto AL, Redente E, Sandahl M, Hunter DM, Strunk KE, Graham DK, and Earp HS.
J Clin Invest. 2013 123(8):3231-42.

Appendix 2.
Efferocytosis produces a prometastatic landscape during postpartum mammary gland involution.
Stanford JC, Young C, Hicks D, Owens P, Williams A, Vaught DB, Morrison MM, Lim J, Williams M, Brantley-Sieders DM, Balko JM, Tonetti D, Earp HS 3rd, ***Cook RS***.
J Clin Invest. 2014 Nov;124(11):4737-52.

Appendix 3.
Clearance of dying cells accelerates malignancy.
Vaught DB and ***Cook RS***.
Oncotarget. 2015 Sept. 22; 6(28): 24590-24591. Pubmed PMID:26387138.

Appendix 1.

MerTK inhibition in tumor leukocytes decreases tumor growth and metastasis.

Cook RS, Jacobsen KM, Woffard AM, DeRyckere D, Stanford JC, Prieto AL, Redente E, Sandahl M, Hunter DM, Strunk KE, Graham DK, and Earp HS.

J Clin Invest. 2013 123(8):3231-42.

MerTK inhibition in tumor leukocytes decreases tumor growth and metastasis

Rebecca S. Cook,[1,2] Kristen M. Jacobsen,[3,4] Anne M. Wofford,[5] Deborah DeRyckere,[4] Jamie Stanford,[1] Anne L. Prieto,[6] Elizabeth Redente,[7] Melissa Sandahl,[8] Debra M. Hunter,[8] Karen E. Strunk,[8] Douglas K. Graham,[3,4] and H. Shelton Earp III[8]

[1]Department of Cancer Biology, Vanderbilt University School of Medicine, Nashville, Tennessee, USA. [2]Ingram Cancer Center, Nashville, Tennessee, USA. [3]Department of Integrated Immunology and [4]Department of Pediatrics, University of Colorado, Anschutz Medical Campus, Aurora, Colorado, USA. [5]Wake Forest School of Medicine, Winston-Salem, North Carolina, USA. [6]Department of Psychological and Brain Science, Indiana University, Bloomington, Indiana, USA. [7]Department of Pediatrics, National Jewish Health, Denver, Colorado, USA. [8]Departments of Pharmacology and Medicine and UNC Lineberger Comprehensive Cancer Center, University of North Carolina School of Medicine, Chapel Hill, North Carolina, USA.

MerTK, a receptor tyrosine kinase (RTK) of the TYRO3/AXL/MerTK family, is expressed in myeloid lineage cells in which it acts to suppress proinflammatory cytokines following ingestion of apoptotic material. Using syngeneic mouse models of breast cancer, melanoma, and colon cancer, we found that tumors grew slowly and were poorly metastatic in *MerTK*$^{-/-}$ mice. Transplantation of *MerTK*$^{-/-}$ bone marrow, but not wild-type bone marrow, into lethally irradiated *MMTV-PyVmT* mice (a model of metastatic breast cancer) decreased tumor growth and altered cytokine production by tumor CD11b^{+} cells. Although MerTK expression was not required for tumor infiltration by leukocytes, *MerTK*$^{-/-}$ leukocytes exhibited lower tumor cell–induced expression of wound healing cytokines, e.g., IL-10 and growth arrest-specific 6 (GAS6), and enhanced expression of acute inflammatory cytokines, e.g., IL-12 and IL-6. Intratumoral CD8^{+} T lymphocyte numbers were higher and lymphocyte proliferation was increased in tumor-bearing *MerTK*$^{-/-}$ mice compared with tumor-bearing wild-type mice. Antibody-mediated CD8^{+} T lymphocyte depletion restored tumor growth in *MerTK*$^{-/-}$ mice. These data demonstrate that MerTK signaling in tumor-associated CD11b^{+} leukocytes promotes tumor growth by dampening acute inflammatory cytokines while inducing wound healing cytokines. These results suggest that inhibition of MerTK in the tumor microenvironment may have clinical benefit, stimulating antitumor immune responses or enhancing immunotherapeutic strategies.

Introduction

MerTK is a member of a receptor tyrosine kinase (RTK) family that also includes AXL and TYRO3. Family members undergo ligand-induced homodimerization, followed by catalytic tyrosine kinase activation and intracellular signaling (1–4). Cross-phosphorylation has also been demonstrated within this RTK family, suggesting heterodimerization (5). These RTKs are widely expressed in many epithelial tissues and in cells of the immune, nervous, and reproductive systems (2, 6). The MerTK ligands include growth arrest-specific 6 (GAS6) (7, 8), protein-S (9, 10), tubby and tubby-like protein-1 (TULP1) (11), and galectin-3 (12). Several of these ligands are present in serum, and all are expressed locally in some tissues. These ligands bind to the extracellular domain of MerTK, resulting in tyrosine kinase activation.

With respect to neoplastic diseases, MerTK is expressed in non-neoplastic cells found in the tumor microenvironment. MerTK is also ectopically expressed or overexpressed in many hematologic and epithelial malignant cells. Moreover, expression of MerTK and GAS6 correlates with poor prognosis or chemoresistance in some human tumor types (1, 2, 13–19). However, the mechanisms by which increased MerTK signaling contributes to tumor malignancy remain unknown.

Studies using mice devoid of MerTK revealed its critical role at the interface of innate and adaptive immunity (4, 20, 21). Innate immunity requires rapid and robust activation in response to pathogens or wounding. However, this response must be restrained to prevent inflammation-associated tissue damage or immunity against self-antigens. MerTK signaling plays a central role in dampening the innate immune response in DCs and macrophages (21). One mechanism by which MerTK performs this task is through efferocytosis, the physiological process by which apoptotic cells are engulfed by phagocytes (22). MerTK ligands, including GAS6, simultaneously bind to MerTK expressed on phagocytes and to phosphatidylserine presented on the outer plasma membrane leaflets of apoptotic cells (23, 24). This complex ligand (GAS6 bound to externalized phosphatidylserine) activates MerTK tyrosine kinase signaling, initiates phagocytosis of apoptotic material, and drives transcriptional changes that cause suppression of proinflammatory cytokines, such as IL-12, and increases in inflammatory repressors, such as IL-10 (25, 26). Therefore, MerTK-mediated efferocytosis is necessary to maintain tissue homeostasis in organs harboring abundant apoptotic materials, such as the retina and the postlactational mammary gland (27, 28).

MerTK similarly dampens TLR-induced production of proinflammatory cytokines, such as IL-6, IL-12, and type I interferons (IFNs), which fail to be downregulated in *MerTK*$^{-/-}$ mice (4, 24, 29). For example, low doses of lipopolysaccharide in *MerTK*$^{-/-}$ mice resulted in death from endotoxic shock associated with high levels of TNF-α (30). Failure to dampen acute innate immunity leads to secondary pathological activation of T and B lymphocytes directed at self-antigens (4, 26, 29, 31, 32). This is especially important

Conflict of interest: The authors have declared that no conflict of interest exists.

Note regarding evaluation of this manuscript: Manuscripts authored by scientists associated with Duke University, The University of North Carolina at Chapel Hill, Duke-NUS, and the Sanford-Burnham Medical Research Institute are handled not by members of the editorial board but rather by the science editors, who consult with selected external editors and reviewers.

Citation for this article: *J Clin Invest.* 2013;123(8):3231–3242. doi:10.1172/JCI67655.

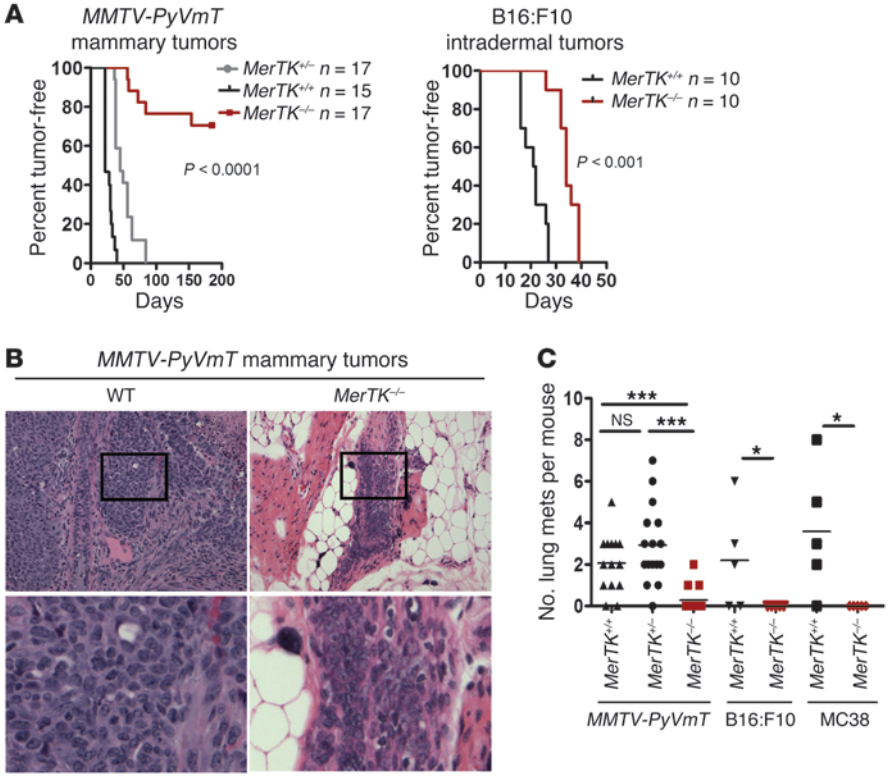

Figure 1

Decreased tumor malignancy in *MerTK*$^{-/-}$ microenvironment. (**A**) *MMTV-PyVmT* mammary tumor cells injected into the mammary fat pads and B16:F10 tumor cells injected intradermally formed tumors with a delayed latency in *MerTK*$^{-/-}$ mice as compared with that in *MerTK*$^{+/+}$ and *MerTK*$^{+/-}$ mice. *P* values comparing *MerTK*$^{+/+}$ to *MerTK*$^{-/-}$ were determined using the log-rank (Mantel-Cox) test. (**B**) H&E-stained sections of tumors harvested 30 days after tumor cell injection in *MerTK*$^{+/+}$ mice and 180 days after tumor cell injection in *MerTK*$^{-/-}$ mice. Boxed regions are shown at higher magnification below and indicate the monotonous sheets of tumor cells in *MerTK*$^{+/+}$ mice and the compartmentalized nature of the implanted tumor cells in *MerTK*$^{-/-}$ mice. Original magnification, ×100 (top row); ×600 (bottom row). (**C**) Lung metastases were enumerated in tumor-bearing mice at 14 days after *MMTV-PyVmT* tumor palpation (n = 14–16), at 7 days after B16:F10 tumor palpation (n = 5), and at 7 days after MC38 tumor palpation of subcutaneously implanted MC38 cells. Horizontal bars represent average numbers of lung metastases per mouse. *P* values were calculated using Student's t test for *MMTV-PyVmT* tumors (comparing *MerTK*$^{+/+}$ to *MerTK*$^{-/-}$) and using a 1-tailed Mann-Whitney test for B16:F10 and MC38 tumors. *$P < 0.05$. ***$P < 0.001$.

given that apoptotic cells accumulate in the absence of MerTK (23, 28), providing an enriched source for intracellular "self" antigens in the context of heightened acute inflammatory signals and enhanced B and T lymphocyte activity. Therefore, MerTK signaling on macrophages and DCs lies at the interface of the innate and adaptive immune systems. Combined loss of MerTK, AXL, and TYRO3 results in a highly active autoimmune state, with massive lymphocyte proliferation and lupus-like autoimmunity (33).

Numerous studies indicate that tumor-associated macrophages correlate with a poor prognosis in patients with cancer (34–36). Reduction of macrophage presence in mouse models of breast cancer by genetic loss of *CSF1*, or by antibody-mediated blockade of CSF1 receptor signaling, substantially reduced tumor metastasis (37, 38), demonstrating that malignant tumor progression is promoted by macrophages. Tumor-associated macrophages generally secrete wound healing cytokines that increase growth of epithelial tumor and stromal cells in experimental models (39–41). Tumor-associated macrophages also produce immune-modulating cytokines such as IL-10, which may decrease antitumor immunity by suppressing proinflammatory cytokine expression, limiting antigen presentation, and dampening of T lymphocyte–mediated tumor cell cytotoxicity (41, 42). For example, antigen presentation in the context of increased IL-12 results in clonal expansion of CD8$^+$ T lymphocytes (43); the suppression of IL-12 in the tumor microenvironment suggests a mechanism by which tumor-associated macrophage-mediated changes in antigen presentation and cytokine production may directly decrease T cell–mediated antitumor immunity.

Interestingly, the characteristically low IL-12/high IL-10 production observed in tumor-associated macrophages is also seen in macrophages and DCs following efferocytosis. Because MerTK appears to be a central regulator of the transition from proinflammatory to wound healing cytokine production following efferocytosis, and because *MerTK*-deficient macrophages produce increased proinflammatory cytokines, we tested the hypothesis that MerTK in the tumor microenvironment aids malignant tumor progression by suppressing antitumor immunity. We show here that loss of MerTK in the tumor microenvironment of *MerTK*$^{-/-}$ mice (30) slowed the establishment, growth, and metastasis of mammary tumors and melanomas in immune competent, syngeneic mice. These findings were recapitulated in spontaneous mammary tumors in recipients of *MerTK*$^{-/-}$ bone marrow transplants. Very early immune responses to syngeneic tumor cell implantation in *MerTK*$^{-/-}$ mice included decreased IL-10 and increased IL-12 production, increased leukocyte proliferation, and a higher level of tumor CD8$^+$ T lymphocytes as compared with early tumor-induced responses in *MerTK*$^{+/+}$ mice. Isolation of CD11b$^+$ cells from tumors revealed MerTK-dependent repression of proinflammatory cytokines. Antibody-based depletion of CD8$^+$ T lymphocytes restored tumor growth in *MerTK*$^{-/-}$ hosts. These results suggest that MerTK in the immune compartment of the tumor microenvironment suppresses innate immunity and promotes tumor progression. They also suggest that inhibition of MerTK signaling may produce an immunomodulatory, therapeutic benefit in some human tumors.

Results

Prolonged tumor latency and decreased metastasis in MerTK$^{-/-}$ *hosts*. To determine whether host-derived MerTK in the tumor microenvironment affects tumor formation and growth, primary mouse mammary tumor cells derived from female *MMTV-PyVmT* mice (43) (inbred into the C57BL/6 genetic background) were injected

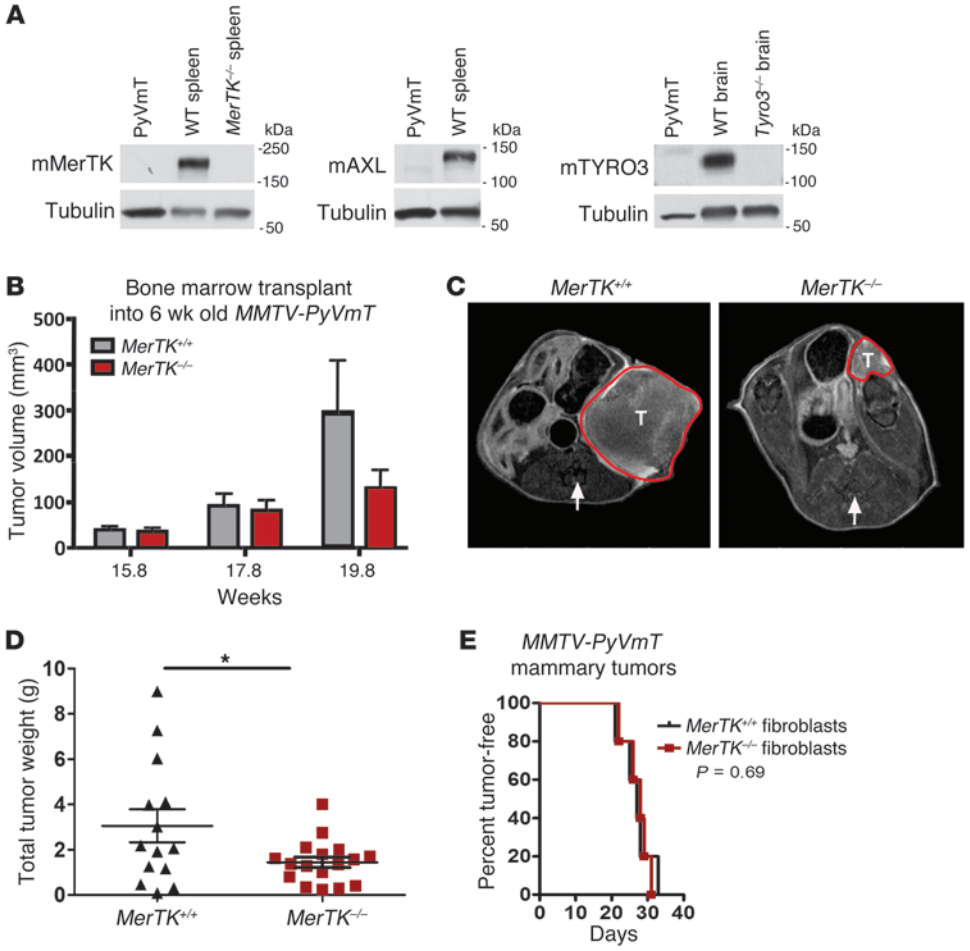

Figure 2

MerTK-deficient leukocytes confer tumor resistance to *MerTK*$^{+/+}$ mice. (**A**) Whole cell lysates harvested from *MMTV-PyVmT* primary mammary tumor cells were assessed by Western analysis using antibodies indicated. Whole spleen lysates harvested from *MerTK*$^{+/+}$ and *MerTK*$^{-/-}$ mice were used as positive and negative controls, respectively, for MerTK expression. Whole spleen lysates harvested from *MerTK*$^{+/+}$ mice were used as a positive control for AXL expression. Whole brain lysates harvested from *Tyro3*$^{+/+}$ and *Tyro3*$^{-/-}$ mice were used as positive and negative controls from TYRO3 expression. (**B**–**D**) Bone marrow harvested from *MerTK*$^{+/+}$ or *MerTK*$^{-/-}$ donors was delivered by tail vein injection into lethally irradiated 6-week-old female *MMTV-PyVmT* recipients. (**B**) Average tumor volume ± SEM measured in live mice by MRI at 15.8, 17.8, and 19.8 weeks of age. (**C**) Representative transverse MRI slices of age-matched *MMTV-PyVmT* recipients of *MerTK*$^{+/+}$ or *MerTK*$^{-/-}$ bone marrow in the lower abdomen/pelvic region. The arrows indicate the location of the spine, while the tumor (T) margins are identified by the red dotted line. (**D**) Total tumor weight measured at 21 weeks of age (time of necropsy). Horizontal bars represent average total tumor weight ± SEM ($n = 14$). The P value was calculated using Student's t test. *$P < 0.05$. (**E**) Mammary fibroblasts harvested from *MerTK*$^{+/+}$ and *MerTK*$^{-/-}$ mice were cotransplanted with *MMTV-PyVmT* tumor cells into the mammary fat pads of *MerTK*$^{+/+}$ mice, and tumor latency was measured.

orthotopically into the inguinal mammary fat pads of female wild-type (*MerTK*$^{+/+}$) and *MerTK*$^{-/-}$ recipient mice. While tumors formed in *MerTK*$^{+/+}$ mice with an average latency of 28 days, latency was delayed in *MerTK*$^{-/-}$ littermates ($P < 0.001$). Tumors remained unpalpable in 70% of *MerTK*$^{-/-}$ mice throughout the entire study period of 198 days (Figure 1A). Mice carrying one functional *MerTK* allele (*MerTK*$^{+/-}$ mice) formed tumors with an average latency of 49 days, which was intermediate between *MerTK*$^{+/+}$ mice ($P < 0.001$) and *MerTK*$^{-/-}$ mice ($P < 0.001$, Mantel-Cox test). This suggests that MerTK signaling in the stromal environment enhances tumor growth in a dose-dependent manner. C57BL/6-derived B16:F10 mouse melanoma cells injected orthotopically formed intradermal tumors in *MerTK*$^{+/+}$ mice with an average latency of 26 days, compared with 48 days in *MerTK*$^{-/-}$ littermates ($P < 0.0001$; Figure 1A). Similarly, a third syngeneic model demonstrated prolonged latency. C57B1/6 MC38 colon cancer cells were implanted subcutaneously; in *MerTK*$^{+/+}$ mice tumors formed with an average latency of 27 days as compared with 46 days in *MerTK*$^{-/-}$ mice ($P < 0.0001$, data not shown).

Histological analysis of *MMTV-PyVmT* tumors that formed in *MerTK*$^{-/-}$ mice revealed distinct differences from those growing in *MerTK*$^{+/+}$ mice. Tumors harvested from *MerTK*$^{+/+}$ mice displayed densely packed solid sheets of cells, with prominent hyperchromatic nuclei and little cytoplasm, regions of central necrosis, and invasion into skeletal muscle (Figure 1B). In contrast, tumors harvested from *MerTK*$^{-/-}$ mice were small and harbored more connective tissue as opposed to the frank cellularity of tumors in *MerTK*$^{+/+}$ hosts (Figure 1B). *MerTK*$^{-/-}$ mice were less prone to formation of lung metastases (Figure 1C), with only 3 out of 15 *MerTK*$^{-/-}$ mice presenting with lung micrometastases derived from *MMTV-PyVmT* primary tumors, as compared with 13 out of 15 wild-type mice and 16 out of 17 *MerTK*$^{+/-}$ mice exhibiting *MMTV-PyVmT* lung metastases. Lung metastases were not detected in any *MerTK*$^{-/-}$ mice bearing B16:F10 tumors, while 3 out of 5 wild-type mice displayed B16:F10 lung metastases. Likewise, 4 out of 5 subcutaneously implanted MC38 colon cancer cell tumors in *MerTK*$^{+/+}$ mice yielded lung metastases, whereas none were detected in the *MerTK*$^{-/-}$ mice (Figure 1C). These data suggest that MerTK signaling in the tumor microenvironment leads to increased tumor growth and malignant progression.

MerTK$^{-/-}$ *leukocytes confer tumor resistance in MerTK*$^{+/+}$ *mice.* There are complex autocrine and paracrine interactions between tumor-associated macrophages and the epithelial cells in preclinical breast cancer models and presumably in human breast cancer. These have been well characterized in the polyoma middle T model. To rule out a potential role of MerTK in our C57/Bl6

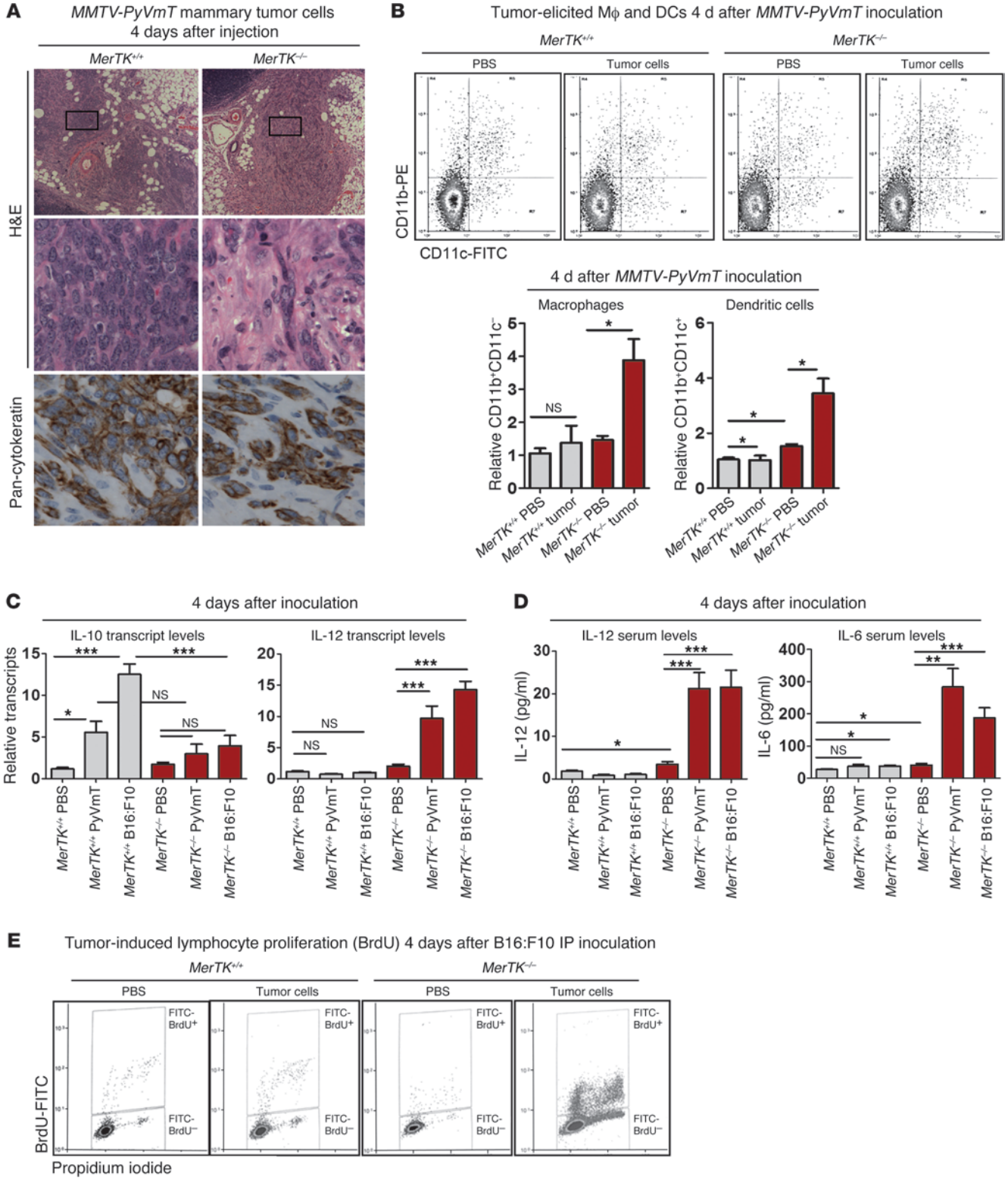

Figure 3
Altered early tumor response in *MerTK*-deficient mice. (**A**) Representative H&E-stained and cytokeratin-stained sections of mammary glands 4 days after injection with *MMTV-PyVmT* cells are shown. Boxed regions are shown at higher magnification below. Original magnification, ×100 (top row); ×600 (bottom rows). (**B**) Single cell mammary suspensions harvested 4 days after intramammary tumor cell injections were stained for CD11b and CD11c. Proportions of $CD11b^+CD11c^-$ macrophages and $CD11b^+CD11c^+$ dendritic cells relative to total PBS-treated $MerTK^{+/+}$ $CD11b^+CD11c^+$ population is shown. $^*P < 0.05$. (**C**) RNA harvested 4 days after PBS, *MMTV-PyVmT*, or B16:F10 injection into the inguinal mammary fat pad was assessed by qPCR to detect IL-10 and IL-12p40 transcripts. (**D**) Serum collected 4 days after injection of PBS, *MMTV-PyVmT*, or B16:F10 tumor cells into the inguinal mammary fat pad was assessed by ELISA to measure IL-12p70 and IL-6. (**C** and **D**) Values shown, calculated using the (**C**) δδCT method or (**D**) serum levels, represent the average ± SD ($n = 6$), relative to the level detected in PBS-treated $MerTK^{+/+}$ samples. $^*P < 0.05$; $^{**}P < 0.01$; $^{***}P < 0.001$. (**E**) Mice were inoculated with B16:F10 cells by i.p. injection. After 4 days, mice were treated with BrdU. Splenocytes harvested after 1 hour treatment with BrdU were stained with anti-BrdU and propidium iodide and assessed by flow cytometry.

PyVmT cells, we measured MerTK protein expression by Western analysis. Protein lysates from cultured tumor cells did not express MerTK. MerTK was detected in whole spleen lysates harvested from $MerTK^{+/+}$ mice but not $MerTK^{-/-}$ mice (Figure 2A). Certain paracrine ligands (e.g., GAS6) might bind to other members of this RTK family in PyVmT cells; therefore, we examined the protein expression of AXL and TYRO3. Neither AXL nor TYRO3 were expressed in the PyVmT breast cancer cells. qPCR of RNA levels confirmed these findings (data not shown).

However, as MerTK is expressed in hematopoietic cells, we used bone marrow reconstitution assays to determine the impact of MerTK ablation within bone marrow–derived subpopulations of the tumor microenvironment. We harvested bone marrow from $MerTK^{-/-}$ × *UBC-GFP* and $MerTK^{+/+}$ × *UBC-GFP* donors and delivered marrow to lethally irradiated 6-week-old C57BL/6 female transgenic *MMTV-PyVmT* mice. After 4 weeks, mice exhibiting >75% GFP^+ hematopoietic cells were used for further analysis. At this time point (10 weeks of age), the majority of mice had already developed tumors, consistent with the published average tumor latency in this aggressive tumor model (44). Therefore, it was not feasible to detect potential differences in tumor latency. Instead, tumor growth was measured by MRI over the following 11 weeks, revealing reduced tumor volume in $MerTK^{-/-}$ bone marrow recipients as compared with that in $MerTK^{+/+}$ bone marrow recipients (Figure 2, B and C). Similarly, upon sacrifice at the study end point (21 weeks of age), total tumor weight was decreased nearly 2 fold in $MerTK^{-/-}$ bone marrow recipients as compared with that in $MerTK^{+/+}$ bone marrow recipients (Figure 2D). To measure the burden of apoptotic material in these tumors, immunofluorescent detection of apoptotic cells by TUNEL analysis in these late-stage tumors (19.8 weeks of age) was performed. The number of apoptotic tumor cells within $F4/80^+$ macrophages was not altered in recipients of $MerTK^{-/-}$ bone marrow as compared to what was seen in tumors harvested from $MerTK^{+/+}$ bone marrow recipients (Supplemental Figure 1; supplemental material available online with this article; doi:10.1172/JCI67655DS1).

Because bone marrow–derived mesenchymal stem cells might give rise to fibroblasts in the tumor microenvironment that could modulate tumor growth and metastasis (45), we investigated the impact of $MerTK^{-/-}$ fibroblasts in the tumor microenvironment. 10^6 mammary fibroblasts harvested from $MerTK^{-/-}$ and $MerTK^{+/+}$ donors were cotransplanted with *MMTV-PyVmT* tumor cells into $MerTK^{+/+}$ mammary fat pads. The rate of tumor formation was similar in mice receiving $MerTK^{-/-}$ or $MerTK^{+/+}$ fibroblasts (Figure 2E). Together, these data suggest that loss of MerTK from the immune compartment, but not the fibroblast compartment, of the tumor microenvironment is sufficient to delay tumor formation.

Altered early tumor response in $MerTK^{-/-}$ mice. To examine early immune response in the tumor microenvironment, inguinal mammary glands were harvested 4 days after *MMTV-PyVmT* tumor inoculation. At this time, tumor cells were evident in the injected mammary glands of both $MerTK^{+/+}$ and $MerTK^{-/-}$ mice, as shown in H&E-stained sections and by immunohistochemical detection of pan-cytokeratin (Figure 3A). However, higher-power magnification of the injection site revealed histological differences at this early stage, including an abundance of matrix deposition and reduced tumor cellularity in $MerTK^{-/-}$ samples as compared with that in $MerTK^{+/+}$ samples (Figure 3A). After removal of the intramammary lymph node, mammary cell suspensions were stained with antibodies against CD11b and CD11c to identify tumor-recruited macrophages and DCs. To control for injection-induced changes in the cell populations, we injected sterile phosphobuffered saline (PBS) into the contralateral mammary fat pads. The results revealed that, in early-stage implanted tumors, there are differences in basal macrophage and DC levels in $MerTK^{-/-}$ mammary glands as compared with those in $MerTK^{+/+}$ mammary glands (Figure 3B). At 4 days after tumor inoculation into the mammary gland, the percentages of macrophages and DCs were relatively unchanged in $MerTK^{+/+}$ mice as compared to those in PBS-injected $MerTK^{+/+}$ mice. In contrast, tumor cell injection in $MerTK^{-/-}$ fat pads generated a >4-fold increase in macrophages and >3.5-fold increase in DCs over PBS-injected $MerTK^{-/-}$ mammary glands.

RNA isolated from single cell mammary suspensions harvested at 4 days after tumor (or PBS) inoculation revealed increased transcript levels encoding the wound healing/tolerogenic cytokine IL-10 in $MerTK^{+/+}$ samples but not in $MerTK^{-/-}$ samples (Figure 3C). Conversely, transcripts encoding the proinflammatory cytokine IL-12 were elevated 10 fold at 4 days after *MMTV-PyVmT* tumor cell inoculation in $MerTK^{-/-}$ mice but not in $MerTK^{+/+}$ mice. We similarly assessed *Il10* and *Il12* mRNA levels 4 days following implantation of B16:F10 mouse melanoma cells into the mouse mammary fat pad. Tumor-recruited cells were collected 4 days after tumor cell injection. *Il10* transcript levels were substantially increased in samples from tumor cell–inoculated $MerTK^{+/+}$ mice as compared with those from PBS-inoculated $MerTK^{+/+}$ mice. However, *Il10* transcript levels were unchanged in cells harvested from tumor cell–inoculated $MerTK^{-/-}$ mice (Figure 3C). While *Il12* transcript levels remained relatively unchanged in $MerTK^{+/+}$ cells harvested from PBS- and tumor cell–treated mice, cells harvested from $MerTK^{-/-}$ mice expressed more *Il12* transcripts 4 days after tumor cell injection as compared with 4 days after PBS injection (Figure 3C). Serum IL-12p70 and IL-6 levels were increased 4 days after intramammary *MMTV-PyVmT* tumor cell injection into $MerTK^{-/-}$ mice, but not $MerTK^{+/+}$ mice, over what was seen in PBS-injected $MerTK^{-/-}$ and $MerTK^{+/+}$ mice, respectively (Figure 3D). Mammary fat pad injection of B16:F10 tumor cells also generated increased serum IL-12p70 and IL-6 levels in $MerTK^{-/-}$ mice (Figure 3D). We repeated this analysis 4 days after injection of B16:F10 tumor cells i.p. into $MerTK^{+/+}$ and $MerTK^{-/-}$ mice, yielding

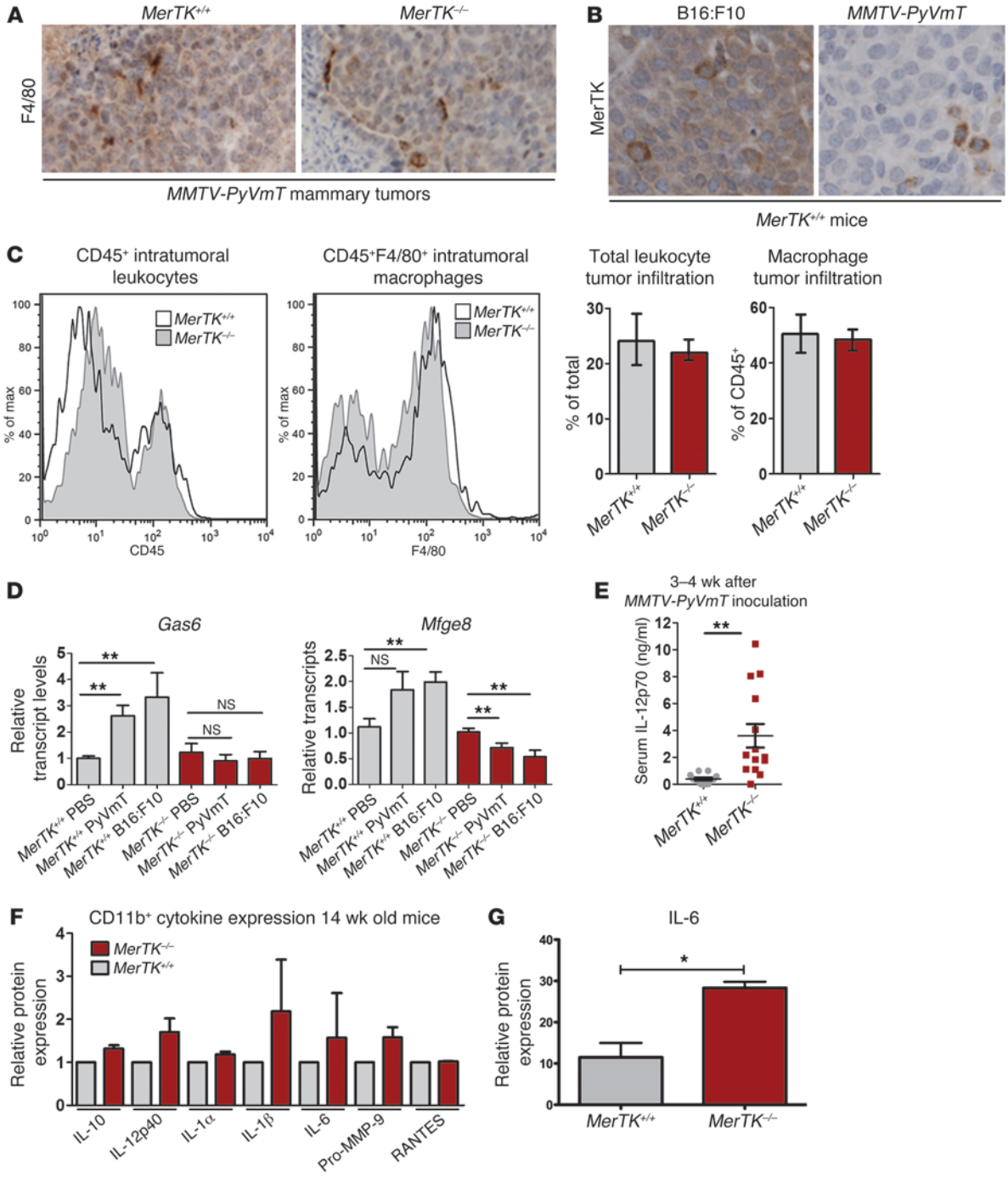

Figure 4

Altered cytokine production in *MerTK*$^{-/-}$ tumor microenvironment. (**A** and **B**) Immunohistochemistry for (**A**) F4/80 and (**B**) MerTK in tumors from (**A**) *MerTK*$^{+/+}$ and *MerTK*$^{-/-}$ mice and (**B**) *MerTK*$^{+/+}$ mice. Original magnification, ×400 (**A**); ×600 (**B**). (**C**) Single cell *MMTV-PyVmT* tumor suspensions harvested from *MerTK*$^{+/+}$ (solid line) and *MerTK*$^{-/-}$ (tinted area) mice were stained for CD45 and F4/80. Representative plots for live cells are shown. Average ± SEM; $n = 4$. (**D**) Total RNA harvested 4 days after PBS, *MMTV-PyVmT*, or B16:F10 injection was assessed by qPCR for *Gas6* and *Mfge8*. δδCT values shown represent average ± SD ($n = 6$) relative to PBS-injected *MerTK*$^{+/+}$ values. $^{**}P < 0.01$. (**E**) Serum IL-12p70 was measured by ELISA in serum harvested 3–4 weeks after tumor cell inoculation ($n = 13$). $^{**}P < 0.01$. (**F** and **G**) CD11b^{+} cells were harvested from *MMTV-PyVmT* tumors (**F**) 8 weeks and (**G**) 15 weeks after bone marrow transplant. GFP^{+}CD45^{+}CD11b^{+} cells were purified from tumors and cell lysates were analyzed by cytokine array. $^{*}P < 0.05$.

similar results. Cells harvested by peritoneal lavage were used to assess expression of transcripts encoding IL-10 and IL-12. *Il10* transcripts were elevated in cells isolated from *MerTK*$^{+/+}$ mice inoculated with B16:F10 cells by i.p. injection as compared with those in cells from *MerTK*$^{+/+}$ mice inoculated with PBS (Supplemental Figure 2). In contrast, *Il10* transcripts were not elevated in *MerTK*$^{-/-}$ mice inoculated with B16:F10 cells. Elevated *Il12* transcripts were observed in peritoneal lavage cells harvested from tumor-inoculated *MerTK*$^{-/-}$ mice as compared with what was seen in PBS-inoculated mice or tumor-inoculated *MerTK*$^{+/+}$ mice. Serum IL-6 was also elevated in *MerTK*$^{-/-}$ mice inoculated i.p. with B16:F10 tumor cells (Supplemental Figure 2). We used the B16:F10 i.p. inoculation model to assess splenocyte proliferative activity. BrdU labeling of mice for 1 hour, 4 days after i.p. tumor cell or PBS inoculation, revealed that BrdU incorporation into splenocytes was similar in *MerTK*$^{+/+}$ and *MerTK*$^{-/-}$ mice inoculated with sterile PBS and that BrdU incorporation increased in both *MerTK*$^{+/+}$ and *MerTK*$^{-/-}$ splenocytes harvested 4 days after i.p. tumor cell injection as compared with splenocytes from PBS-injected, genotype-matched mice (Figure 3E). However, the tumor-induced increase in BrdU-positive splenocytes was substantially greater in *MerTK*$^{-/-}$ mice compared with that in tumor-treated *MerTK*$^{+/+}$ mice, suggesting that tumor-induced leukocyte proliferation was exaggerated in the absence of MerTK.

Altered tumor microenvironment in established tumors in MerTK$^{+/+}$ *and MerTK*$^{-/-}$ *mice*. Immunohistochemical detection of F4/80, a macrophage marker, demonstrated macrophage infiltration of orthotopic *MMTV-PyVmT* tumors grown in *MerTK*$^{+/+}$ and *MerTK*$^{-/-}$ mice (Figure 4A). MerTK staining was detected in B16:F10 and *MMTV-PyVmT* tumor macrophages grown in *MerTK*$^{+/+}$ mice (Figure 4B). To verify that *MerTK*$^{-/-}$ macrophages were capable of infiltrating spontaneously forming tumors, we generated single cell suspensions from *MMTV-PyVmT* mice harboring *MerTK*$^{-/-}$ and *MerTK*$^{+/+}$ immune cells and stained cell suspensions for CD45, a cell surface marker of leukocytes, and F4/80. *MerTK*$^{+/+}$ and *MerTK*$^{-/-}$ CD45$^+$ leukocytes were detected at similar proportions of the total cell population (Figure 4C), revealing similar levels of CD45$^+$ tumor leukocytes and comparable levels of *MerTK*$^{+/+}$ and *MerTK*$^{-/-}$ tumor-associated macrophages in these established tumors.

Transcripts encoding the MerTK ligand, GAS6, were identified by qRT-PCR in RNA isolated from mammary glands 4 days after *MMTV-PyVmT* tumor cell injection into the mammary fat pads of *MerTK*$^{+/+}$ and *MerTK*$^{-/-}$ mice. *Gas6* levels in *MerTK*$^{+/+}$ mammary glands were >3-fold higher in tumor cell–injected glands as compared with those seen in the contralateral PBS-injected mammary gland, suggesting that GAS6 is elevated in the tumor microenvironment within 4 days (Figure 4D). Increased *Gas6* mRNA levels were also detected in *MerTK*$^{+/+}$ samples harvested 4 days after B16:F10 cell inoculation, consistent with previous reports of elevated *Gas6* levels in the tumor microenvironment (46). However, *Gas6* remained unchanged in the *MerTK*$^{-/-}$ mice after tumor cell inoculation with *MMTV-PyVmT* or *B16:F10* cells. Because the *MerTK*$^{-/-}$ tumor microenvironment did not induce *Gas6* expression, it is possible that MerTK signaling may be part of the mechanism by which tumors upregulate GAS6 in the microenvironment. *MFGE8* encodes another phosphatidylserine-interacting ligand used for efferocytosis by macrophages (47). Similar to *Gas6*, *Mfge8* transcript levels were elevated in response to tumors in *MerTK*$^{+/+}$ but not *MerTK*$^{-/-}$ samples (Figure 4D).

Cytokine expression in the microenvironment of established tumors was examined to determine whether the cytokine expression patterns seen 4 days after tumor cell injection were sustained. Serum IL-12p70 was measured 3–4 weeks after mammary fat pad injection of *MMTV-PyVmT* tumor cells. As compared with that in tumor-bearing *MerTK*$^{+/+}$ mice, serum IL-12p70 was increased in tumor-bearing *MerTK*$^{-/-}$ mice (Figure 4E), confirming that MerTK signaling in the tumor microenvironment suppresses proinflammatory cytokine production in both early and late stages of tumor progression. To specifically assess MerTK-dependent cytokine modulation in macrophages and DCs in the tumor microenvironment, we harvested CD11b$^+$ cells from transgenic *MMTV-PyVmT* mice 8 weeks after lethal irradiation and bone marrow transplantation from *MerTK*$^{+/+}$ or *MerTK*$^{-/-}$ donors. Protein lysates from CD11b$^+$ cells were assessed by cytokine array, revealing increased levels of IL-1β, IL-6, and IL-12p40 in tumor-associated *MerTK*$^{-/-}$ CD11b$^+$ cells as compared with levels seen in *MerTK*$^{+/+}$ CD11b$^+$ cells (Figure 4F). CD11b$^+$ cells from transgenic *MMTV-PyVmT* mice harvested 15 weeks after bone marrow transplant revealed significantly elevated IL-6 levels in *MerTK*$^{-/-}$ tumor-associated CD11b$^+$ cells (Figure 4G). M1- and M2-programmed tumor-associated F4/80$^+$ macrophages were identified in situ using antibodies against inducible nitric oxide synthase (iNOS) and arginase-1 (Arg1), respectively. These results confirmed that the density of macrophages in the tumor microenvironment was relatively similar in tumors grown in *MerTK*$^{+/+}$ or *MerTK*$^{-/-}$ bone marrow recipients. Recipients of *MerTK*$^{-/-}$ bone marrow showed a modest decrease in the ratio of M2 to M1 tumor-associated macrophages as compared with what was seen in tumors harvested from *MerTK*$^{+/+}$ bone marrow recipients, although this trend was not statistically significant (Supplemental Figure 3). Taken together, these data demonstrate that targeted loss of MerTK from tumor-associated CD11b$^+$ cells increases and sustains expression of proinflammatory cytokines, suggesting that MerTK signaling within tumor-associated monocyte-derived cells limits the expression of proinflammatory cytokines.

CD8$^+$ *T lymphocytes are more abundant in the MerTK*$^{-/-}$ *tumor microenvironment*. Four days after *MMTV-PyVmT* tumor cell inoculation into the mammary fat pad, mammary lymph nodes were removed and the remaining tissue was used to generate single cell suspensions. Staining for CD8 and CD4 revealed that the total CD8$^+$CD4$^-$ population was decreased in tumor-inoculated *MerTK*$^{+/+}$ samples (Figure 5A) but remained unchanged in tumor-inoculated *MerTK*$^{-/-}$ mice. Because NK cells express MerTK and also express CD8, we measured the relative presence of NK cells in the early tumor microenvironment by staining the CD8$^+$CD4$^-$ population with NK1.1. Although a slight increase in NK1.1$^+$CD8$^+$CD4$^-$ levels was observed in tumor-inoculated *MerTK*$^{+/+}$ mice, this did not reach statistical significance (Figure 5B). Similar levels were seen in *MerTK*$^{-/-}$ mice treated with either PBS or with tumor cells. While these results do not rule out the impact of MerTK on tumor-infiltrating NK cell behavior, these data suggest that NK cell numbers are not greatly affected in the early tumor microenvironment by MerTK. Immunohistochemical detection of granzyme B was used to detect cytotoxic leukocytes (such as CD8$^+$ T lymphocytes, NK cells, or NKT cells) in the tumor microenvironment of *MMTV-PyVmT* tumors 3–8 weeks after tumor transplant. Granzyme B–positive cells were more abundant in tumors grown in *MerTK*$^{-/-}$ mice as compared with those in tumors grown in *MerTK*$^{+/+}$ littermates (Figure 5C). In contrast to what was seen with the CD8$^+$CD4$^-$ population (Figure 5A), we found an early tumor-elicited increase in the CD8$^-$CD4$^+$ population in *MerTK*$^{+/+}$

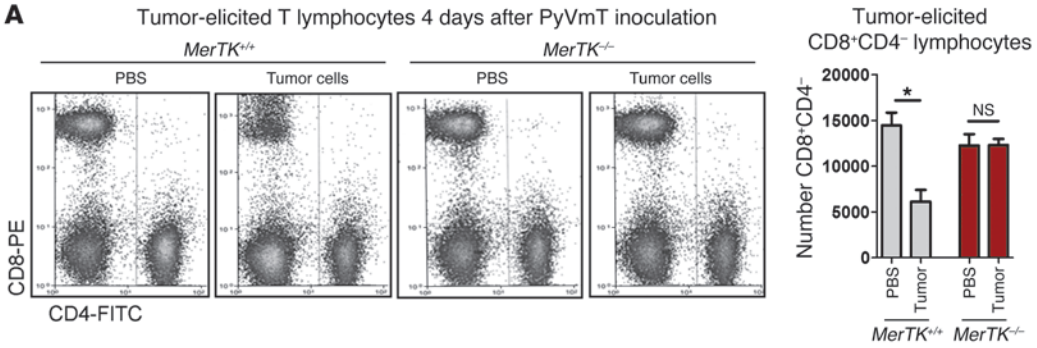

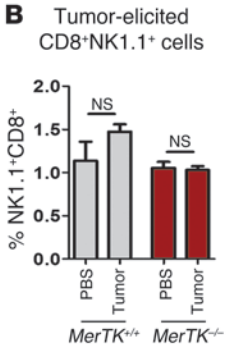

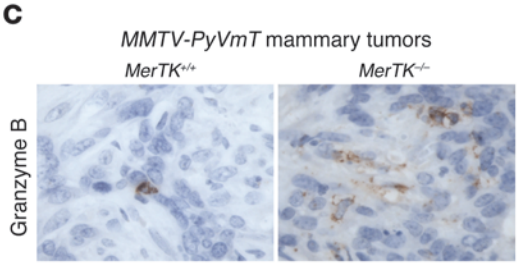

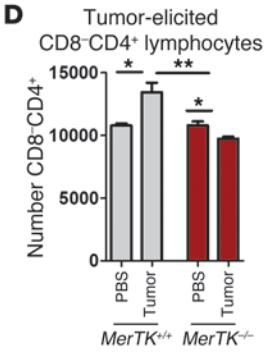

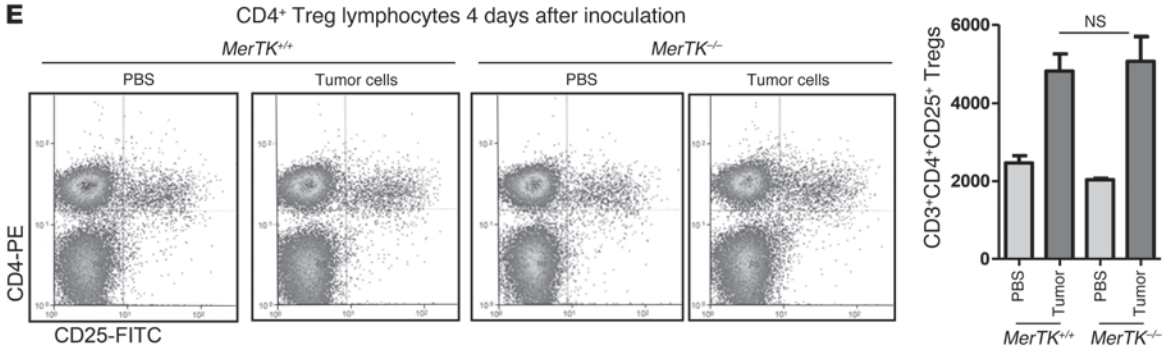

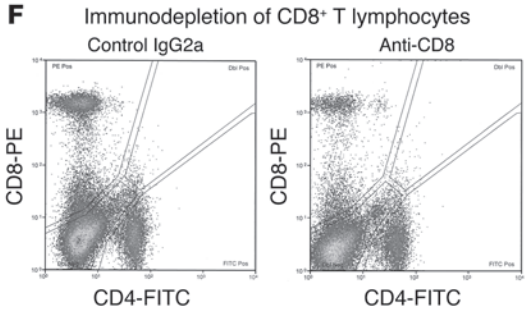

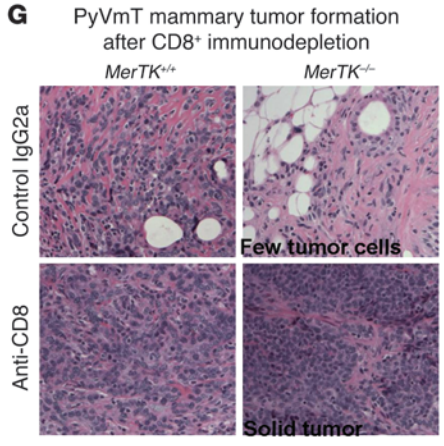

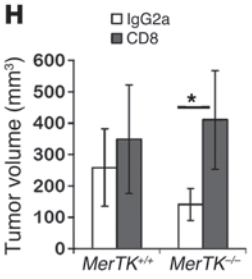

Figure 5
Increased presence of CD8+ T lymphocytes in *MerTK*$^{-/-}$ microenvironment is required for inhibition of tumor growth. (**A** and **B**) Flow cytometric analysis of CD8/CD4– and NK1.1+CD8+–stained mammary gland suspensions 4 days after *MMTV-PyVmT* or PBS injection, with quantification (n = 6). (**C**) Immunohistochemistry for granzyme B. Original magnification, ×600. (**D** and **E**) Flow cytometry and quantitation of (**D**) CD8–CD4+ and (**E**) CD25+CD4+ cells in mammary gland suspensions collected 4 days after intramammary injection of tumor cells or PBS. (**F**–**H**) *MMTV-PyVmT* tumor cells were injected into mammary fat pads of anti-CD8 antibody–treated mice. Mammary glands/tumors were collected after 28 days for analysis. (**F**) CD8/CD4–stained tumor suspensions were assessed by flow cytometry. (**G**) Representative histological sections are shown. Original magnification, ×200. (**H**) Average *MMTV-PyVmT* tumor volume at 28 days after inoculation is shown ± SD (n = 8). P values were calculated using Student's t test. *P < 0.05; **P < 0.01.

mice but a slight decrease in *MerTK*$^{-/-}$ mice (Figure 5D). We further examined this population for expression of CD25 to identify Tregs. Similar basal levels of CD4+CD25+ cells were identified 4 days after PBS injection into *MerTK*$^{+/+}$ and *MerTK*$^{-/-}$ mice (Figure 5E). Although levels of CD4+CD25+ cells increased in response to tumors, the increase was similar in *MerTK*$^{+/+}$ and *MerTK*$^{-/-}$ mice.

Depletion of CD8+ T lymphocytes restores tumor growth in MerTK$^{-/-}$ *mice*. CD8+ T lymphocytes were depleted from *MerTK*$^{+/+}$ and *MerTK*$^{-/-}$ mice using antibodies against CD8. Mice were pretreated with anti-CD8 for 1 week prior to *MMTV-PyVmT* tumor inoculation into mammary fat pads, and antibody treatment was maintained for 3 weeks following tumor inoculation. Tumor cell suspensions were stained with antibodies against CD4 and CD8, revealing decreased presence of CD8+CD4– cells in the tumor microenvironment of mice treated with anti-CD8 antibody, as compared with those treated with isotype-matched antibody control (Figure 5F). Histological examination revealed that, while *MerTK*$^{-/-}$ mice treated with the isotype control antibody developed small tumors comprising primarily matrix and stromal cells (Figure 5G), *MerTK*$^{-/-}$ mice treated with anti-CD8 antibodies developed larger, more aggressive tumors, with densely packed tumor epithelial cells, closely resembling the histological appearance of tumors grown in *MerTK*$^{+/+}$ mice (Figure 5G). Tumors grown in *MerTK*$^{-/-}$ mice were nearly 3-fold larger upon CD8 depletion as compared with those grown in IgG2a-treated *MerTK*$^{-/-}$ mice (Figure 5H). These data suggest that, in the *MerTK*$^{-/-}$ tumor microenvironment, CD8+ T lymphocytes are, at least in part, responsible for decreased tumor mass.

Discussion

The stromal microenvironment in which a tumor exists greatly influences its pathophysiology. Specifically, tumor-associated macrophages in human and mouse tumors have been correlated with poor prognosis and increased malignant progression. This was illustrated by studies in which targeted inhibition of CSF1 receptor signaling in tumor-associated macrophages, through gene targeting or through antibody-based pharmacologic strategies, decreased tumor growth and metastasis in mice (37, 38, 41, 48, 49). Therefore, tumor macrophages are valid therapeutic targets. Macrophages and DCs can produce the cytokines and growth factors that encourage tumor progression and metastasis, such as IL-10, which dampen antitumor immune responses (40). We demonstrate here that the *MerTK*$^{+/+}$ microenvironment responds very rapidly after tumor cell implantation by increasing production of IL-10 and GAS6 and decreasing production of IL-12. These cytokine changes are correlated with a decreased local presence of CD8+ T lymphocytes in the tumor. IL-10 and GAS6 induction in the tumor microenvironment required MerTK, as tumor-induced IL-10 and GAS6 expression was not observed in *MerTK*-deficient mice. This is consistent with previous data suggesting that MerTK is required in the innate immune system to induce IL-10 following efferocytosis and TLR activation (3, 4, 21, 50, 51). We also showed that *MerTK*-deficient cells in the tumor microenvironment express increased IL-12 and IL-6, proinflammatory cytokines known to be repressed by MerTK signaling in response to efferocytosis or TLR activation (4, 32).

Our results demonstrating upregulation of GAS6 in the tumor microenvironment of *MerTK*$^{+/+}$ mice are consistent with a previously published study, demonstrating GAS6 expression in tumor macrophages and showing that genetic loss of *Gas6* in the microenvironment of syngeneic tumor transplants decreases tumor growth (46). In these studies, GAS6 was not required for tumor infiltration by macrophages; this is consistent with our finding that tumor-associated macrophage numbers are not altered by loss of MerTK. MerTK was needed for full induction of GAS6 in the tumor microenvironment, supporting a model in which MerTK signaling induces GAS6 expression in tumor macrophages, creating positive feed-forward signaling through MerTK. Sustained MerTK signaling would maintain the repression of proinflammatory cytokines and induce wound healing/tolerogenic cytokines, ultimately resulting in decreased antitumor immunity. In the PyVmT models, we have demonstrated that the GAS6 receptors MerTK, AXL and TYRO3 are absent and, thus, the production or lack of production of GAS6 is irrelevant to the tumor cell per se.

Several studies using genetic disruption of MerTK, AXL, and TYRO3 in mice demonstrated that the innate immune system responds to pathogen-mimicking agents (TLR activation) with an early increase in IL-12, IL-6, and type I IFN production, followed by MerTK-, AXL-, and TYRO3-dependent reduction of proinflammatory cytokine expression, and finally with induction of wound healing and tolerogenic cytokines (IL-10, TGF-β) (3, 4, 21, 50, 51). In the absence of these receptors, the innate immune system is unable to dampen expression of proinflammatory cytokines and unable to induce production of tolerogenic cytokines. Similarly, we found that early responses of the innate immune system in the *MerTK*$^{+/+}$ tumor microenvironment were characterized by dampened levels of IL-12 and increased levels of IL-10. However, loss of MerTK from the tumor microenvironment caused sustained IL-12 induction (for up to 14 weeks), without induction of IL-10. Therefore, it is possible that the innate immune system uses MerTK signaling in the tumor microenvironment in a way that parallels MerTK function in wounding responses.

Alternatively, MerTK in the tumor microenvironment may respond to efferocytosis. Apoptosis occurs in all tissues, and generally apoptosis rates are higher in rapidly proliferating tumors as compared with quiescent tissues. One major physiological role of MerTK is to clear apoptotic material through efferocytosis (23). To ensure that presentation of self-antigens does not stimulate autoimmunity following efferocytosis, macrophages suppress IL-12 production upon efferocytosis and induce IL-10 production (47). This limits CD8+ T lymphocyte expansion and reduces antigen presentation. It is possible that macrophage-mediated efferocytosis of apoptotic tumor cells drives the cytokine expression patterns that characterize tumor-associated macrophages. This scenario,

while not proven, would predict that modulating the consequence of chronic efferocytosis, through targeted inhibition of MerTK, would increase IL-12 levels, decrease IL-10 levels, increase tumor $CD8^+$ T lymphocytes, and decrease malignant progression. However, this hypothesis remains to be tested, requiring a systematic evaluation of efferocytosis in the tumor microenvironment. We did not observe major differences in apoptotic material in the microenvironment of *MerTK*$^{+/+}$ and *MerTK*$^{-/-}$ mice in late-stage tumors (Supplemental Figure 1). However, dramatic differences in apoptotic cell numbers are only seen in acute challenges in *MerTK*$^{-/-}$ mice (23). Other macrophage receptors eventually clear apoptotic material, but these alternative clearance mechanisms do not suppress the inflammatory response to the extent that MerTK does. This conclusion is substantiated by the autoimmune phenotype seen in the *MerTK*$^{-/-}$ mice.

IL-12 stimulates antitumor immunity in several models of epithelial tumors in part by promoting $CD8^+$ T lymphocyte expansion (43). Because MerTK suppresses IL-12 production in the tumor microenvironment, MerTK signaling may suppress antitumor immunity through suppression of $CD8^+$ T lymphocyte proliferation. Consistent with this idea, we found that depletion of $CD8^+$ T lymphocytes restored tumor growth in the *MerTK*-deficient tumor microenvironment. In the case of AXL/TYRO3/MerTK triple-deficient mice, sustained IL-12 levels in normal tissues correlated with increased presence of $CD8^+$ T lymphocytes and induction of adaptive immunity against self-antigens (21). While this response would be undesirable in normal tissues, immunity against tumor-specific antigens may improve the outcome of patients with cancer. This is supported by increasing evidence gained by expression microarrays that correlates tumors bearing a Th1 (e.g., IL-6, IL-12, CD8, granzyme B) gene expression signature with an improved outcome over tumors bearing a Th2 (e.g., IL-10, TGF-β, IL-4, cathepsin, IL-13, CD4) signature (38, 52, 53). Recent work has shown that tumors can orchestrate the immune response in a manner advantageous for tumor growth, metastasis, and escape from immune surveillance (54). The present data suggest that inhibition of MerTK signaling may be a promising therapeutic intervention that can break the deleterious immune suppression cycle by directly targeting the tumor-associated innate immune system. This could shift the immune response toward a more favorable antitumor one. MerTK inhibition that would set the stage for an antitumor Th1 response combined with new clinical agents designed to prolong antitumor T cell action may well provide an additive antitumor effect.

Methods

Mice. All mice regardless of genotype were inbred to C57BL/6 for at least 10 generations. *MerTK*$^{-/-}$ mice, originally referred to as *Mer*^{KD} mice, have been previously described (30).To generate *MerTK*$^{+/+}$ and *MerTK*$^{-/-}$ siblings, *MerTK*$^{+/-}$ males and females were mated to generate the expected Mendelian ratios of offspring, which were genotyped using the following primers: forward 5′-GAATTTACCTTTCACAGGTTGCGG; reverse 5′-TCGTCAAGAAGGCGATAGAAGGCG. Mice were maintained in American Association for Accreditation of Laboratory Animal Care–approved animal facilities at the University of North Carolina under an approved IACUC protocol. Where indicated, mice were treated with BrdU (10 mg/kg in sterile PBS) by i.p. injection 1 hour prior to tissue collection.

Transplantation of tumor cells. Primary mammary tumor cells were derived from a female *MMTV-PyVmT* mouse inbred to C57BL/6 for 6 generations as previously described (54). B16:F10 cells were obtained from American Type Tissue Culture Collection. For orthotopic injections into the mammary fat pads, 10^6 *MMTV-PyVmT* cells were resuspended in 100 μl sterile PBS (in the presence or absence of 0.5×10^6 mouse mammary fibroblasts harvested from 6-week-old virgin *MerTK*$^{+/+}$ or *MerTK*$^{-/-}$ female C57BL/6 mice) and injected centrally in the right no. 4 inguinal fat pad of 6-week-old virgin mice. For orthotopic injections into the dermis, 10^3 B16:F10 melanoma cells were resuspended in 100 μl PBS and injected intradermally between the scapulae of 6-week-old mice. For subcutaneous injection, 1×10^4 MC38 colon cancer cells were injected into the flank. Tumors were detected by manual palpation. Statistical analysis of average tumor latency was assessed by log-rank test. Where indicated, i.p. injection of 3×10^3 B16:F10 cells was performed in 100 μl PBS, and cells were collected in MEM by peritoneal lavage after 4 days.

Histological analysis and immunohistochemistry. Tumors and mammary glands were harvested and immediately fixed in 10% formalin (VWR Scientific). Paraffin-embedded tumors and mammary glands were sectioned (5 μm), rehydrated, and peroxidase-quenched with 3% H_2O_2. Rehydrated slides were stained with H&E by the UNC Lineberger Animal Histopathology Core Facility. Immunohistochemistry was performed as previously described (55, 56) using the following polyclonal antibodies: F4/80 (6A545, Santa Cruz Biotechnology Inc.; diluted 1:200), MerTK (produced by the Earp laboratory) against a peptide in the intracellular domain of human MerTK; diluted 1:100), pan-cytokeratin (H240, Santa Cruz Biotechnology Inc.; diluted 1:500), and granzyme B (Santa Cruz Biotechnology Inc.; diluted 1:200). Slides were washed in PBST and then incubated in biotinylated anti-rabbit or anti-rat antibody (Vector Laboratories) and developed using the Vectastain Kit (Vector Laboratories). Sections were photographed using the Zeiss LCM 210 microscope and Scion Image 2.0 software.

Western blot analysis. *MMTV-PyVmT* tumor cells were lysed in lysis buffer (50 mM HEPES, pH 7.5, 150 mM NaCl, 10 mM EDTA, 10% glycerol, and 1% Triton X-100) supplemented with phosphatase inhibitors (1 mM Na_3VO_4 and 0.1 mM Na_2MoO_4) and protease inhibitors (Complete Mini, Roche Applied Science). Whole spleen lysates harvested from *MerTK*$^{+/+}$ and *MerTK*$^{-/-}$ mice and whole brain lysates harvested from *Tyro3*$^{+/+}$ and *Tyro3*$^{-/-}$ mice were prepared in sodium chloride–Tris-EDTA buffer and sonicated. Whole protein lysates were separated on 8% Tris-glycine SDS-PAGE gels (Life Technologies) and then transferred to nitrocellulose membranes (iBlot, Life Technologies). Membranes were probed with primary antibodies: anti-mouse MerTK (AF591, R&D Systems; diluted 1:2,000), anti-mouse AXL (AF854, R&D Systems; diluted 1:1,000), and anti-TYRO3 rabbit sera (produced by the Prieto laboratory; diluted 1:20,000)

Bone marrow transplantation. Six-week-old female *MMTV-PyVmT* mice were lethally irradiated with 9.5 Gy split over 2 doses. 1×10^6 bone marrow cells from *C57BL/6-Tg(UBC-GFP)30Scha/J* (The Jackson Laboratory) *MerTK*$^{+/+}$ or *MerTK*$^{-/-}$ donors were delivered to irradiated mice by tail vein injection. After 4 weeks, recipient mice that expressed ≥75% GFP in peripheral blood indicated successful engraftment and were included for further analysis. Animals were housed and experimental procedures were done in accordance with the regulatory standards approved by the University of Colorado, Anschutz Medical Campus' IACUC.

Tumor measurement by MRI. Mammary gland tumor growth was measured over time by MRI. Mice were anesthetized with 1.5% to 2.5% inhaled isoflurane and were placed in the 4.7 Tesla Bruker MRI/MRS PharmaScan. Gadolinium-DTPA bismethylamide (gadodiamide, OMNISCAN) was administered intravenously as a contrast agent. Axial plane images of the animals were obtained using conventional T1-, T2-, and proton density–weighted MRI. Additional fast imaging with steady-state precession (FISP) images were required in order to exclude cysts from the tumor volume calculations, and all images were processed using Bruker ParaVision software. The total tumor volume of each tumor was calculated from the resulting images by multiplying the pixel volume by the number of pixels within

the tumor area by hand-tracing the ROI with "track" command from each set of slices. All MRI acquisitions and data analysis were performed at the University of Colorado Cancer Center Animal Imaging Core.

qRT-PCR. Total RNA was isolated using RNeasy (Qiagen) from single mammary cell suspensions and from peritoneal lavage collections. Total RNA (10 ng) was reverse transcribed with transcript-specific primers and then amplified with transcript-specific primers using SyBR Green (Invitrogen), according to manufacturer's instructions, with a temperature of 62°C. The following primers and probes were used. *Gas6*, 5′-TCTTCTCACACTGTGCTGTTGCG and 5′-GGTCAGGCAAGTTCTGAACACAT; mouse *Il12p40*, 5′-TTATGTTGTAGAGGTGGACTGG and 5′-TTTCTTTGCACCAGCCATGAGC; mouse *Il10*, 5′-TGGCCCAGAAATCAAGGAGC and 5′-CAGCAGACTCAATACACACT; mouse *Mfge8*, forward: 5′-GGGCCTGAAGAATAACACGA and 5′-AGGGCAACTTGGACAACAAC; and mouse *Gapdh*, 5′-AACGACCCCTTCATTGAC-3′ and 5′-TCCACGACATACTCAGCAC. The CT for each transcript within each sample was corrected for the CT of *Gapdh* within each sample, normalized to the CT of a single sample, and converted into relative levels of expression using the δδCT method, such that all values are presented as a fold change in reference to a single sample. Samples were analyzed 6 times.

ELISA. Serum was collected by cardiac puncture and immediately stored in frozen aliquots. Neat serum was analyzed by ELISA for mouse IL-12p70 (R&D Systems) and IL-6 (R&D Systems) according to manufacturer's directions. Standard curves generated using manufacturer-supplied IL-12 and IL-6 were used to calculate serum concentrations of each protein.

Flow cytometry. Single cell suspensions of tumors or mammary glands were generated by mechanical tissue disruption using razor blades followed by 30 minutes in 1 mg/ml collagenase A (Sigma-Aldrich) in DMEM, 10 minutes in 1 mg/ml dispase (BD Biosciences), 2 minutes in 0.25% trypsin (BD Biosciences), and 5 minutes in DNase I (Stem Cell Technologies). Single cell splenocyte suspensions were generated by forcing spleens through 70-μ and 40-μ mesh filters. Cells (1.5×10^6) were blocked with mouse Fcγ III/II Receptor Block (BD Biosciences) for 10 minutes prior to 30-minute incubation at room temperature with the following fluorescence-conjugated BD Pharmingen antibodies (BD Biosciences) diluted 1:200: rat anti-mouse Thy1 (53-2.1), rat anti-mouse CD8 (53-6.7), rat anti-mouse CD4 (GK1.5), rat anti-mouse CD3 (500A2), rat anti-mouse CD45 (30F11), rat anti-mouse CD11b (M1/70), hamster anti-mouse CD11c (HL3), and mouse IgG2a anti-mouse NK1.1 (PK136). Alternatively, splenocytes were fixed and permeabilized (BD Cytofix/Cytoperm, BD Biosciences), DNA was denatured using 1 M HCl for 15 minutes, and cells were stained with FITC-conjugated anti-BrdU antibody (1:100, BD Biosciences) for 1 hour. Cells were washed and counterstained with propidium iodide. Cells were analyzed at the UNC Flow Cytometry Core Facility on a Cytek-modified 5-color FACSCalibur using hardware single-color compensation.

Tumor-associated macrophage isolation. $CD11b^+$ tumor-associated macrophages were isolated from freshly digested (serum-free DMEM with 0.1% Collagenase I [Sigma-Aldrich] and DNaseI [EMD Millipore] at 37°C for 45 minutes) single cell suspensions, which were enriched using CD11b magnetic beads (Miltenyi Biotec) and MS Columns (Miltenyi Biotec) according to the manufacturer's directions.

Cytokine array. Whole cell lysates were prepared in lysis buffer (50 mM HEPES, pH 7.5, 150 mM NaCl, 10 mM EDTA, 10% glycerol, and 1% Triton X-100) supplemented with phosphatase inhibitors (1 mM Na_3VO_4 and 0.1 mM Na_2MoO_4) and protease inhibitors (Complete Mini, Roche Applied Science). Relative protein expression was analyzed on custom cytokine arrays, using 100 μg lysates according to the manufacturer's instructions (RayBiotech). The cytokine membranes were quantified by densitometric analysis using ImageJ 1.44o (NIH) with the MicroArray Profile plug-in (OptiNav).

Antibody-mediated immune-depletion of $CD8^+$ cells. Mice were treated by i.p. injection of anti-mouse CD8 antibody (clone 53.6.7, BioXCell) at 2.5 mg/kg in sterile PBS twice weekly for 2 weeks prior to inoculation with *MMTV-PyVmT* tumor cells and afterward for an additional 4 weeks.

In situ identification of TUNEL-positive cells and macrophage-programming markers. Immunofluorescent in situ staining of apoptotic cells in paraffin-embedded tumors and mammary glands was done using the Dead End Fluorometric TUNEL system (Promega). Sections were subsequently stained with anti–F4/80-PE (Serotec; diluted 1:100) and DAPI. Triple staining to identify macrophage-programming status was performed using antibodies against F4/80-PE (Serotec; diluted 1:100), iNOS-FITC (BD Biosciences; diluted 1:100), and Arginase I-AMCA (Santa Cruz Biotechnology Inc.; 1:100) as previously described (57). Images were acquired on a Zeiss Axioplan 2 epifluorescent microscope.

Statistics. Data represent the mean ± SEM of all experiments, unless otherwise noted. Statistical significance was calculated by Mantel-Cox test (tumor latency), Student's *t* test, Student's *t* test with Welch's correction for unequal variance (tumor weight, tumor volume), or analysis of variance using Prism 5 (GraphPad Software) unless otherwise noted.

Study approval. All studies involving mice were performed with approval from the IACUCs of the University of North Carolina, Chapel Hill, North Carolina, USA, or the University of Colorado, Anschutz Medical Campus.

Acknowledgments

This work was supported by the Breast Cancer Research Foundation (to H.S. Earp III), the UNC Breast Cancer SPORE P50 CA058223 (to H.S. Earp III), NIH R01 CA143126 (to R.S. Cook), VICC Breast Cancer SPORE P50 CA98131, and Susan G. Komen for the Cure KG100677 (to R.S. Cook). The Animal Imaging Core at University of Colorado is supported by the following grants: NCI Cancer Center P30 CA046934; NCRR CTSA UL1 RR025780. The authors thank Kendra Huber (RT MRI/CT) for her help with all MRI studies and data analysis.

Received for publication November 8, 2012, and accepted in revised form May 10, 2013.

Address correspondence to: H. Shelton Earp III, UNC Lineberger Comprehensive Cancer Center, University of North Carolina Chapel Hill, 450 West Avenue, CB 7295, 1st Floor Administration Office, Chapel Hill, North Carolina 27599, USA. Phone: 919.966.2335; Fax: 919.966.3015; E-mail: hse@med.unc.edu.

1. Linger RM, Keating AK, Earp HS, Graham DK. Taking aim at Mer and Axl receptor tyrosine kinases as novel therapeutic targets in solid tumors. *Expert Opin Ther Targets*. 2010;14(10):1073–1090.
2. Linger RM, Keating AK, Earp HS, Graham DK. TAM receptor tyrosine kinases: biologic functions, signaling, and potential therapeutic targeting in human cancer. *Adv Cancer Res*. 2008;100:35–83.
3. Lemke G, Rothlin CV. Immunobiology of the TAM receptors. *Nat Rev Immunol*. 2008;8(5):327–336.
4. Rothlin CV, Lemke G. TAM receptor signaling and autoimmune disease. *Curr Opin Immunol*. 2010; 22(6):740–746.
5. Brown J, Krodel M, Pazos M, Lai C, Prieto A. Cross-phosphorylation, signaling and proliferative functions of the Tyro-3 and Axl receptors in Rat2 cells. *PLoS One*. 2012;7(5):e36800.
6. Graham DK, Dawson TL, Mullaney DL, Snodgrass HR, Earp HS. Cloning and mRNA expression analysis of a novel human protooncogene, c-mer. *Cell Growth Differ*. 1994;5(6):647–657.
7. Nagata K, et al. Identification of the product of growth arrest-specific gene 6 as a common ligand for Axl, Sky, and Mer receptor tyrosine kinases. *J Biol Chem*. 1996;271(47):30022–30027.
8. Varnum B, et al. Axl receptor tyrosine kinase stimulated by the vitamin K-dependent protein encoded by growth-arrest-specific gene 6. *Nature*. 1995;373(6515):623–626.
9. Hafizi S, Dahlback B. Gas6 and protein S. Vitamin K-

dependent ligands for the Axl receptor tyrosine kinase subfamily. *FEBS J*. 2006;273(23):5231–5244.
10. Stitt TN, et al. The anticoagulation factor protein S and its relative, Gas6, are ligands for the Tyro 3/Axl family of receptor tyrosine kinases. *Cell*. 1995; 80(4):661–670.
11. Caberoy NB, Zhou Y, Li W. Tubby and tubby-like protein 1 are new MerTK ligands for phagocytosis. *EMBO J*. 2010;29(23):3898–3910.
12. Caberoy NB, Alvarado G, Bigcas J, Li W. Galectin-3 is a new MerTK-specific eat-me signal. *J Cell Physiology*. 2011;227(2):401–407.
13. Wang Y, et al. Mer receptor tyrosine kinase promotes invasion and survival in glioblastoma multiforme. *Oncogene*. 2013;32(7):872–882.
14. Png KJ, Halberg N, Yoshida M, Tavazoie SF. A microRNA regulon that mediates endothelial recruitment and metastasis by cancer cells. *Nature*. 2012; 481(7380):190–194.
15. Jansen FH, et al. Profiling of antibody production against xenograft-released proteins by protein microarrays discovers prostate cancer markers. *J Proteome Res*. 2012;11(2):728–735.
16. Tworkoski K, et al. Phosphoproteomic screen identifies potential therapeutic targets in melanoma. *Mol Cancer Res*. 2011;9(6):801–812.
17. Keating AK, et al. Inhibition of Mer and Axl receptor tyrosine kinases in astrocytoma cells leads to increased apoptosis and improved chemosensitivity. *Mol Cancer Ther*. 2010;9(5):1298–1307.
18. Graham DK, et al. Ectopic expression of the proto-oncogene Mer in pediatric T-cell acute lymphoblastic leukemia. *Clin Cancer Res*. 2006;12(9):2662–2669.
19. Keating AK, et al. Lymphoblastic leukemia/lymphoma in mice overexpressing the Mer (MerTK) receptor tyrosine kinase. *Oncogene*. 2006;25(45):6092–6100.
20. Behrens EM, Gadue P, Gong SY, Garrett S, Stein PL, Cohen PL. The mer receptor tyrosine kinase: expression and function suggest a role in innate immunity. *Eur J Immunol*. 2003;33(8):2160–2167.
21. Rothlin CV, Ghosh S, Zuniga EI, Oldstone MB, Lemke G. TAM receptors are pleiotropic inhibitors of the innate immune response. *Cell*. 2007; 131(6):1124–1136.
22. Fadok VA, Voelker DR, Campbell PA, Cohen JJ, Bratton DL, Henson PM. Exposure of phosphatidylserine on the surface of apoptotic lymphocytes triggers specific recognition and removal by macrophages. *J Immunol*. 1992;148(7):2207–2216.
23. Scott RS, et al. Phagocytosis and clearance of apoptotic cells is mediated by MER. *Nature*. 2001; 411(6834):207–211.
24. Seitz HM, Camenisch TD, Lemke G, Earp HS, Matsushima GK. Macrophages and dendritic cells use different Axl/Mertk/Tyro3 receptors in clearance of apoptotic cells. *J Immunol*. 2007;178(9):5635–5642.
25. Tibrewal N, et al. Autophosphorylation docking site Tyr-867 in Mer receptor tyrosine kinase allows for dissociation of multiple signaling pathways for phagocytosis of apoptotic cells and down-modulation of lipopolysaccharide-inducible NF-kappaB transcriptional activation. *J Biol Chem*. 2008;283(6):3618–3627.
26. Filardy AA, et al. Proinflammatory clearance of apoptotic neutrophils induces an IL-12(low) IL-10(high) regulatory phenotype in macrophages. *J Immunol*. 2010;185(4):2044–2050.
27. Gal A, et al. Mutations in MERTK, the human orthologue of the RCS rat retinal dystrophy gene, cause retinitis pigmentosa. *Nat Genet*. 2000;26(3):270–271.
28. Sandahl M, Hunter DM, Strunk KE, Earp HS, Cook RS. Epithelial cell-directed efferocytosis in the post-partum mammary gland is necessary for tissue homeostasis and future lactation. *BMC Dev Biol*. 2010;10:122.
29. Cohen PL, et al. Delayed apoptotic cell clearance and lupus-like autoimmunity in mice lacking the c-mer membrane tyrosine kinase. *J Exp Med*. 2002; 196(1):135–140.
30. Camenisch TD, Koller BH, Earp HS, Matsushima GK. A novel receptor tyrosine kinase, Mer, inhibits TNF-alpha production and lipopolysaccharide-induced endotoxic shock. *J Immunol*. 1999;162(6):3498–3503.
31. Shao WH, Eisenberg RA, Cohen PL. The Mer receptor tyrosine kinase is required for the loss of B cell tolerance in the chronic graft-versus-host disease model of systemic lupus erythematosus. *J Immunol*. 2008;180(11):7728–7735.
32. Shao WH, et al. Disrupted Mer receptor tyrosine kinase expression leads to enhanced MZ B-cell responses. *J Autoimmun*. 2010;35(4):368–374.
33. Lu Q, et al. Tyro-3 family receptors are essential regulators of mammalian spermatogenesis. *Nature*. 1999;398(6729):723–728.
34. Pollard JW. Tumour-educated macrophages promote tumour progression and metastasis. *Nat Rev Cancer*. 2004;4(1):71–78.
35. Pollard JW. Trophic macrophages in development and disease. *Nat Rev Immunol*. 2009;9(4):259–270.
36. Ruffell B, Affara NI, Coussens LM. Differential macrophage programming in the tumor microenvironment. *Trends Immunol*. 2012;33(3):119–126.
37. Lin EY, Nguyen AV, Russell RG, Pollard JW. Colony-stimulating factor 1 promotes progression of mammary tumors to malignancy. *J Exp Med*. 2001; 193(6):727–740.
38. Denardo DG, et al. Leukocyte complexity predicts breast cancer survival and functionally regulates response to chemotherapy. *Cancer Discov*. 2011; 1(1):54–67.
39. Wyckoff J, et al. A paracrine loop between tumor cells and macrophages is required for tumor cell migration in mammary tumors. *Cancer Res*. 2004; 64(19):7022–7029.
40. Qian B, et al. A distinct macrophage population mediates metastatic breast cancer cell extravasation, establishment and growth. *PLoS One*. 2009;4(8):e6562.
41. Qian BZ, Pollard JW. Macrophage diversity enhances tumor progression and metastasis. *Cell*. 2010; 141(1):39–51.
42. Grivennikov SI, Greten FR, Karin M. Immunity, inflammation, and cancer. *Cell*. 2010;140(6):883–899.
43. Trinchieri G. Interleukin-12 and the regulation of innate resistance and adaptive immunity. *Nat Rev Immunol*. 2003;3(2):133–146.
44. Guy CT, Cardiff RD, Muller WJ. Induction of mammary tumors by expression of polyomavirus middle T oncogene: a transgenic mouse model for metastatic disease. *Mol Cell Biol*. 1992;12(3):954–961.
45. Kidd S, et al. Origins of the tumor microenvironment: quantitative assessment of adipose-derived and bone marrow-derived stroma. *PLoS One*. 2012; 7(2):e30563.
46. Loges S, et al. Malignant cells fuel tumor growth by educating infiltrating leukocytes to produce the mitogen Gas6. *Blood*. 2010;115(11):2264–2273.
47. Friggeri A, Yang Y, Banerjee S, Park YJ, Liu G, Abraham E. HMGB1 inhibits macrophage activity in efferocytosis through binding to the alphavbeta3-integrin. *Am J Physiol Cell Physiol*. 2010; 299(6):C1267–C1276.
48. Nowicki A, et al. Impaired tumor growth in colony-stimulating factor 1 (CSF-1)-deficient, macrophage-deficient op/op mouse: evidence for a role of CSF-1-dependent macrophages in formation of tumor stroma. *Int J Cancer*. 1996;65(1):112–119.
49. O'Brien J, et al. Alternatively activated macrophages and collagen remodeling characterize the postpartum involuting mammary gland across species. *Am J Pathol*. 2010;176(3):1241–1255.
50. Lemke G, Lu Q. Macrophage regulation by Tyro 3 family receptors. *Curr Opin Immunol*. 2003; 15(1):31–36.
51. Lu Q, Lemke G. Homeostatic regulation of the immune system by receptor tyrosine kinases of the Tyro 3 family. *Science*. 2001;293(5528):306–311.
52. Kristensen VN, et al. Integrated molecular profiles of invasive breast tumors and ductal carcinoma in situ (DCIS) reveal differential vascular and interleukin signaling. *Proc Natl Acad Sci U S A*. 2012; 109(8):2802–2807.
53. Teschendorff AE, et al. Improved prognostic classification of breast cancer defined by antagonistic activation patterns of immune response pathway modules. *BMC Cancer*. 2010;10:604.
54. Coussens L, Zitvogel L, Palucka K. Neutralizing tumor-promoting chronic inflammation: a magic bullet? *Science*. 2013;339(6117):286–291.
55. Cook RS, et al. ErbB3 ablation impairs PI3K/Akt-dependent mammary tumorigenesis. *Cancer Res*. 2011;71(11):3941–3951.
56. Balko JM, et al. The receptor tyrosine kinase ErbB3 maintains the balance between luminal and basal breast epithelium. *Proc Natl Acad Sci U S A*. 2012;109(1):221–226.
57. Redente EF, Orlicky DJ, Bouchard RJ, Malkinson AM. Tumor signaling to the bone marrow changes the phenotype of monocytes and pulmonary macrophages during urethane-induced primary lung tumorigenesis in A/J mice. *Am J Pathol*. 2007; 170(2):693–708.

Appendix 2.

Efferocytosis produces a prometastatic landscape during postpartum mammary gland involution.

Stanford JC, Young C, Hicks D, Owens P, Williams A, Vaught DB, Morrison MM, Lim J, Williams M, Brantley-Sieders DM, Balko JM, Tonetti D, Earp HS 3rd, ***Cook RS***.

J Clin Invest. 2014 Nov;124(11):4737-52.

Efferocytosis produces a prometastatic landscape during postpartum mammary gland involution

Jamie C. Stanford,[1] Christian Young,[2] Donna Hicks,[1] Philip Owens,[1] Andrew Williams,[1] David B. Vaught,[1] Meghan M. Morrison,[1] Jiyeon Lim,[1] Michelle Williams,[1] Dana M. Brantley-Sieders,[2] Justin M. Balko,[2] Debra Tonetti,[3] H. Shelton Earp III,[4] and Rebecca S. Cook[1,5]

[1]Department of Cancer Biology and [2]Department of Medicine, Vanderbilt University School of Medicine, Nashville, Tennessee, USA. [3]University of Illinois, Chicago, Illinois, USA. [4]Department of Biomedical Sciences, UNC-Lineberger Comprehensive Cancer Center, University of North Carolina, Chapel Hill, North Carolina, USA. [5]Vanderbilt Ingram Cancer Center, Nashville, Tennessee, USA.

Breast cancers that occur in women 2–5 years postpartum are more frequently diagnosed at metastatic stages and correlate with poorer outcomes compared with breast cancers diagnosed in young, premenopausal women. The molecular mechanisms underlying the malignant severity associated with postpartum breast cancers (ppBCs) are unclear but relate to stromal wound-healing events during postpartum involution, a dynamic process characterized by widespread cell death in milk-producing mammary epithelial cells (MECs). Using both spontaneous and allografted mammary tumors in fully immune–competent mice, we discovered that postpartum involution increases mammary tumor metastasis. Cell death was widespread, not only occurring in MECs but also in tumor epithelium. Dying tumor cells were cleared through receptor tyrosine kinase MerTK–dependent efferocytosis, which robustly induced the transcription of genes encoding wound-healing cytokines, including IL-4, IL-10, IL-13, and TGF-β. Animals lacking MerTK and animals treated with a MerTK inhibitor exhibited impaired efferocytosis in postpartum tumors, a reduction of M2-like macrophages but no change in total macrophage levels, decreased TGF-β expression, and a reduction of postpartum tumor metastasis that was similar to the metastasis frequencies observed in nulliparous mice. Moreover, TGF-β blockade reduced postpartum tumor metastasis. These data suggest that widespread cell death during postpartum involution triggers efferocytosis-induced wound-healing cytokines in the tumor microenvironment that promote metastatic tumor progression.

Introduction

Although pregnancy at a young age decreases a woman's lifetime breast cancer risk (1, 2), the first 5 years following a pregnancy at any age are associated with increased breast cancer risk, a risk that continues to increase with age (3–6). Given the societal trends in Western cultures of postponing childbirth later into women's lives, the incidence of malignant postpartum breast cancer is expected to increase. Currently, breast cancers diagnosed 2–5 years postpartum account for nearly 25% of all premenopausal breast cancers (7). Importantly, breast cancers diagnosed 2–5 years postpartum are diagnosed more frequently as metastatic disease and correlate with decreased disease-free survival (DFS) versus breast cancers occurring in premenopausal nulliparous women (4, 7, 8). In contrast, many studies have shown that breast cancers diagnosed during pregnancy do not correlate with decreased DFS (8, 9), although there remains some debate about this conclusion. The observation that postpartum breast cancers (ppBCs) correlate with reduced DFS suggests that events occurring in the postpartum breast augment the malignant severity of tumors existing therein. This hypothesis is supported by studies in which breast cancer cells transplanted into involuting mouse mammary fat pads grow and invade more rapidly than do cells transplanted into mammary glands of nulliparous mice (10–12). This postpartum transplantation model elegantly distinguished the microenvironmental influences of the involuting postpartum mammary gland versus the mammary gland at other reproductive stages (3, 10–15). Thus, it is imperative to understand how the changing landscape of the postpartum breast accelerates cancer progression in order to design more effective therapies for patients suffering from ppBC or strategies to limit the alterations leading to ppBCs.

M2-like macrophages are a critical driving force of malignancy in the postpartum mammary microenvironment through enhanced cyclooxygenase 2 (COX2) production and through enhanced extracellular matrix (ECM) remodeling (16, 17). However, it is unclear what triggers macrophage polarization during postpartum involution toward an M2-like phenotype. Further, cytokines produced by M2-like macrophages (e.g., IL-4, IL-10, IL-13, TGF-β1, and EGF) (18–21) are associated with increased breast cancer malignancy (22–25). It should be noted that these cytokines, which are involved in wound healing and immune suppression, are produced abundantly during postpartum involution to support mammary remodeling (26–29), consistent with their potential involvement in ppBC progression. In addition, our

Note regarding evaluation of this manuscript: Manuscripts authored by scientists associated with Duke University, The University of North Carolina at Chapel Hill, Duke-NUS, and the Sanford-Burnham Medical Research Institute are handled not by members of the editorial board but rather by the science editors, who consult with selected external editors and reviewers.

Conflict of interest: The authors have declared that no conflict of interest exists.

Submitted: March 31, 2014; **Accepted:** August 13, 2014.

Reference information: *J Clin Invest*. 2014;124(11):4737–4752. doi:10.1172/JCI76375.

previous work shows that MerTK, an RTK required for efficient efferocytosis by macrophages and epithelial cells, is elevated during postpartum involution (30) and is involved in the accumulation of Th2-like tumor-associated leukocytes in preclinical mammary tumor models (31).

We have used the *MMTV PyVmT* transgenic mouse model (32) to assess how postpartum mammary involution and remodeling affects malignant progression of spontaneous mammary tumors within the context of their native microenvironment and within a fully competent immune system. Tumor metastasis was elevated 10-fold by events occurring during postpartum involution, triggered by stromal responses to widespread tumor cell death, including increased M2-like macrophage characteristics and enhanced production of wound-healing and immunosuppressive cytokines. These changes in the stromal microenvironment were orchestrated by MerTK, which is responsible in large part for the clearance of dying cells (efferocytosis) by macrophages or other efferocytes. We demonstrate that MerTK inhibition or gene targeting abolished efferocytosis, M2-like macrophage polarization, production of wound-healing cytokines, and reduced tumor metastasis in the postpartum setting. Our data reveal a critical role for MerTK and efferocytosis in driving stromal wound-healing and remodeling events that contribute to ppBC malignancy.

Results

Increased metastasis of tumors in the postpartum mammary gland. Previous studies demonstrated that breast tumor cell lines transplanted into mouse mammary glands just prior to postpartum involution are more invasive and metastatic than the same tumor cells transplanted into the mammary fat pads of age-matched virgin mice (11, 12). We recapitulated these findings using primary mammary tumor cells (PMTCs) derived from *MMTV PyVmT* mice, which we transplanted into the mammary fat pads of WT FVB female mice. Prior to tumor cell injection, age-matched mice (42 days of age) were randomized into 2 groups: 1 remaining nulliparous and 1 that would breed for 1 to 3 days. Primary tumor cells were injected when mice were 59–61 days of age, corresponding to 14.5 to 16.5 dpc in the parous group (Figure 1A), such that partuition occurred 4–7 days after tumor injection. Pups were withdrawn from dams at partuition to initiate postpartum involution in the parous group. Tumors became palpable 11 days (on average) after tumor cell injection in both groups, corresponding to involution day 6 (Inv d6) in the parous group and suggesting that late pregnancy and postpartum events did not affect tumor latency (T_{50} = 11 days, $P > 0.05$, log-rank test). Tumors in parous mice grew at a modestly increased rate compared with what was observed in virgin mice (Figure 1B). However, lungs harvested at postinjection day 39 revealed that metastatic lung lesions occurred in 5 of 6 parous mice, but were not detected in age-matched virgin mice (0 of 6 mice, Supplemental Figure 1; supplemental material available online with this article; doi:10.1172/JCI76375DS1).

We extended these findings using spontaneous tumors arising in *MMTV PyVmT* transgenic mice, with the added advantages of endogenously forming tumors within a fully intact immune system (32). Female mice remained as virgin mice or were impregnated at 42 to 44 days of age. Synchronized pregnancies within this 3-day window allowed us to make age-matched comparisons between genetically comparable animals, establishing reproductive history as the major experimental variable (Figure 1C). In the parous group, pups were withdrawn at partuition because *MMTV PyVmT* dams are unable to nurse their offspring. Pregnancy did not affect average tumor latency (T_{50} = 56 ± 5 days in virgin mice; T_{50} = 52 ± 3 days in parous mice) (Supplemental Figure 2, left panel), total tumor burden (Supplemental Figure 2, right panel), tumor cell proliferation (Supplemental Figure 3), or PyVmT expression (Figure 1D). Histological differences were apparent between virgin and parous groups, including milk within the ductal lumens of parous mouse tumors (but not virgin mouse tumors) at partuition/64 days of age, which was resorbed during the course of postpartum involution (Supplemental Figure 4). Although the number of lung metastases was similar in 64-day-old virgin and parous mice (partuition in the parous group) and in 71-day-old virgin and parous mice (Inv d7 in the parous group), lung metastases in the parous group increased by 10-fold in 85-day-old parous mice (Inv d21) as compared with the metastases seen in 85-day-old virgin mice (Figure 1, E and F). These models demonstrate that changes occurring in the mammary microenvironment during involution have a profound impact on metastasis, without affecting primary tumor burden.

We investigated phosphorylation of STAT3 (p-STAT3) in tumors from virgin and parous mice, as p-STAT3 is an early event in the involution signaling cascade and is known to correlate with increased aggressiveness in several tumor models. We found relatively equal levels of p-STAT3 in parous and virgin mice at 71 days of age (corresponding to Inv d7 in the parous group) and at 85 days of age (corresponding to Inv d21 in the parous group, Figure 1D). We also measured p-AKT and p-ERK, which revealed similar levels of each in virgin and parous mice at 71 days of age (Inv d7 in parous group). At 84 days of age, AKT and ERK phosphorylation was modestly decreased in the parous group (Inv d21) as compared with that detected in the virgin group.

Increased cell death and efferocytosis in postpartum mammary tumors. To begin understanding how postpartum involution might establish a prometastatic tumor microenvironment (TME), we examined the physiological events that characterize postpartum involution in the normal breast. A remarkable feature of postpartum involution is transient but widespread cell death throughout the milk-producing mammary epithelium (33). However, it is currently unknown whether tumors within the breast during postpartum involution are similarly subjected to a vast presence of dying cells. Using TUNEL analysis to measure dying/dead tumor cells, we found very few TUNEL$^+$ cells in tumors from virgin mice at 64 days, 71 days, 85 days, and 104 days of age (Figure 2, A and B). However, the frequency of TUNEL$^+$ cells increased more than 5-fold in tumors harvested from 71-day-old parous mice (Inv d7) and diminished at later involution time points. This is the first demonstration to our knowledge that mammary tumors also experience a peak in cell death during postpartum involution.

During physiological postpartum involution, dying mammary epithelial cells (MECs) are cleared from the mammary gland through efferocytosis, a process by which macrophages and other phagocytes recognize, bind to, and engulf dying cells (34, 35). Macrophages require the RTK MerTK to engulf dying cells, particularly during postpartum involution, when dying cells are

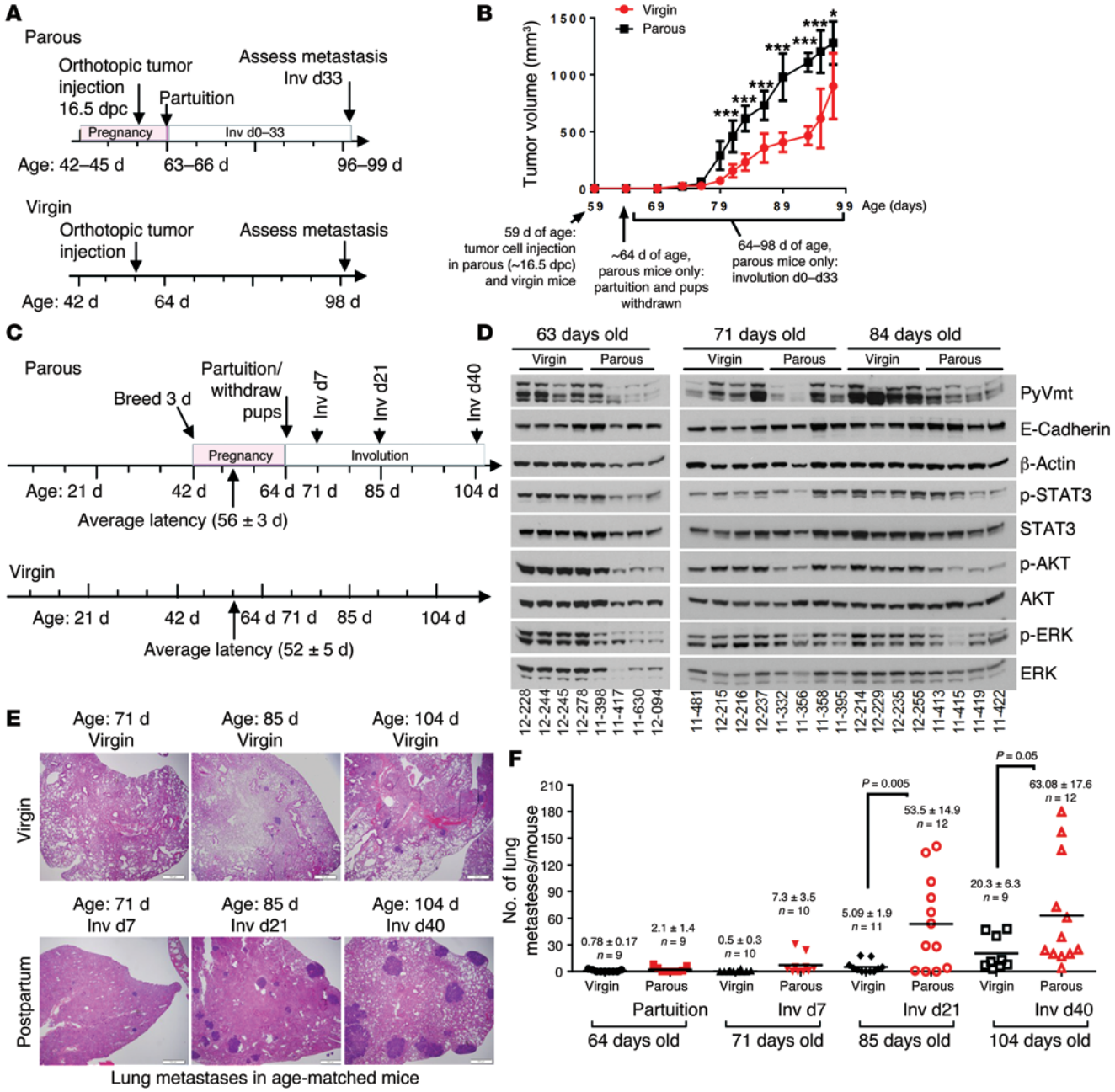

Figure 1. Postpartum involution increases metastasis of mammary tumors. (**A** and **B**) Orthotopic allograft model of ppBC. (**A**) Approach used to model ppBCs in WT female virgin mice. 42-day-old mice were randomized into 2 groups: (a) one that remained nulliparous and (b) one bred for 3 days with WT male mice. Tumors in 56- to 59-day-old mice (14.5–16.5 dpc) were injected. Pups were withdrawn at partuition. Tumors and lungs were harvested from 97-day-old mice (Inv d33 in the parous group). (**B**) Tumor volume, measured 2–3 times per week, is shown as the average tumor volume ± SD. n = 6–8 per group. ; $^*P < 0.05$; $^{***}P < 0.001$. (**C**–**F**) Immune-competent, spontaneous ppBC model. (**C**) Approach used to model ppBCs in *MMTV PyVmT* mice. Female mice were randomized at 42 days of age into 2 groups: (a) one that remained nulliparous and (b) one bred for 3 days with WT male mice. P = NS by log-rank test. (**D**) Whole-tumor lysates assessed by Western blot analysis using the indicated antibodies. Each lane represents tumor lysates harvested from a distinct mouse. (**E**) Representative images of histological lung sections. Original magnification, ×400. (**F**) Quantification of the number of lung metastases per mouse; each point represents a single mouse. Midline represents the average. n = 9–12 per group. P values were calculated by Student's t test.

very abundant (30). In normal mammary glands, MerTK expression is low during puberty, maturity, and pregnancy, but is rapidly induced during postpartum involution, when cell death peaks (30). To determine whether MerTK is similarly induced in postpartum mammary tumors during involution, we used Western blot analysis of whole-tumor lysates collected at partuition (Inv d0) and at postpartum involution time points (Inv d7, Inv d21, and Inv d40). We found that tumor MerTK expression was low at the end of pregnancy (Inv d0, 64 days of age), but was strongly elevated in tumors harvested at Inv d7 (Figure 2C), a time point when TUNEL$^+$ dead tumor cells were at their peak (Figure 2B). Tumor lysates harvested from age-matched *MerTK*$^{-/-}$ mice did not show

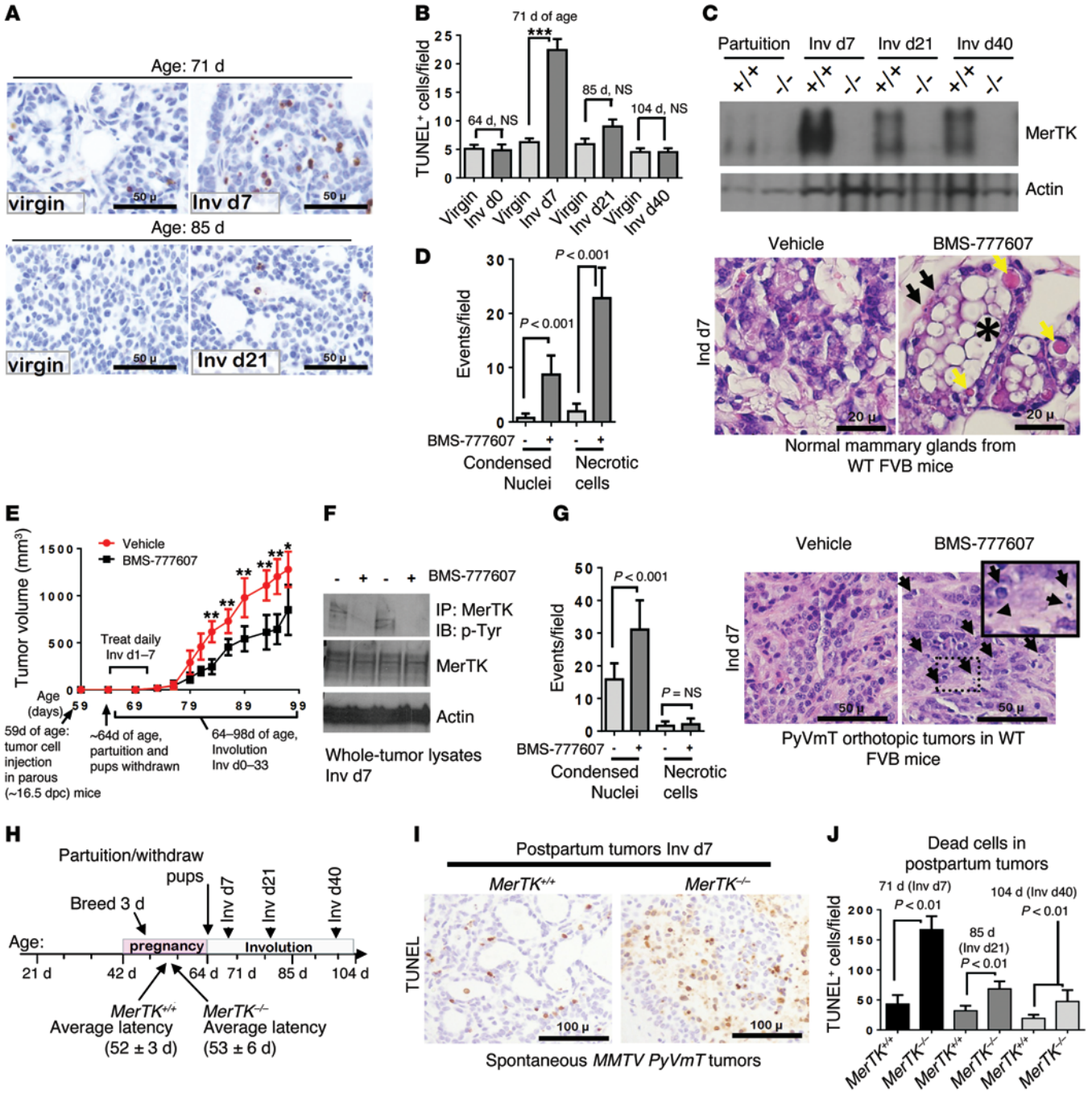

Figure 2. Increased tumor cell death and efferocytosis in ppBCs. (**A**) TUNEL analysis of tumors from virgin and postpartum mice. Representative images are shown. Original magnification, ×400. (**B**) Average TUNEL$^+$ cells per field (5 random fields/sample; n = 4–6). ***$P < 0.001$ by Student's t test. (**C**) Western blot analysis of whole-tumor lysates harvested at partuition (64 days old), Inv d7 (71 days old), Inv d21 (85 days old), and Inv d40 (104 days old). $^{+/+}$ denotes *MerTK*$^{+/+}$ *PyVmT* tumors; $^{-/-}$ denotes *MerTK*$^{-/-}$ *PyVmT* tumors. (**D**) WT mice treated with BMS-777607 (Inv d1–7). Representative histological sections of mammary glands harvested 1 hour after final treatment. Black arrows indicate hypercondensed nuclei of dead cells; yellow areas indicate necrotic cells; single asterisk indicates milk fat globule. Original magnification, ×400. (**E**–**G**) Allografted ppBCs treated with BMS-777607 (Inv d1–7). (**E**) Tumor volume was measured 2–3 times per week and is shown as the average tumor volume ± SD. n = 6–8 per group. **$P < 0.01$; *$P < 0.05$. (**F**) Whole-tumor lysates and MerTK immunoprecipitates from tumor lysates were assessed by Western blot analysis. (**G**) Representative histological sections of tumors harvested 1 hour after final treatment on Inv d7. Arrows indicate hypercondensed nuclei of dead cells. Original magnification, ×400; ×600 (inset). (**H**) Schematic approach to assess ppBCs in *MerTK*$^{+/+}$ *PyVmT* and *MerTK*$^{-/-}$ *PyVmT* mice. Average latency is indicated on timeline. P = NS by log-rank test. (**I**) TUNEL analysis of tumors at Inv d7. Representative images are shown. Original magnification, ×400. (**J**) Average TUNEL$^+$ cells per field (5 fields/sample; n = 4–6 per condition). $P < 0.01$ by Student's t test.

any MerTK expression, as expected. In *MerTK*$^{+/+}$ tumors, postpartum tumor MerTK levels remained elevated throughout Inv d40, as compared with what was detected in tumors harvested at Inv d0, consistent with the hypothesis that MerTK plays an important role in directing efferocytosis in postpartum mammary tumors.

To test this hypothesis directly, we used the MerTK tyrosine kinase inhibitor (TKI) BMS-777607 (36) to impair MerTK activity in mammary tumors during postpartum involution. We first confirmed that BMS-777607 impaired efferocytosis during postpartum involution in normal mammary glands. Beginning at Inv d1, mice were treated with BMS-777607 once daily through Inv d7. MerTK inhibition produced a substantial accumulation of dying/dead cell bodies, necrotic cells, and lipid (milk fat) globules in postpartum mammary glands (Figure 2D), similar to what has been reported in MerTK-deficient mammary glands during postpartum involution (30) and thus confirming that BMS-777607 inhibits MerTK-dependent efferocytosis. Next, we modified the allografted ppBC model shown in Figure 1A, adding daily treatments with BMS-777607 beginning at Inv d1 and ending on Inv d7 (Figure 2E). This brief treatment window coincided with the peak in dying tumor cell burden (Figure 2B) and with the peak induction of MerTK expression (Figure 2C). BMS-777607 treatment for the first 7 days of involution did not affect tumor latency, but caused a slight decrease in the postpartum tumor growth rate. Western blot analysis of MerTK immunoprecipitates from tumor lysates harvested on Inv d7 showed decreased MerTK tyrosine phosphorylation in BMS-777607–treated samples compared with what was detected in vehicle-treated tumors (Figure 2F). Importantly, dead cell bodies were abundant in BMS-777607–treated tumors on Inv d7, but not in vehicle-treated tumors, demonstrating that MerTK signaling is necessary for efferocytosis in postpartum mammary tumors (Figure 2G).

Because BMS-777607 can inhibit other RTKs related to MerTK, we confirmed our findings using genetic MerTK ablation. *MerTK*$^{-/-}$ mice (inbred to FVB) crossed with *MMTV PyVmT* mice were randomized into virgin or breeding groups in which pregnancies were synchronized in 42-day-old mice, as described in Figure 1D. MerTK loss was confirmed in tumors from virgin mice by Western blot analysis of whole-tumor lysates (Supplemental Figure 5A). MerTK loss in virgin mice did not affect tumor latency, total tumor burden, tumor cell proliferation, or tumor cell death (Supplemental Figure 5, B–E). Tumors from virgin *MerTK*$^{-/-}$ and *MerTK*$^{+/+}$ mice were histologically similar (Supplemental Figure 5F). These data are consistent with reports that MerTK expression is not detected in the tumor epithelial cell population of *MMTV PyVmT* tumors (31), explaining in part why MerTK loss had no overt effect on tumor latency or growth in nulliparous mice. However, given the profound burden of dying cells that require clearance from the mammary gland (11, 28, 29, 37) and mammary tumors (Figure 2B) during postpartum involution and the known role of MerTK in efferocytosis, it is possible that MerTK loss uniquely affects tumor progression in the context of postpartum involution.

We examined this hypothesis in tumors harvested from parous *MerTK*$^{+/+}$ and *MerTK*$^{-/-}$ mice at the end of pregnancy/Inv d0 (when pups were withdrawn), Inv d7, Inv d21, and Inv d40 (Figure 2H). MerTK loss was confirmed by Western blot analysis at each time point (Figure 2C). We found that MerTK loss did not affect tumor latency in parous mice (Figure 2H; log-rank test). However, TUNEL analysis revealed a dramatic increase in the presence of dead cell bodies in *MerTK*$^{-/-}$ *PyVmT* tumors at Inv d7 (Figure 2I). Dead cell bodies in *MerTK*$^{-/-}$ tumors remained prominent throughout postpartum Inv d40 (Figure 2J). Because we did not observe increased TUNEL staining in mammary tumors from virgin *MerTK*$^{-/-}$ mice (Supplemental Figure 5E) and because previous studies demonstrate that MerTK is poorly expressed in *MMTV PyVmT* tumor cells (31), these data suggest that MerTK loss did not increase tumor cell death per se, but caused an accumulation of dead cell bodies throughout postpartum involution due to a failure in efferocytosis. This is supported by annexin V staining of purified, cultured *MerTK*$^{+/+}$ *PyVmT* and *MerTK*$^{-/-}$ *PyVmT* primary tumor cells, which revealed similar levels of cell death in both groups (Supplemental Figure 5G).

Pharmacological or genetic MerTK ablation decreases postpartum mammary tumor metastasis. To define the potential relationship between (a) widespread postpartum tumor cell death, (b) efferocytosis of dying tumor cells, and (c) postpartum tumor progression, we examined the impact of pharmacological MerTK inhibition on metastasis of postpartum mammary tumors in our allografted model of ppBC (described in Figure 2E), in which tumor-bearing mice were treated daily with BMS-777607 beginning on Inv d1 and ending on Inv d7. Tumor metastases were counted in lungs harvested at Inv d33 (Figure 3A), revealing metastatic lung lesions in 5 of 6 parous mice treated for 7 days with vehicle, but in only 1 of 6 parous mice treated for 7 days with BMS-777607. These data suggest that MerTK inhibition during early postpartum involution decreases mammary tumor metastasis. Metastases were not detected in the lungs of tumor-bearing virgin mice (with or without BMS-777607 treatment) age-matched to the postpartum group.

These findings were confirmed using genetic MerTK ablation in our spontaneous tumor model of ppBC (described in Figure 2H). We found that although genetic MerTK loss in virgin mice did not affect the number of lung metastases (Figure 3B), MerTK loss in parous mice diminished the number of metastatic lung lesions by more than 3-fold and by more than 6-fold at Inv d21 and Inv d40, respectively (Figure 3C). Importantly, MerTK loss did not affect total tumor burden in parous mice at Inv d0, d7, d21, or d40 (Supplemental Figure 6A), although histological changes associated with impaired efferocytosis were apparent in MerTK-deficient postpartum mammary tumors, such as accumulation of dead cells in fluid-filled lumens (Supplemental Figure 6B), which we confirmed by TUNEL analysis (Supplemental Figure 6C). Taken together, these data establish a relationship between MerTK-mediated efferocytosis and the prometastatic environment in postpartum mammary tumors.

Increased expression of wound-healing cytokines in postpartum mammary tumors. Genes including *Il4*, *Il10*, and *Tgfb1* encoding wound-healing and immunosuppressive cytokines are often induced in response to efferocytosis(38–40). Transcriptional induction of wound-healing and immunosuppressive cytokine signatures is a major feature of the normal mouse mammary gland during postpartum involution (26, 28, 37, 41), due at least in part to high levels of efferocytosis occurring in this setting (30). We used a publicly available quantitative reverse transcription-PCR (qRT-PCR) dataset measuring expression of Th2 cytokine genes

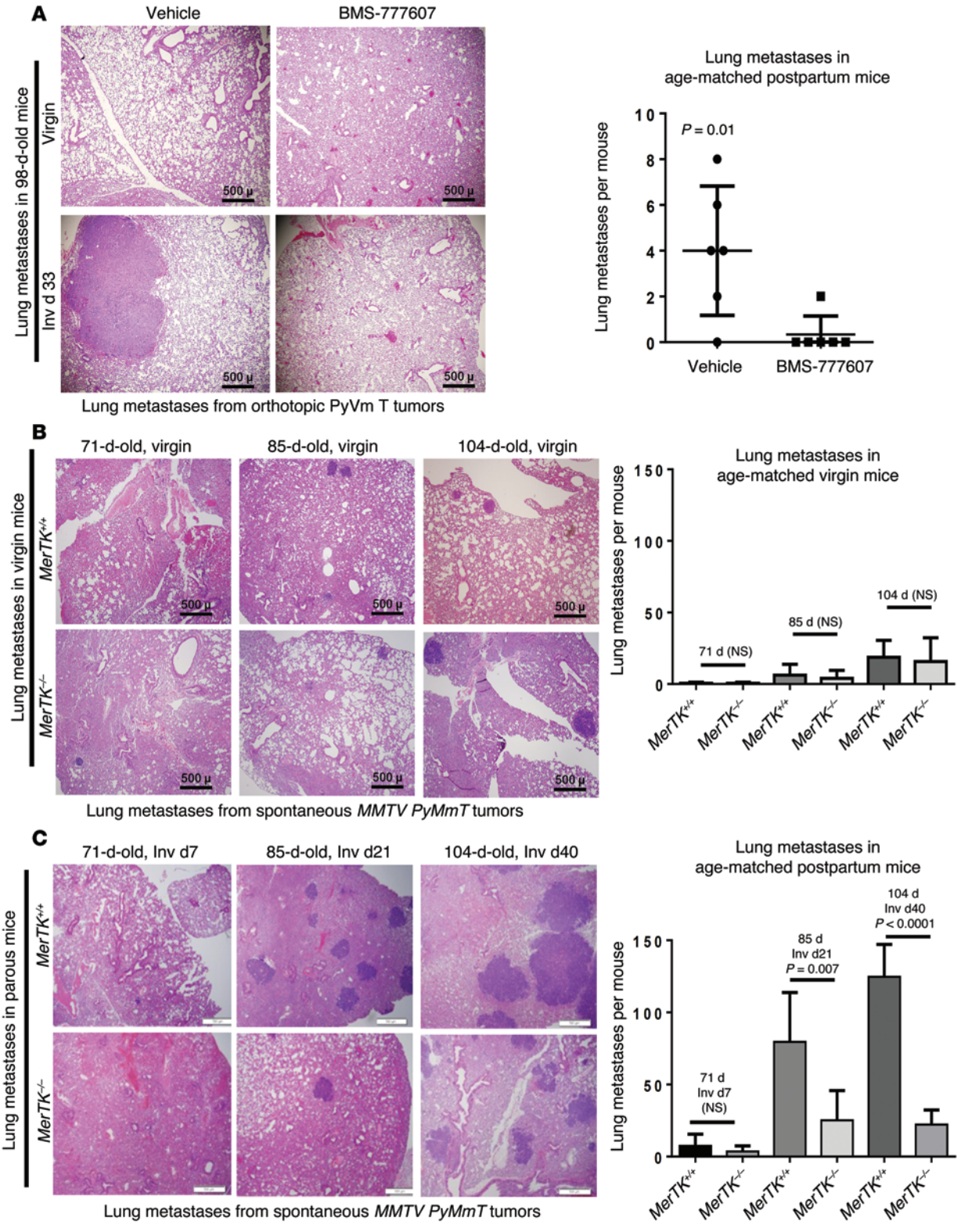

Figure 3. Postpartum involution increases metastasis of ppBCs in a MerTK-dependent manner. (**A**) Left panels: Representative images of histological lung sections harvested from 98-day-old virgin and parous mice harboring orthotopic allografts of mammary tumor cells (corresponding to 38 days after tumor cell injection in both groups and corresponding to Inv d33 in the parous group). Mice were treated with BMS-777607 for 7 days beginning at 64 days of age (corresponding to Inv d1 in the parous group). Right panels: Metastatic burden was quantified from H&E-stained lung sections from all 5 lung lobes in each mouse. $P < 0.01$ by Student's *t* test. Original magnification, ×40. (**B** and **C**) Left panels: Representative histological lung sections from virgin (**B**) and parous (**C**) *MerTK*$^{+/+}$*PyVmT* and *MerTK*$^{-/-}$*PyVmT* mice. Original magnification, ×40. Right panels: Metastatic burden was quantified from H&E-stained lung sections from all 5 lung lobes in each mouse. *P* values were calculated by Student's *t* test.

in human breast tissue specimens collected from premenopausal women who were either nulliparous or who were within 0 to 2 years of a recent full-term pregnancy (27). These data revealed elevated *IL13* and *TGFB1* levels in postpartum samples (n = 4–13) compared with what was seen in samples from nulliparous women (n = 4–20) (Figure 4A). *IL4* was not reported in this dataset, although mouse models have shown upregulation of *Il4* during postpartum involution (16, 26, 42). Levels of *CD68* (a molecular marker for total macrophage content), *IFNG* (a Th1-like cytokine), and *CDH1* (encoding E-cadherin, to control for epithelial content) were similar in samples harvested from nulliparous and postpartum women. These findings suggest that transcripts encoding wound-healing or Th2-like cytokines are locally elevated in postpartum breast tissue in humans, similar to what is seen in mice, supporting the utility of mouse mammary tumor models to understand how postpartum changes in the breast microenvironment contribute to deadly tumor metastasis.

To determine whether postpartum mammary tumors upregulate wound-healing and immune-suppressive cytokines, we compared cytokine levels in spontaneous *MMTV PyVmT* tumors harvested from 71-day-old virgin and parous (Inv d7) mice. Using a cytokine antibody array to gain a broad and unbiased view of cytokine expression in postpartum mammary tumors (Supplemental Figure 7), we found that IL-4 and IL-10 were detected at very low levels in tumors from virgin mice, but were upregulated in tumors from postpartum (Inv d7) mice (Figure 4B). Most cytokines examined were similar in virgin and postpartum tumors (Supplemental Figure 7), including osteopontin (Figure 4B). Cytokine transcripts measured by qRT-PCR analysis of whole-tumor RNA harvested confirmed *Il10*, *Il4*, and *Tgfb1* upregulation in postpartum mammary tumors over what was seen in tumors from virgin mice (Figure 4C), demonstrating that these wound-healing cytokines are locally synthesized in the postpartum mammary TME. It should be noted that wound-healing Th2-like cytokines are frequently detected in clinical breast tumors (24, 43) and are associated with decreased DFS in breast cancer patients (24, 43).

Decreased wound-healing cytokines in postpartum MerTK$^{-/-}$ tumors. Macrophage-mediated efferocytosis is known to trigger the production of wound-healing Th2-like cytokines, including IL-10 and TGF-β1, although the link between tumor cell efferocytosis and TME cytokine levels has not been widely investigated. If efferocytosis in postpartum breast tumors is the primary trigger for the production of Th2-like cytokines, we predicted that the blockade of efferocytosis through MerTK inhibition would prevent postpartum induction of wound-healing cytokines in tumors. We tested this hypothesis using a cytokine antibody array of whole-tumor lysates from postpartum *MerTK*$^{+/+}$ and *MerTK*$^{-/-}$ mammary tumors harvested at Inv d7 (Figure 4D). Postpartum *MerTK*$^{-/-}$ tumors exhibited decreased IL-4, IL-10, and IL-13 levels as compared with the levels detected in *MerTK*$^{+/+}$ tumors (Figure 4E). Most of the cytokines we examined were measured at similar levels in postpartum *MerTK*$^{+/+}$ and *MerTK*$^{-/-}$ tumors (Supplemental Figure 8). These results were confirmed by qRT-PCR analysis of whole-tumor RNA, revealing reduced *Il4*, *Il10*, and *Tgfb1* transcripts in postpartum *MerTK*$^{-/-}$ mammary tumors as compared with those detected in postpartum *MerTK*$^{+/+}$ tumors (Figure 4F). Similarly, whole-tumor RNA from allografted tumors treated with BMS-777607 from Inv d1 to Inv d7 revealed decreased *Il10* and *Tgfb1* mRNAs, although *Il4* transcripts were not altered by BMS-777607 (Figure 4G). These studies suggest that MerTK-mediated efferocytosis enhances wound-healing Th2-like cytokine levels in postpartum mammary tumors.

Efferocytosis of dying breast cancer cells induces Th2-like cytokine expression. To investigate a mechanistic link between postpartum tumor cell death and cytokine modulation by tumor-associated macrophages, we generated a coculture-based model in which dying breast cancer cells could be engulfed by neighboring macrophages. To generate a model of dying mammary tumor cells, we transduced PyVmT primary mammary tumor cells expressing fluorescent mCherry with adenovirus expressing herpes simplex virus-thymidine kinase (HSV-TK), rendering these cells sensitive to gancyclovir-inducible cell death (Figure 5A). After 32 hours in the presence of gancyclovir, *PyVmT mCherry TK* cells displayed more than 85% cell death (Figure 5B and Supplemental Figure 9). These *PyVmT mCherry TK* cells were cocultured with GFP-labeled mouse macrophages (Raw267.4), followed by treatment of cocultures with gancyclovir to induce cell death specifically in the tumor cell population (but not in neighboring macrophages) (Figure 5B and Supplemental Figure 9). BMS-777607 was used in this coculture model to block MerTK activity. Cocultures treated with BMS-777607 (1 μM) displayed reduced MerTK tyrosine phosphorylation (Figure 5C), as did cocultures treated with a goat anti-mouse MerTK-neutralizing antibody (ref. 44 and Supplemental Figure 10).

Fluorescence microscopy demonstrated that many dying *PyVmT mCherry TK* tumor cells were contained within cytoplasmic vacuoles of GFP$^+$ macrophages (Figure 5D, white arrows), while others remained free in culture (Figure 5D, yellow arrows). However, cocultures treated with BMS-777607 failed to exhibit any mCherry$^+$ inclusions within GFP$^+$ macrophages, confirming that efferocytosis was blocked by BMS-777607. *PyVmT mCherry TK* cells remaining in culture after 32 hours were counted, revealing a loss of 68.7% of gancyclovir-treated *PyVmT mCherry TK* tumor cells after 32 hours in coculture with macrophages, as compared with the number of recovered *PyVmT mCherry TK* tumor cells lacking gancyclovir treatment or lacking macrophage coculture (Figure 5E). Importantly, BMS-777607 blocked the clearance of dying *PyVmT mCherry TK* tumor cells. We obtained similar findings using *MCF7 mCherry* human breast cancer cells infected with Ad.TK (Supplemental Figure 9), which revealed reduced recovery of dying *MCF7 mCherry TK* cells in the presence of macrophages. BMS-777607 inhibited clearance of dying *MCF7 mCherry TK* tumor cells by Raw264.7 macrophages (Figure 5F). Similarly, preincubation of cocultures with a neutralizing anti-mouse MerTK antibody prior to treatment with gancyclovir impaired the clearance of dying *MCF7 mCherry TK* tumor cells, confirming the role of MerTK in this macrophage-mediated process (Figure 5F).

To investigate efferocytosis-induced changes in cytokines, the efferocytosis coculture assay required modification because Ad.TK altered cytokine levels, even in the absence of efferocytosis (not shown). Therefore, we induced cell death in nonadherent suspensions of MCF7 cells using the Bcl-2/Bcl-xL inhibitor ABT-263 (1 μM) in combination with the phosphatidylinositol-3 kinase (PI3K) inhibitor BKM-120 (1 μM) for 4 hours (Figure 5G). Cells were washed 5 times to remove residual drug, then were cultured

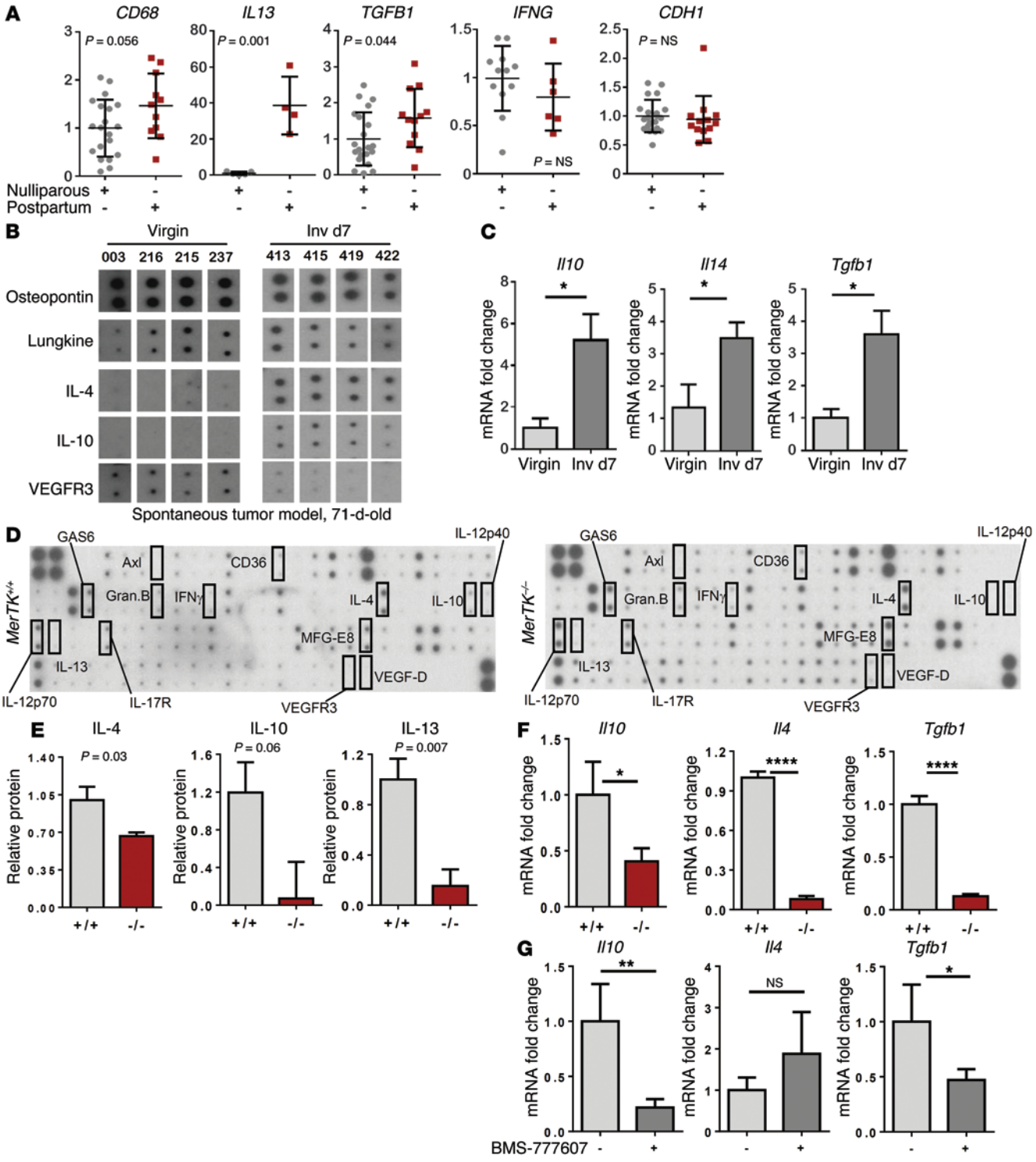

Figure 4. Increased expression of Th2-like cytokines in postpartum tumors requires MerTK. (**A**) A publicly available qRT-PCR dataset of RNA expression levels in normal breast biopsies harvested from premenopausal nulliparous women and premenopausal women 0–2 years after a full-term pregnancy (27) was queried for relative expression levels of the indicated transcripts, which were normalized to dataset housekeeping genes. *P* values were calculated by Student's *t* test. *n* = 4–20 per group. (**B**) Cytokine antibody array was performed using lysates from spontaneous *MMTV PyVmT* tumors harvested from 71-day-old mice (*n* = 4 tumors per group). Individual cytokine spots are shown from identical exposures. (**C**) Whole-tumor RNA from 71-day-old virgin and postpartum (Inv d7) mice was assessed by qRT-PCR for *Il10*, *Il4*, and *Tgfb1*. Values are the average relative transcripts levels ± SD. *n* = 4 tumors analyzed in 6 replicate experiments. **P* < 0.05 by Student's *t* test. (**D**) Cytokine antibody array was performed using lysates from *MerTK*$^{+/+}$ *PyVmT* and *MerTK*$^{-/-}$ *PyVmT* postpartum tumors (Inv d7). *n* = 4. (**E**) Densitometry-based quantitation of relative cytokine levels in whole-tumor lysates. Selected cytokines of interest are shown. Values are the average ± SD. *n* = 4. *P* values were calculated by Student's *t* test. (**F**) RNA isolated from whole tumors collected from 71-day-old parous *MerTK*$^{+/+}$ *PyVmT* and *MerTK*$^{-/-}$ *PyVmT* mice at Inv d7 was assessed by qRT-PCR to quantify *Il10*, *Il4*, and *Tgfb1*. Values shown are the average ± SD. *n* = 4. **P* < 0.05; *****P* < 0.0001 by Student's *t* test. (**G**) RNA isolated from whole tumors from parous mice treated from Inv d0 to Inv d7 with or without BMS-777607 was assessed by qRT-PCR to quantify *Il10*, *Il4*, and *Tgfb1*. Values shown are the average ± SD. *n* = 4. **P* < 0.05; ***P* < 0.01 by Student's *t* test.

alone or in combination with Raw267.4 mouse macrophages. Annexin V staining revealed that this approach induced cell death in more than 70% of all MCF7 cells (Supplemental Figure 11). After 16 hours of coculture, we used ELISAs to measure protein levels of mouse IL-4 (mIL-4) and mIL-10 in the cultured media. The use of mouse macrophages to engulf human breast cancer cells allowed us to exploit antibody specificity to capture mouse cytokines (macrophage-derived, in this case), while excluding human cytokines (tumor cell–derived, in this case). When macrophages, dying MCF7 cells, or live MCF7 cells were cultured alone in serum-free media, only low levels of mIL-4 and mIL-10 were detected (Figure 5H). However, coculture of macrophages with dying MCF7 cells, but not live MCF7 cells, significantly increased mIL-4 and mIL-10 (Figure 5H). Whole-cell RNA after 16 hours revealed increased *Tgfb1* transcript levels in macrophages cocultured with dying MCF7 cells, but not with live MCF7 cells (Figure 5H). Further, MerTK inhibition using BMS-777607 or goat anti-mouse MerTK-neutralizing antibody decreased mIL-4 levels in cultured media (Figure 5I). We found that induction of mIL-10 occurred when macrophages were cocultured with dead MCF7 cells, but not in the presence of the neutralizing MerTK antibody (Supplemental Figure 12). These data suggest that MerTK-dependent efferocytosis of dying breast cancer cells induces Th2-like cytokines in the postpartum TME.

Increased infiltration of tumor-associated macrophages in postpartum mammary tumors. During physiological postpartum involution, macrophages expressing M2-like (alternatively activated) molecular markers, such as arginase 1 (ARG1) or CD206, are the predominant macrophage population in the mammary gland (16, 45, 46). Importantly, M2 macrophages increase the malignancy of ppBCs in transplantable models (10, 13). We examined the impact of postpartum involution on macrophages in spontaneous *MMTV PyVmT* tumors (Figure 6A). Immunofluorescence detection of the macrophage marker F4/80 revealed that macrophage density was similar in tumors from 71-day-old virgin and postpartum mice (Inv d7) (Figure 6B). However, macrophages localized to the tumor periphery in samples from virgin mice, but infiltrated the tumor epithelium of postpartum tumors, in agreement with what is known regarding macrophages in postpartum involution (16). We measured ARG1 by IHC in mammary tumors from virgin or postpartum (Inv d7) mice (Figure 6C), finding substantially increased ARG1 in tumors harvested during postpartum involution compared with what was found in virgin samples (Figure 6D). Expression of *Mrc1*, the gene encoding the M2 molecular marker CD206, was also markedly elevated in whole-tumor RNA harvested at Inv d7 (Figure 6E). These findings were confirmed in samples harvested from allografted PyVmT tumors, revealing that *Mrc1* levels were also higher in tumors harvested at postpartum Inv d7 compared with what we observed in tumors from age-matched virgin mice (Figure 6E). In contrast, *Nos2* (encoding iNOS, a marker of M1-like macrophages) was expressed at similar levels in tumors from 71-day-old virgin and 71-day-old postpartum mice (Supplemental Figure 13). Thus, postpartum involution increases intratumoral M2-like macrophages, consistent with what has been reported for the normal mammary gland during involution and in other models of ppBC.

To determine whether MerTK-mediated efferocytosis is a critical driving force for M2 macrophage polarization in postpartum mammary tumors, we assessed macrophages in spontaneous *MMTV PyVmT* mammary tumors from parous $MerTK^{+/+}$ and $MerTK^{-/-}$ mice at postpartum Inv d7 (Figure 6F). Loss of MerTK did not affect total macrophage density and did not affect the number of intratumoral macrophages (Figure 6G), suggesting that MerTK and efferocytosis are not required to recruit tumor macrophages during postpartum involution. However, postpartum $MerTK^{-/-}$ tumors harvested at Inv d7 harbored fewer $ARG1^{+}$ cells (the M2-like marker) (Figure 6, H and I) and expressed decreased *Mrc1* levels as compared with postpartum $MerTK^{+/+}$ mammary tumors (Figure 6J). Additionally, pharmacological inhibition of MerTK using BMS-777607 from Inv d1 to Inv d7 resulted in decreased *Mrc1* expression levels (Figure 6J). These data suggest that MerTK signaling in the TME during postpartum involution does not affect macrophage recruitment to tumors, but enhances the acquisition or maintenance of M2-like phenotypes of macrophages in postpartum tumors. Importantly, these data indicate that MerTK inhibition can be used to diminish M2-like macrophage phenotypes in postpartum mammary tumors.

Increased TGF-β signaling increases mammary tumor metastasis during postpartum involution. To determine the impact of efferocytosis-induced cytokines on postpartum mammary tumor metastasis, we used an antibody-based approach to neutralize 2 candidate cytokines, IL-4 and TGF-β1, in postpartum tumors (Figure 7A). Beginning at partuition, tumor-bearing WT mice were treated with the mIL-4 antibody 11B11 twice weekly through Inv d14. Western blot analysis of whole-tumor lysates confirmed immune depletion of IL-4 from postpartum tumors (Figure 7B). Despite decreased IL-4 in the TME, the number of metastatic lung lesions was statistically similar in mice treated with 11B11 compared with the number of lesions in mice treated with an isotype-matched IgG (Figure 7C).

In contrast, tumor-bearing mice treated with the anti-mouse TGF-β–neutralizing antibody 1D11 twice weekly through Inv d14 displayed reduced levels of p-Smad2 in whole-tumor lysates at Inv d15 (Figure 7D) and reduced numbers of metastatic lung lesions at Inv d40 (Figure 7E) as compared with tumors treated with isotype-matched IgG. These findings suggest that efferocytosis-induced TGF-β expression increases TGF-β signaling in mammary tumor cells during postpartum involution to enhance tumor metastasis. Interestingly, postpartum tumors treated with the IL-4 antibody 11B11 displayed a further increase in *Tgfb1* mRNA (Supplemental Figure 14A) and increased p-Smad2, a TGF-β–activated transcription factor (Supplemental Figure 14B).

TGF-β signaling is known to increase motility and invasion of mammary tumor cells. To determine whether efferocytosis is capable of inducing TGF-β–mediated tumor cell invasion, we first established efferocytosis cocultures composed of dead MCF7 cells (as established in Figure 5G) cocultured with Raw267.4 macrophages and collected the cultured media after 16 hours (efferocytosis-conditioned media) (Figure 7F). We used media from cocultures of live MCF7 cells with Raw267.4 macrophages for comparison (live cell–cocultured media). We used efferocytosis-conditioned media to stimulate serum-starved recipient PyVmT primary tumor cells in

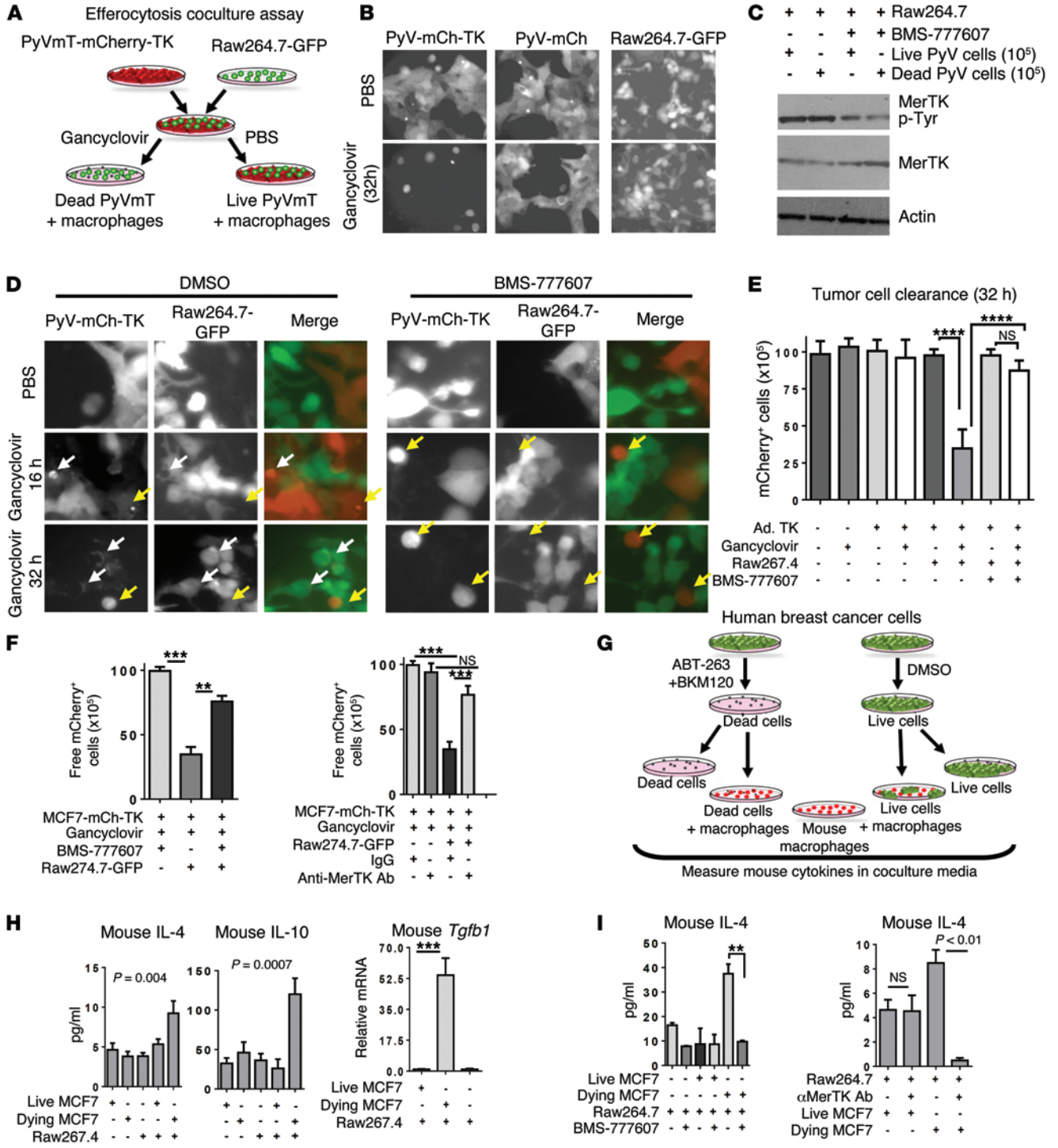

Figure 5. MerTK-dependent efferocytosis of dying breast cancer cells induces production of TGF-β, IL-10, and IL-4. (**A**) Schematic of a novel breast cancer efferocytosis coculture assay. PyVmT cells expressing mCherry and HSV-TK were cocultured with GFP-Raw264.7 macrophages. Gancyclovir caused cell death in HSV-TK$^+$ PyVmT cells. BMS-777607 or neutralizing anti-MerTK antibody was used to block MerTK-dependent efferocytosis. (**B**) Gancyclovir-inducible cell death in PyVmT cells. Original magnification, ×400. (**C**) Western blot analysis of whole-cell lysates or MerTK immunoprecipitates from cocultures treated with or without BMS-777607 (1 μM) for 16 hours. (**D**) Representative fluorescent images of cocultures. White arrows indicate condensed mCherry$^+$ tumor cells within cytoplasmic vacuoles of GFP$^+$ macrophages; yellow arrows indicate condensed mCherry$^+$ cells free in culture. Original magnification, ×400. (**E**) mCherry$^+$ cells remaining after 32 hours in coculture. $^{****}P < 0.0001$ by Student's *t* test. (**F**) Remaining MCF7-mCherry cells were quantified. Values represent the average ± SD. $^{**}P < 0.01$; $^{***}P < 0.001$. $n = 6$. (**G**) MCF7-mCherry cells were cultured for 4 hours in suspension with BKM120 (1 μM) plus ABT-263 (2 μM) to induce cell death, then seeded over adherent Raw264.7 cells and cocultured for 16 hours with or without BMS-777607 or anti-MerTK antibody. (**H**) Mouse IL-4 and IL-10 ELISA of cultured media and qPCR to measure mouse *Tgfb1* transcripts in whole coculture RNA. Values represent the average ± SD. $n = 4$, each assessed in duplicate. $^{**}P < 0.01$. (**I**) Mouse IL-4 ELISA of cocultured media. $n = 4$, each sample assessed in duplicate. Values are the average ± SD. $^{**}P < 0.01$ by Student's *t* test. PyV-mCh-TK, PyVmT-mCherry-TK; PyV-mCh, PyVmT-mCherry.

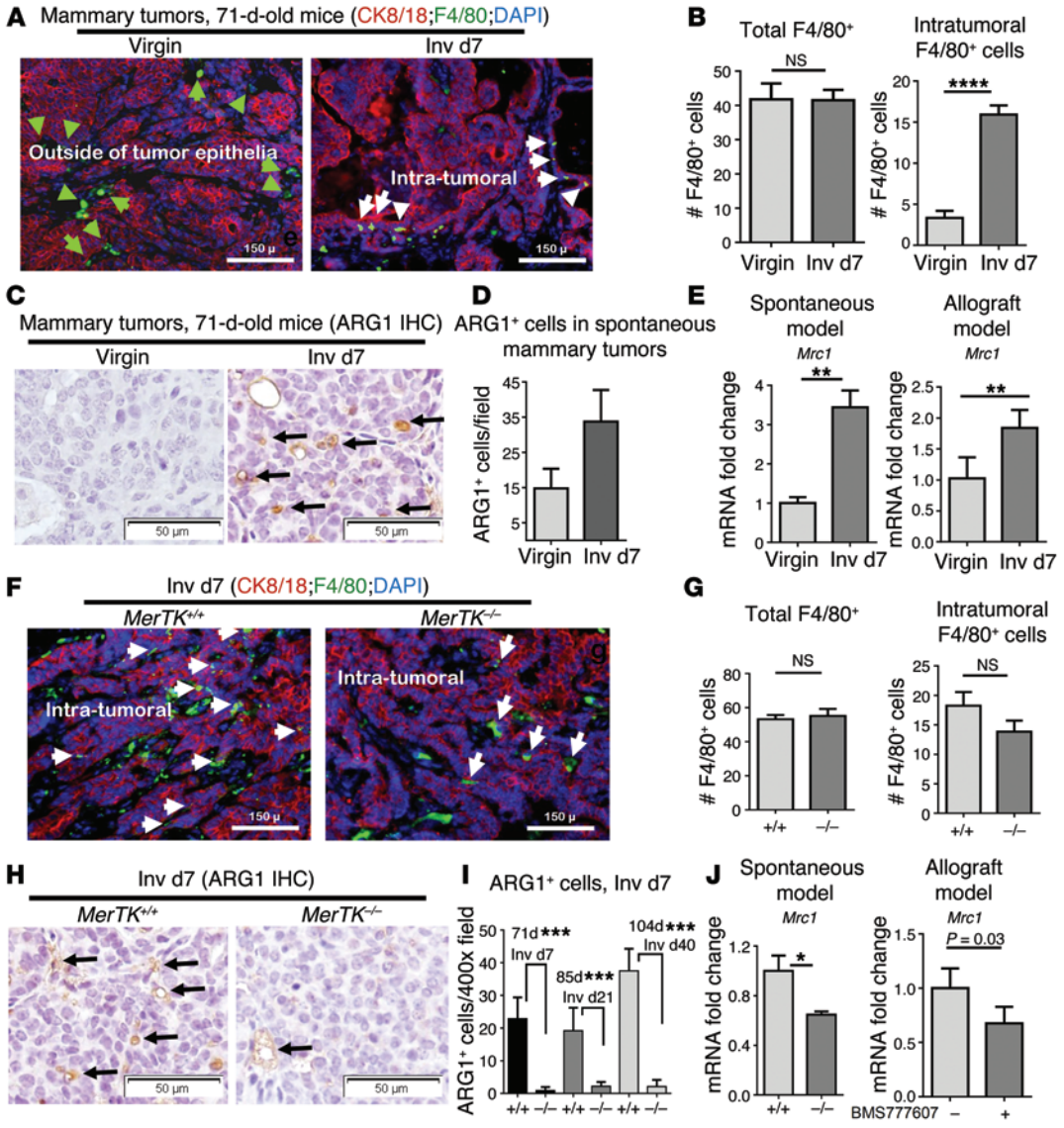

Figure 6. M2 polarization of postpartum tumor–associated macrophages requires MerTK. (**A**–**E**) Tumor sections of *MMTV PyVmT* spontaneous mammary tumors from 71-day-old virgin and postpartum mice were used for analysis. (**A**) Representative immunofluorescent images showing CK8/18 (red) and F4/80 (green) staining; nuclei were counterstained with DAPI (blue). $n = 4$. Green arrows indicate peritumoral F4/80$^+$ macrophages; white arrows indicate intratumoral macrophages. Original magnification, ×100. (**B**) Average (± SD) number of total (left panel) and intratumoral (right panel) macrophages per ×400 field. $n = 4$, 5 fields per sample. $^{****}P < 0.0001$ by Student's t test. (**C**) Representative images of IHC ARG1 staining. $n = 4$. Original magnification, ×400. (**D**) Average number of ARG1$^+$ cells per ×400 field. ($n = 4$). Values are the average ± SD. $P < 0.001$ by Student's t test. (**E**) Whole-tumor RNA assessed by qRT-PCR to quantify relative *Mrc1*. Values shown are the average ± SD. $n = 4$. $^{**}P < 0.01$ by Student's t test. (**F**–**J**) *MerTK*$^{+/+}$ *PyVmT* and *MerTK*$^{-/-}$ *PyVmT* postpartum mammary tumors from 71-day-old mice. (**F**) Representative immunofluorescent images of CK8/18 (red) and F4/80 (green) staining; nuclei were counterstained with DAPI (blue). $n = 4$. White arrows indicate intratumoral macrophages. (**G**) Total (left panel) and intratumoral macrophages (right panel) per ×400 field. $n = 4$, 5 fields per sample. Values are the average ± SD. Student's t test. (**H**) Representative IHC images of ARG1 staining. Original magnification, ×400. (**I**) Average number of ARG1$^+$ cells per ×400 field. $n = 4$. Values are the average ± SD. $^{***}P < 0.001$ by Student's t test. (**J**) Whole-tumor RNA assessed by qRT-PCR to quantify *Mrc1*. Values are the average ± SD. $n = 4$. $^{*}P < 0.05$ by Student's t test.

culture, inducing p-Smad2 to a greater extent than cultured media harvested from "live cell" cocultures (Figure 7G). We found that p-Smad2 induced in response to efferocytosis-conditioned media was inhibited by the TGF-β receptor type 1 (TβR1) inhibitor SD208 (1 μM), confirming that bioavailable TGF-β is upregulated in response to efferocytosis. Efferocytosis-conditioned media increased invasion of PyVmT primary tumor cells through Matrigel-coated Transwell filters (Figure 7H), as did recombinant TGF-β1 (2 pg/ml). Invasion through Transwell filters in response to both efferocytosis-conditioned media and TGF-β1 was blocked by the TβR1 inhibitor SD208.

These results suggest that efferocytosis induces TGF-β in the postpartum mammary TME, thus enhancing tumor cell invasion and migration. This hypothesis was tested in a 3D invasion assay, in which spheroids generated from human breast cancer–derived cell lines (MDA-MB-361 and SKBR3) were embedded in a collagen matrix (2.5 mg/ml), then cultured for 24 hours. Cultures were imaged at 0 and 24 hours following TGF-β1 treatment, revealing that TGF-β1 increased cellular invasion away from spheroids into the surrounding collagen matrix (Figure 7I). We observed that tumor cell invasion from spheroids was inhibited by SD208 (Figure 7J). Similarly, efferocytosis-conditioned media (but not live cell–conditioned media) induced invasion of tumor cells from the spheroid into the collagen matrix, but was blocked upon treatment with SD208. Altogether, these data suggest that increased metastasis of postpartum breast tumors is due in large part to efferocytosis-dependent cytokine modulation in the postpartum mammary gland and identify MerTK and TGF-β as potential therapeutic targets to improve the outcome for young women diagnosed with ppBC (Figure 7K).

Discussion

Premenopausal breast cancers diagnosed during postpartum involution are more frequently diagnosed at metastatic stages as compared with premenopausal breast cancers diagnosed in nulliparous women, pregnant women, or women whose pregnancies occurred more than 10 years before diagnosis (5–8). We have used a spontaneous model of breast cancer to study postpartum mammary tumors within the context of the native TME and a fully competent immune system. Postpartum involution profoundly increased tumor metastasis in this spontaneous tumor model. We verified the results using an allografted mammary tumor model introduced at late pregnancy, which would be less influenced by pregnancy-associated events. Results from the present study establish a causal relationship between the tissue remodeling events of physiological postpartum involution and the increased metastasis of postpartum mammary tumors. Both scenarios are characterized by a transient widespread wave of cell death, efferocytosis, M2 macrophage polarization, and production of key wound-healing cytokines, of which the latter 2 correlate with advanced disease and reduced DFS in breast cancer patients (16, 24, 25, 43).

Our results suggest that increased tumor cell death during postpartum involution triggers efferocytosis, which then induces a stromal wound-healing response that enhances tumor malignancy. Importantly, we identified that MerTK, a critical regulator of efferocytosis in physiological postpartum involution (30), is also required for efferocytosis in postpartum mammary tumors during involution, driving M2 macrophage polarization and wound-healing cytokine production. Pharmacological MerTK inhibition using BMS-777607 reduced efferocytosis, wound-healing cytokines, and metastasis in postpartum mammary tumors. Although BMS-777607 also inhibits Met, Ron, Axl, and Tyro3 (36), we confirmed that MerTK uniquely performs these roles in postpartum mammary tumors using genetic MerTK ablation (Supplemental Figure 15). Additional studies will be required to determine how these other RTKs contribute to postpartum tumor progression, but we propose that BMS-777607 might be used for short durations during postpartum breast remodeling as a potential strategy to inhibit MerTK-mediated efferocytosis and the wound-healing events that follow.

A widespread burden of dying cells in any healthy or injured tissue requires a mechanism to clear dying cells (47–49). In some tissues, such as the epidermis or the gut, dying cells can be sloughed. However, in other tissues, including the retina or the involuting mammary gland, removal of dying cells is achieved through efferocytosis, a process that relies on MerTK (49–52). MerTK recognizes, binds to, and engulfs dying cells marked by phosphatidyl serine (PS), doing so in conjunction with its ligands (Gas6, protein-S, galectin-3, Tubby, and Tubby-like protein 1 [TULP-1]; reviewed in ref. 39]. Efferocytosis is known to produce a shift in macrophage phenotypes toward M2-like characteristics (albeit through unknown mechanisms) and to induce transcription of Th2-like cytokines, including *Il10* and *Tgfb1* (53–55). Genetically engineered mouse models demonstrated that signaling through IL-4 and TGF-β also enhances M2 macrophage polarization (21, 56, 57). Thus, it is possible that MerTK initiates M2 macrophage polarization through efferocytosis-mediated induction of IL-4 and TGF, although this hypothesis remains to be tested. Based on our findings herein, we propose that MerTK-dependent efferocytosis is the driving force behind changes in cytokine levels during physiological postpartum involution and in postpartum mammary tumors. This hypothesis is supported by previous studies showing that MerTK loss from the mammary gland during physiological postpartum involution reduces efferocytosis of dying MECs, causing impaired upregulation of *Il10* and *Tgfb1* (30). Other studies demonstrated that MerTK-mediated efferocytosis of dying neutrophils or injured cardiomyocytes, liver cells, or lung epithelial cells induces the transcription of wound-healing cytokines that promote resolution of acute inflammation and tissue repair (47, 50, 54, 58–62). While MerTK-mediated efferocytosis is desirable in physiological (e.g., postpartum involution of the breast) or pathological (e.g., tissue damage) wound-healing situations, our results suggest that efferocytosis-mediated tissue repair in tumors would enhance tumor metastasis. We show herein that MerTK was in large part responsible for the exaggerated metastasis of ppBCs and for a robust M2-like macrophage presence in postpartum tumors, without affecting total tumor macrophage content. Thus, our studies provide the first illustration to our knowledge of how efferocytosis promotes malignant cancer progression in the endogenous TME.

These findings are consistent with previous reports indicating that loss of MerTK or its ligand Gas6 decreases tumor malignancy in transplantable tumor models in virgin mice, without affecting macrophage recruitment to tumors (31, 63). The previous studies reported that adoptive transfer of MerTK-deficient bone marrow reduced tumor growth over the course of 20 weeks and altered tumor cytokine levels, although lung metastasis and efferocytosis were not reported in this model (31). Together, the current and previous studies suggest that MerTK inhibition reduces tumor malignancy through impaired efferocytosis-induced cytokine modulation. Conversely, increased MerTK expression correlates with decreased DFS in many cancers and may decrease tumor response to chemotherapies (64–66), albeit through unknown mechanisms.

Our results indicate that efferocytosis-induced expression of TGF-β1 increases invasion and motility of mammary tumors cells and that blocking MerTK for the first 7 days of involution, or blocking TGF-β for the first 14 days of involution, is sufficient to impair formation of lung metastases through later time points. The observation that a 7-day time course of MerTK inhibition during early involution was sufficient to provide a therapeutic effect is of great interest, as a potential on-target side effect of sustained MerTK inhibition may be increased autoimmunity. Limited use of a MerTK inhibitor during a short postpartum window would minimize the risk of developing autoimmunity and may be sufficient to limit the profound wound-healing response initiated by efferocytosis during postpartum involution.

In summary, we have shown that changes that occur during physiological postpartum involution, including widespread cell death, MerTK-dependent efferocytosis, and induction of wound-healing cytokines, similarly occur in postpartum mammary tumors, enhancing tumor metastasis. This knowledge will advise new potential strategies for the prevention and treatment of ppBCs.

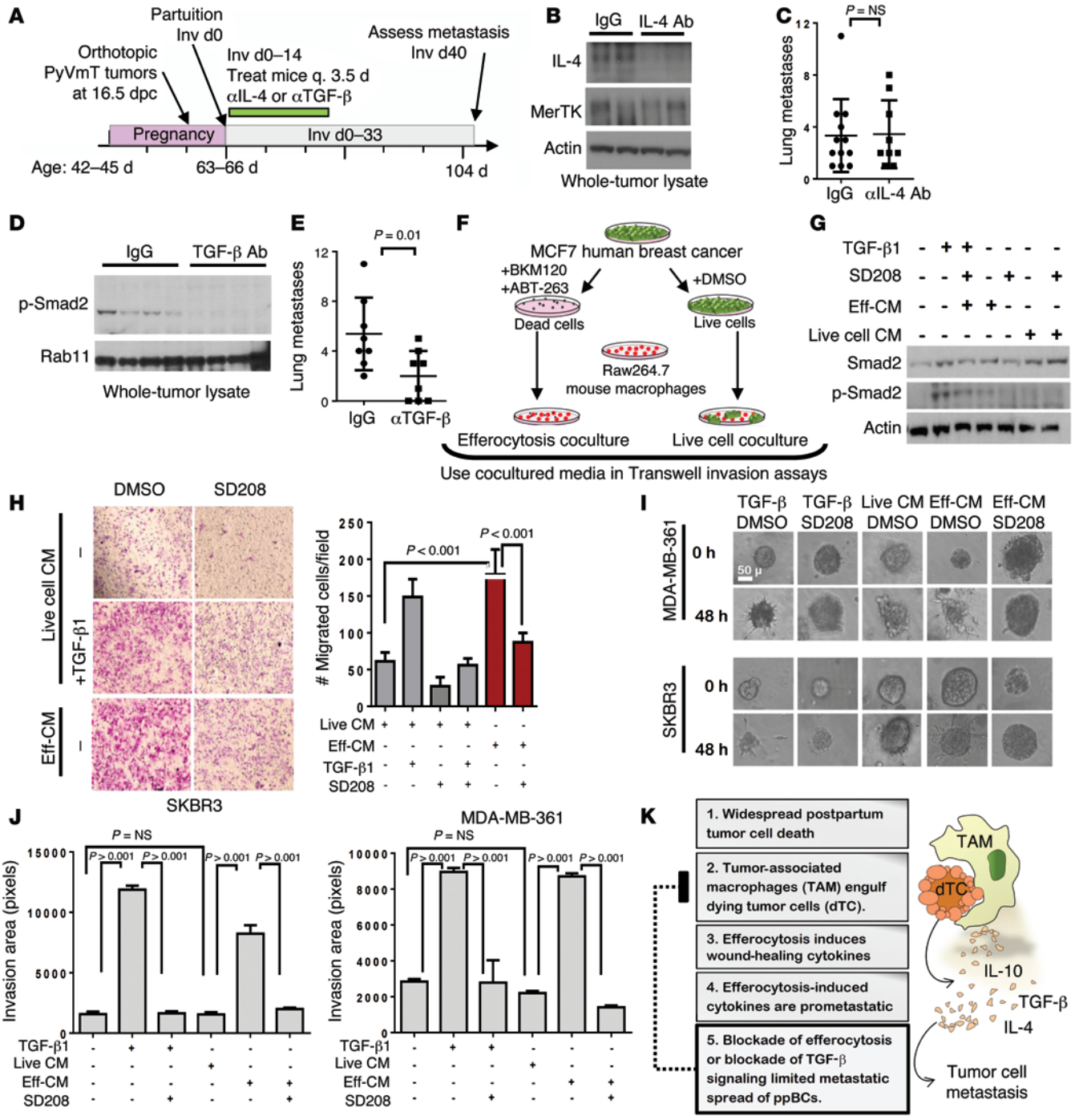

Figure 7. Postpartum TGF-β1 induction increases metastasis of ppBCs. (**A**) Postpartum mammary tumors were treated with antibodies against IL-4 (11B11) or TGF-β (1D11) twice weekly (Inv d1–14). (**B**) Western blot analysis of whole-tumor lysates 24 hours after final treatment. (**C**) Average number of lung metastases per mouse. Each point represents 1 mouse. Midline and whiskers represent the average ± SD. Student's *t* test. $n = 9–12$. (**D**) Western blot analysis of whole-tumor lysates 24 hours after final treatment. (**E**) Average number of lung metastases per mouse. Each point represents 1 mouse. Midline and whiskers represent the average ± SD. Student's *t* test. $n = 8$. (**F**) Cultured media harvested from efferocytosis cocultures and live cell cocultures were used for additional experiments. (**G**) Western blot analysis of PyVmT primary tumor cell lysates cultured in efferocytosis-conditioned, live cell–conditioned or serum-free media with or without TGF-β1 and with or without SD208. (**H**) Invasion of primary PyVmT tumor cells through Matrigel-coated Transwells in response to efferocytosis-conditioned and live cell–conditioned media over a 24-hour period. Representative images of crystal violet–stained Transwell filters are shown. Original magnification, ×40. Right panel: Average cells (± SD) invading through Matrigel-coated Transwells. (**I**) Breast cancer cell–derived spheroids were collagen embedded and overlain with live cell–conditioned, efferocytosis-conditioned, or serum-free media with or without TGF-β1 and with or without SD208. Representative images of spheroids at 0 and 24 hours after embedding per treatment are shown. Original magnification, ×400. (**J**) Average invasion area ± SD. $n = 8–10$. Student's *t* test. (**K**) Schematic model of how efferocytosis contributes to cytokine modulation and metastasis in ppBCs. Eff-CM, efferocytosis–conditioned media.

Methods

Mice. All mice were inbred on an FVB background for more than 10 generations. WT FVB, *MMTV PyVmT* and *MerTK*$^{-/-}$ mice (67), originally referred to as *Mer*^{KD}, were purchased from The Jackson Laboratory. Mice were genotyped by PCR of genomic DNA as previously described (30). Female virgin mice were randomized into 2 groups: (a) 1 group that remained virgin, and (b) 1 group that was bred from 42 to 44 days of age with WT male mice. Pregnancies were timed according to identification of a vaginal semen plug, indicating 0.5 dpc. PyVmT primary mammary tumor cells harvested from *MMTV PyVmT* polyclonal tumors (previously described in ref. 68) were collected by trypsinization, suspended 1:1 in growth factor–reduced Matrigel, and 1×10^6 cells were injected into the inguinal mammary fat pads of 57- to 59-day-old virgin or pregnant (14.5–16.5 dpc) WT female mice. *MMTV PyVmT* mice were bred with *MerTK*$^{-/-}$ mice to generate *MerTK*$^{+/+}$ *PyVmT* and *MerTK*$^{-/-}$ *PyVmT* mice. Mice were monitored daily for tumor formation by manual palpation. Pups were withdrawn at partuition to initiate involution, such that partuition was deemed Inv d0. Mice were maintained until no longer than 104 days of age, corresponding to Inv d40. In some cases, mice were treated by oral gavage with BMS-777607 (Selleck Chemicals) once daily for 7 days at 50 mg/kg in 50 μl of 0.1% Tween 80 and 0.5% methylcellulose. Where indicated in the figures, mice were treated twice weekly with 11B11 or 1D11 or isotype-matched IgGs (10 mg/kg) for 2 weeks beginning at Inv d0. 1D11 (HB-9849) and 11B11 (HB-188) were purchased from ATCC. Hybridomas were cultured, and antibodies were harvested and purified by the Vanderbilt Antibody and Protein Shared Resource.

Western analysis, immunoprecipitation, and cytokine antibody arrays. Cells and tissues were homogenized in ice-cold lysis buffer (50 mM Tris, pH 7.4, 100 mM NaF, 120 mM NaCl, 0.5% NP-40, 100 μM Na_3VO_4, 1X protease inhibitor cocktail [Roche]), sonicated for 10 seconds, and cleared by centrifugation at 4°C, 13,000 *g* for 5 minutes. Protein concentration was determined using the BCA Protein Assay (Pierce Biotechnology). Proteins were separated by SDS-PAGE, transferred to nitrocellulose membranes, blocked in 3% gelatin in TBS-T (Tris-buffered saline, 0.1% Tween 20), incubated in primary antibody overnight and in HRP-conjugated anti-rabbit or anti-mouse for 1 hour, and developed using ECL substrate (Pierce Biotechnology). The following primary antibodies were used: MerTK (α-actin, 1:10,000; Sigma-Aldrich); AKT and S473 P-Akt (1:2,000 and 1:500, respectively; Cell Signaling Technology); S6 and P-S6 (1:1,000; Cell Signaling Technology); Rab11 (1:1,000; Cell Signaling Technology). Immunoprecipitation of MerTK from 1 mg protein lysate or cell lysate was performed using goat anti-mouse MerTK antibody (R&D Systems). For cytokine arrays, whole-tumor lysates were collected and cytokine levels assayed as outlined in the mouse cytokine C1000 (8) antibody array protocol (RayBiotech). Relative cytokine levels were quantified using ImageJ software (NIH).

Histological analysis, IHC, and immunofluorescence. Tumors and mammary glands were fixed in 10% formalin (VWR Scientific), paraffin-embedded, sectioned (5 μm), and stained with H&E at the Vanderbilt University Medical Center Translational Pathology Shared Resource. IHC using rabbit antibodies against PCNA (FL-261, diluted 1:200) or arginase 1 (N-20, diluted 1:100) was performed as previously described (69) and developed using the Vectastain kit (Vector Laboratories). TUNEL analysis was performed with the TUNEL kit (Millipore). Immunofluorescence staining was performed with the following antibodies in 12% fraction V BSA (RPI Corp.): CK8 1:500 (RDI, Fitzgerald); F4/80 1:100 (Invitrogen); and goat anti-hamster and anti-rabbit 1:200 (Molecular Probes, Life Technologies). Slides were mounted in SlowFade with DAPI (Molecular Probes, Life Technologies).

qRT-PCR. Whole-tumor RNA was harvested with an RNeasy kit (QIAGEN), and cDNA was synthesized (High Capacity; Applied Biosystems) and amplified using the murine cDNA-specific primers (Integrated DNA Technologies) listed in Supplemental Methods, along with SYBR Green Supermix (Bio-Rad). The following primers were used: *MRC1* (forward: 5′ CCCTCAGCAAGCGATGTGC 3′; reverse: 5′-GGATACTTGCCAGGT CCCCA-3′); *iNOS* (forward: 5′-GGAGCATCCCAAGTACGAGTGG-3′; reverse: 5′-CGGCCCACTTCCTCCAG); *IL10* (forward: 5′-GGCGCTGTCATCGATTTCTCC; reverse: 5′-GGCCTTGTAGACACCTTGGTC); *Tgfb1* (forward: 5′-CGCAACAACGCCATCTATGAG; reverse: 5′-CGGGACAGCAATGGGGGTTC); *IL4* (forward: 5′-GGTCACAGGAGAAGGGACG; reverse: 5′-GCGAAGCACCTTGGAAGCC);, *IL12b* (forward: 5′-GGAGTGGGATGTGTCCTCAG; reverse: 5′-CGGGAGTCCAGTCCACCTCT); *CCL3* (forward: 5′-CCACTGCCCTTGCTGTTCTTCTCT; reverse: 5′-GGGTGTCAGCTCCATATGGCG); and *Rplp0* (forward: 5′-TCCTATAAAAGGCACACGCGGGC; reverse: 5′-AGACGATGTCACTCCAACGAGGACG). Target gene Ct values were normalized to mRplp0 (housekeeping gene) Ct values according to the formula: $(Ct_{\text{target gene}}\text{-}Ct_{Rplp0})_{\text{Sample A}} - (Ct_{\text{target gene}}\text{-}Ct_{Rplp0})_{\text{Sample B}}$. Values were analyzed as the mean in fold differences (± SE, $n = 4$).

Macrophage, ACs, and efferocytosis coculture assay. PyVmT primary mammary tumor cells and MCF7 human breast cancer cells (ATCC) were transduced with viral particles (Ad.mCherry [Vector Biolabs], Ad.HSV-TK (70), or pBABE-GFP [10668; Addgene], and pLL5.0-LoxP-mCherry [Gateway]) at 5×10^9 particle-forming units per milliliter. Raw264.7 mouse macrophage cells (ATCC) were transduced with pBMN-GFP. Where indicated in the figures, cells were treated with gancyclovir (Sigma-Aldrich). To generate apoptotic MCF7, cells were treated in suspension with 1 μm BKM120 plus 2 μm ABT-263 (both inhibitors from Selleck Chemicals) for 4 hours, washed 5 times with PBS to remove residual drug, and used directly for efferocytosis assays or for annexin V staining. For efferocytosis coculture assays, Raw264.7-GFP cells (10^4/well) and PyVmT or MCF7 cells (72 hours after infection with Ad.mCherry and Ad.HSV-TK) were seeded together in a monolayer in 24-well plates in 2% FBS and cultured for 24 hours prior to the addition PBS or gancyclovir. Cells were imaged at 8, 16, and 32 h after addition of gancyclovir. Cells were collected and counted under fluorescence after 32 hours of coculture. In some experiments, Raw264.7-GFP cells (10^4/well) were seeded in a monolayer in 24-well plates and cultured for 24 hours prior to the addition of 10^3 live MCF7-mCherry or 10^3 dead MCF7-mCherry cells in serum-free media. Where indicated in the figures, BMS-777607 (1 μm) or a neutralizing goat anti-mouse MerTK antibody (AF591, 25 μg/ml; R&D Systems)(44) was added 2 hours prior to the addition of gancyclovir or 2 hours prior to the addition of dead MCF7 cells to macrophage monolayers. Live and dead MCF7 cells were similarly seeded without Raw264.7 cells as single cultures. Media were collected after 16 hours of coculture, passed through a 0.2-μm filter, and used neat (250 μl) to quantify murine IL-10 and IL-4 by ELISA (BioLegend) according to the manufacturer's protocol. Total remaining cells were collected after 16 hours of coculture, lysed, and RNA was collected using an RNeasy kit (QIAGEN).

Collagen invasion assay. MDA-MB-361 and SKBR3 cells were purchased from ATCC and used at low passage. Single-cell suspensions of cells (1×10^5) were cultured in low-adhesion plates (Corning Inc.) for 7 days in serum-free media supplemented with insulin and hydrocortisone to generate spheroids, which were transferred to collagen type I (2.5 mg/ml; Invitrogen), and collagen gels were polymerized according to the manufacturer's directions. Collagen matrices were overlain with uncultured media with or without TGF-β1 (2 pM) and with or without the TRI inhibitor SD208 (1 μM), or with cultured media harvested from Raw264.7 macrophages cocultured with either live cells (live cell–cocultured media) or dead cells (efferocytosis-cultured media) with or without SD-208. Spheroids were photographed immediately (t = 0 hours) and again after 24 hours of culture. The area of each colony at each time point was measured in pixels using Olympus DP2 software. The area at 0 hours was subtracted from the area at 24 hours to obtain the invasion area of the colony over the 24-hour period.

Statistics. All statistical analysis was carried out using GraphPad Prism software. Kaplan-Meier tumor-free survival analysis was used to assess tumor latency. One-way ANOVA or an unpaired 2-tailed Student's t test, with a 95% confidence interval, was used to determine significance for all other data. A P value less than 0.05 was considered significant.

Study approval. Mice were maintained in AAALAC-approved animal facilities at Vanderbilt University. The protocols performed herein were reviewed and approved by the IACUC of Vanderbilt University.

Acknowledgments

This work was supported by grants from the NIH (R01 CA143126, to R.S. Cook), the Vanderbilt-Ingram Cancer Center (VICC) Breast Cancer Specialized Program of Research Excellence (SPORE) (P50 CA98131, to R.S. Cook), and the Congressionally Directed Medical Research Program-Breast Cancer Research Program (CDMRP-BCRP) Idea Award (BC120793, to R.S. Cook).

Address correspondence to: Rebecca S. Cook, Vanderbilt University School of Medicine, Vanderbilt Ingram Cancer Center, Department of Cancer Biology, 2220 Pierce Ave., 759 PRB, Nashville, Tennessee 37232, USA. Phone: 615.936.3813; E-mail: rebecca.cook@vanderbilt.edu.

1. Innes KE, Byers TE. First pregnancy characteristics and subsequent breast cancer risk among young women. *Int J Cancer*. 2004; 112(2):306–311.
2. Pathak DR. Dual effect of first full term pregnancy on breast cancer risk: empirical evidence and postulated underlying biology. *Cancer Causes Control*. 2002;13(4):295–298.
3. Lyons TR, Schedin PJ, Borges VF. Pregnancy and breast cancer: when they collide. *J Mammary Gland Biol Neoplasia*. 2009;14(2):87–98.
4. Martinson HA, Lyons TR, Giles ED, Borges VF, Schedin P. Developmental windows of breast cancer risk provide opportunities for targeted chemoprevention. *Exp Cell Res*. 2013; pii(11):S0014-4827(13)00189-4.
5. Schedin P. Pregnancy-associated breast cancer and metastasis. *Nat Rev Cancer*. 2006; 6(4):281–291.
6. Schedin PJ, Watson CJ. The complexity of the relationships between age at first birth and breast cancer incidence curves implicate pregnancy in cancer initiation as well as promotion of existing lesions. Preface. *J Mammary Gland Biol Neoplasia*. 2009;14(2):85–86.
7. Callihan EB, et al. Postpartum diagnosis demonstrates a high risk for metastasis and merits an expanded definition of pregnancy-associated breast cancer. *Breast Cancer Res Treat*. 2013;138(2):549–559.
8. Faupel-Badger JM, et al. Postpartum remodeling, lactation, and breast cancer risk: summary of a National Cancer Institute-sponsored workshop. *J Natl Cancer Inst*. 2013;105(3):166–174.
9. Amant F, et al. Prognosis of women with primary breast cancer diagnosed during pregnancy: results from an international collaborative study. *J Clin Oncol*. 2013;31(20):2532–2539.
10. Lyons TR, et al. Postpartum mammary gland involution drives progression of ductal carcinoma in situ through collagen and COX-2. *Nat Med*. 2011;17(9):1109–1115.
11. McDaniel SM, et al. Remodeling of the mammary microenvironment after lactation promotes breast tumor cell metastasis. *Am J Pathol*. 2006;168(2):608–620.
12. Schedin P, O'Brien J, Rudolph M, Stein T, Borges V. Microenvironment of the involuting mammary gland mediates mammary cancer progression. *J Mammary Gland Biol Neoplasia*. 2007;12(1):71–82.
13. O'Brien J, Schedin P. Macrophages in breast cancer: do involution macrophages account for the poor prognosis of pregnancy-associated breast cancer? *J Mammary Gland Biol Neoplasia*. 2009;14(2):145–157.
14. O'Brien JH, Vanderlinden LA, Schedin PJ, Hansen KC. Rat mammary extracellular matrix composition and response to ibuprofen treatment during postpartum involution by differential GeLC-MS/MS analysis. *J Proteome Res*. 2012;11(10):4894–4905.
15. Schedin P, Borges V. Breaking down barriers: the importance of the stromal microenvironment in acquiring invasiveness in young women's breast cancer. *Breast Cancer Res*. 2009;11(2):102.
16. O'Brien J, et al. Alternatively activated macrophages and collagen remodeling characterize the postpartum involuting mammary gland across species. *Am J Pathol*. 2010;176(3):1241–1255.
17. Fornetti J, Jindal S, Middleton KA, Borges VF, Schedin P. Physiological COX-2 expression in breast epithelium associates with COX-2 levels in ductal carcinoma in situ and invasive breast cancer in young women. *Am J Pathol*. 2014;184(4):1219–1229.
18. Ruffell B, Affara NI, Coussens LM. Differential macrophage programming in the tumor microenvironment. *Trends Immunol*. 2012;33(3):119–126.
19. Qian BZ, Pollard JW. Macrophage diversity enhances tumor progression and metastasis. *Cell*. 2010;141(1):39–51.
20. Coussens LM, Zitvogel L, Palucka AK. Neutralizing tumor-promoting chronic inflammation: a magic bullet? *Science*. 2013;339(6117):286–291.
21. Denardo DG, et al. Leukocyte complexity predicts breast cancer survival and functionally regulates response to chemotherapy. *Cancer Discov*. 2011;1(1):54–67.
22. Tlsty TD, Coussens LM. Tumor stroma and regulation of cancer development. *Annu Rev Pathol*. 2006;1:119–150.
23. Balkwill F, Charles KA, Mantovani A. Smoldering and polarized inflammation in the initiation and promotion of malignant disease. *Cancer Cell*. 2005;7(3):211–217.
24. Kristensen VN, et al. Integrated molecular profiles of invasive breast tumors and ductal carcinoma in situ (DCIS) reveal differential vascular and interleukin signaling. *Proc Natl Acad Sci U S A*. 2012;109(8):2802–2807.
25. Faghih Z, Erfani N, Haghshenas MR, Safaei A, Talei AR, Ghaderi A. Immune profiles of $CD4^+$ lymphocyte subsets in breast cancer tumor draining lymph nodes. *Immunol Lett*. 2014;158(1):57–65.
26. Clarkson RW, Wayland MT, Lee J, Freeman T, Watson CJ. Gene expression profiling of mammary gland development reveals putative roles for death receptors and immune mediators in post-lactational regression. *Breast Cancer Res*. 2004;6(2):R92–109.
27. Asztalos S, et al. Gene expression patterns in the human breast after pregnancy. *Cancer Prev Res (Phila)*. 2010;3(3):301–311.
28. Stein T, Salomonis N, Nuyten DS, van de Vijver MJ, Gusterson BA. A mouse mammary gland involution mRNA signature identifies biological pathways potentially associated with breast cancer metastasis. *J Mammary Gland Biol Neoplasia*. 2009;14(2):99–116.
29. Flanders KC, Wakefield LM. Transforming growth factor-(beta)s and mammary gland involution; functional roles and implications for cancer progression. *J Mammary Gland Biol Neoplasia*. 2009;14(2):131–144.
30. Sandahl M, Hunter DM, Strunk KE, Earp HS,

Cook RS. Epithelial cell-directed efferocytosis in the post-partum mammary gland is necessary for tissue homeostasis and future lactation. *BMC Dev Biol*. 2010;10:122.
31. Cook RS, et al. MerTK inhibition in tumor leukocytes decreases tumor growth and metastasis. *J Clin Invest*. 2013;123(8):3231–3242.
32. Guy CT, Cardiff RD, Muller WJ. Induction of mammary tumors by expression of polyomavirus middle T oncogene: a transgenic mouse model for metastatic disease. *Mol Cell Biol*. 1992;12(3):954–961.
33. Kreuzaler PA, et al. Stat3 controls lysosomal-mediated cell death in vivo. *Nat Cell Biol*. 2011;13(3):303–309.
34. Seitz HM, Camenisch TD, Lemke G, Earp HS, Matsushima GK. Macrophages and dendritic cells use different Axl/Mertk/Tyro3 receptors in clearance of apoptotic cells. *J Immunol*. 2007;178(9):5635–5642.
35. Zizzo G, Hilliard BA, Monestier M, Cohen PL. Efficient clearance of early apoptotic cells by human macrophages requires M2c polarization and MerTK induction. *J Immunol*. 2012;189(7):3508–3520.
36. Schroeder GM, et al. Discovery of N-(4-(2-amino-3-chloropyridin-4-yloxy)-3-fluorophenyl)-4-ethoxy-1-(4-fluorophenyl)-2-oxo-1,2-dihydropyridine-3-carboxamide (BMS-777607), a selective and orally efficacious inhibitor of the Met kinase superfamily. *J Med Chem*. 2009;52(5):1251–1254.
37. Stein T, et al. Involution of the mouse mammary gland is associated with an immune cascade and an acute-phase response, involving LBP, CD14 and STAT3. *Breast Cancer Res*. 2004;6(2):R75–R91.
38. Wallet MA, et al. MerTK is required for apoptotic cell-induced T cell tolerance. *J Exp Med*. 2008;205(1):219–232.
39. Lemke G, Burstyn-Cohen T. TAM receptors and the clearance of apoptotic cells. *Ann N Y Acad Sci*. 2010;1209:23–29.
40. Rothlin CV, Ghosh S, Zuniga EI, Oldstone MB, Lemke G. TAM receptors are pleiotropic inhibitors of the innate immune response. *Cell*. 2007;131(6):1124–1136.
41. Clarkson RW, Watson CJ. Microarray analysis of the involution switch. *J Mammary Gland Biol Neoplasia*. 2003;8(3):309–319.
42. Watson CJ. Immune cell regulators in mouse mammary development and involution. *J Anim Sci*. 2009;87(13):35–42.
43. Teschendorff AE, et al. Improved prognostic classification of breast cancer defined by antagonistic activation patterns of immune response pathway modules. *BMC Cancer*. 2010;10:604.
44. Park HJ, Baen JY, Lee YJ, Choi YH, Kang JL. The TAM-family receptor Mer mediates production of HGF through the RhoA-dependent pathway in response to apoptotic cells. *Mol Biol Cell*. 2012;23(16):3254–3265.
45. O'Brien J, Martinson H, Durand-Rougely C, Schedin P. Macrophages are crucial for epithelial cell death and adipocyte repopulation during mammary gland involution. *Development*. 2012;139(2):269–275.
46. Hughes K, Wickenden JA, Allen JE, Watson CJ. Conditional deletion of Stat3 in mammary epithelium impairs the acute phase response and modulates immune cell numbers during post-lactational regression. *J Pathol*. 2012;227(1):106–117.
47. Vandivier RW, Henson PM, Douglas IS. Burying the dead: the impact of failed apoptotic cell removal (efferocytosis) on chronic inflammatory lung disease. *Chest*. 2006;129(6):1673–1682.
48. deCathelineau AM, Henson PM. The final step in programmed cell death: phagocytes carry apoptotic cells to the grave. *Essays Biochem*. 2003;39:105–117.
49. Erwig LP, Henson PM. Clearance of apoptotic cells by phagocytes. *Cell Death Differ*. 2008;15(2):243–250.
50. Thorp E, Subramanian M, Tabas I. The role of macrophages and dendritic cells in the clearance of apoptotic cells in advanced atherosclerosis. *Eur J Immunol*. 2011;41(9):2515–2518.
51. Fullerton JN, O'Brien AJ, Gilroy DW. Pathways mediating resolution of inflammation: when enough is too much. *J Pathol*. 2013;231(1):8–20.
52. Fadok VA, Voelker DR, Campbell PA, Cohen JJ, Bratton DL, Henson PM. Exposure of phosphatidylserine on the surface of apoptotic lymphocytes triggers specific recognition and removal by macrophages. *J Immunol*. 1992;148(7):2207–2216.
53. Fadok VA, Bratton DL, Konowal A, Freed PW, Westcott JY, Henson PM. Macrophages that have ingested apoptotic cells in vitro inhibit proinflammatory cytokine production through autocrine/paracrine mechanisms involving TGF-β, PGE2, and PAF. *J Clin Invest*. 1998;101(4):890–898.
54. Filardy AA, et al. Proinflammatory clearance of apoptotic neutrophils induces an IL-12(low) IL-10(high) regulatory phenotype in macrophages. *J Immunol*. 2010;185(4):2044–2050.
55. Huynh ML, Fadok VA, Henson PM. Phosphatidylserine-dependent ingestion of apoptotic cells promotes TGF-beta1 secretion and the resolution of inflammation. *J Clin Invest*. 2002;109(1):41–50.
56. DeNardo DG, et al. CD4(+) T cells regulate pulmonary metastasis of mammary carcinomas by enhancing protumor properties of macrophages. *Cancer Cell*. 2009;16(2):91–102.
57. Gong D, Shi W, Yi SJ, Chen H, Groffen J, Heisterkamp N. TGFβ signaling plays a critical role in promoting alternative macrophage activation. *BMC Immunol*. 2012;13:31.
58. Wan E, et al. Enhanced efferocytosis of apoptotic cardiomyocytes through myeloid-epithelial-reproductive tyrosine kinase links acute inflammation resolution to cardiac repair after infarction. *Circ Res*. 2013;113(8):1004–1012.
59. Choi JY, et al. Upregulation of Mer receptor tyrosine kinase signaling attenuated lipopolysaccharide-induced lung inflammation. *J Pharmacol Exp Ther*. 2013;344(2):447–458.
60. Kazeros A, Harvey BG, Carolan BJ, Vanni H, Krause A, Crystal RG. Overexpression of apoptotic cell removal receptor MERTK in alveolar macrophages of cigarette smokers. *Am J Respir Cell Mol Biol*. 2008;39(6):747–757.
61. Gautier EL, et al. Gene-expression profiles and transcriptional regulatory pathways that underlie the identity and diversity of mouse tissue macrophages. *Nat Immunol*. 2012;13(11):1118–1128.
62. Patin E, et al. Genome-wide association study identifies variants associated with progression of liver fibrosis from HCV infection. *Gastroenterology*. 2012;143(5):1244–1252.
63. Loges S, et al. Malignant cells fuel tumor growth by educating infiltrating leukocytes to produce the mitogen Gas6. *Blood*. 2010;115(11):2264–2273.
64. Linger RM, et al. Mer or Axl receptor tyrosine kinase inhibition promotes apoptosis, blocks growth and enhances chemosensitivity of human non-small cell lung cancer. *Oncogene*. 2013;32(29):3420–3431.
65. Whitman SP, et al. GAS6 expression identifies high-risk adult AML patients: potential implications for therapy. *Leukemia*. 2014;28(6):1252–1258.
66. Keating AK, et al. Inhibition of Mer and Axl receptor tyrosine kinases in astrocytoma cells leads to increased apoptosis and improved chemosensitivity. *Mol Cancer Ther*. 2010;9(5):1298–1307.
67. Scott RS, et al. Phagocytosis and clearance of apoptotic cells is mediated by MER. *Nature*. 2001;411(6834):207–211.
68. Cook RS, et al. ErbB3 ablation impairs PI3K/Akt-dependent mammary tumorigenesis. *Cancer Res*. 2011;71(11):3941–3951.
69. Vaught DB, et al. HER3 is required for HER2-induced preneoplastic changes to the breast epithelium and tumor formation. *Cancer Res*. 2012;72(10):2672–2682.
70. Candolfi M, et al. Release of HMGB1 in response to proapoptotic glioma killing strategies: efficacy and neurotoxicity. *Clin Cancer Res*. 2009;15(13):4401–4414.

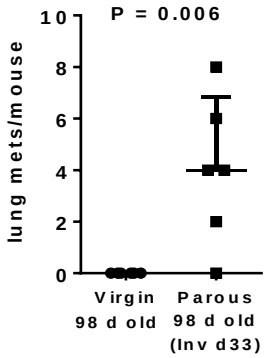

Supplemental Figure S1. The number of lung metastases per mouse was determined in histological lung sections of all five lung lobes. Each point represents lung metastases in one mouse. Midline and whiskers are average and S.D. N = 6. P = 0.006, Student's T-test.

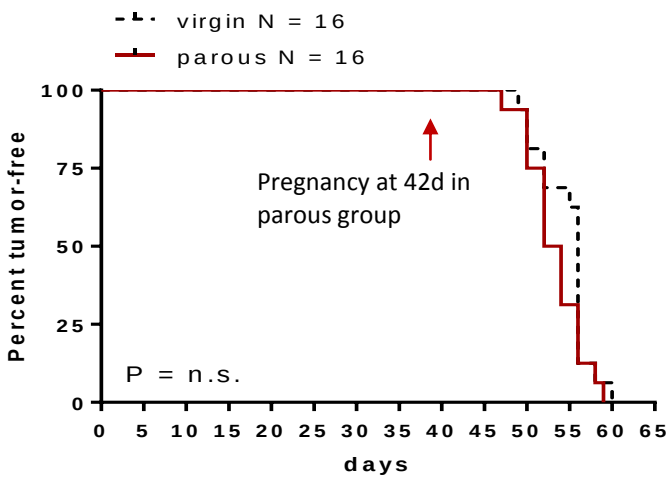

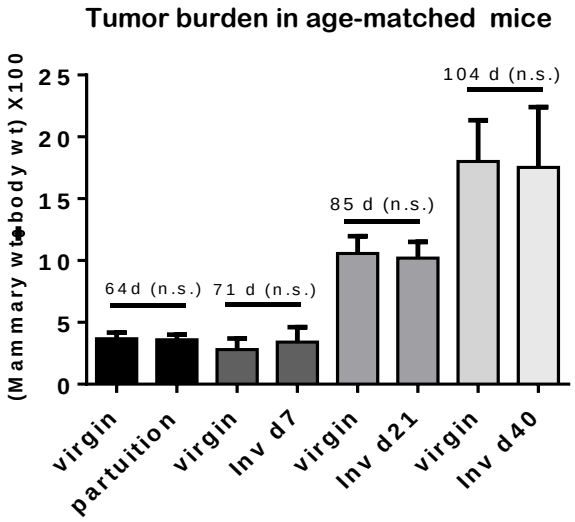

Supplemental Figure S2. A. Kaplan-Meier curve representing the percentage of MMTV-PyVmT mice per group remaining tumor free. n.s., not significant,
B. Total mammary burden was measured as (total mammary weight ÷ mouse weight) X 100. Multi-focal mammary tumors that arise in MMTV-PyVmT grow into each other, making individual tumor volume measurements in live mice unfeasible by current means.

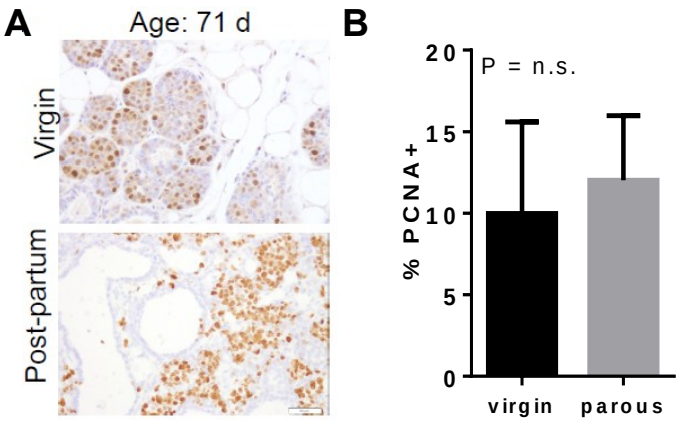

Supplemental Figure S3. Proliferating cell nuclear antigen (PCNA) was used as a molecular marker of cycling tumor cells. **A.** Immunohistochemical detection was performed in tumors harvested from 71 d old virgin mice and 71 d old mice at Inv d7. **B.** The percentage of the tumor population that was PCNA positive was calculated (average ± S.D., N = 4, assessing 5 randomly chosen 400X fields per sample).

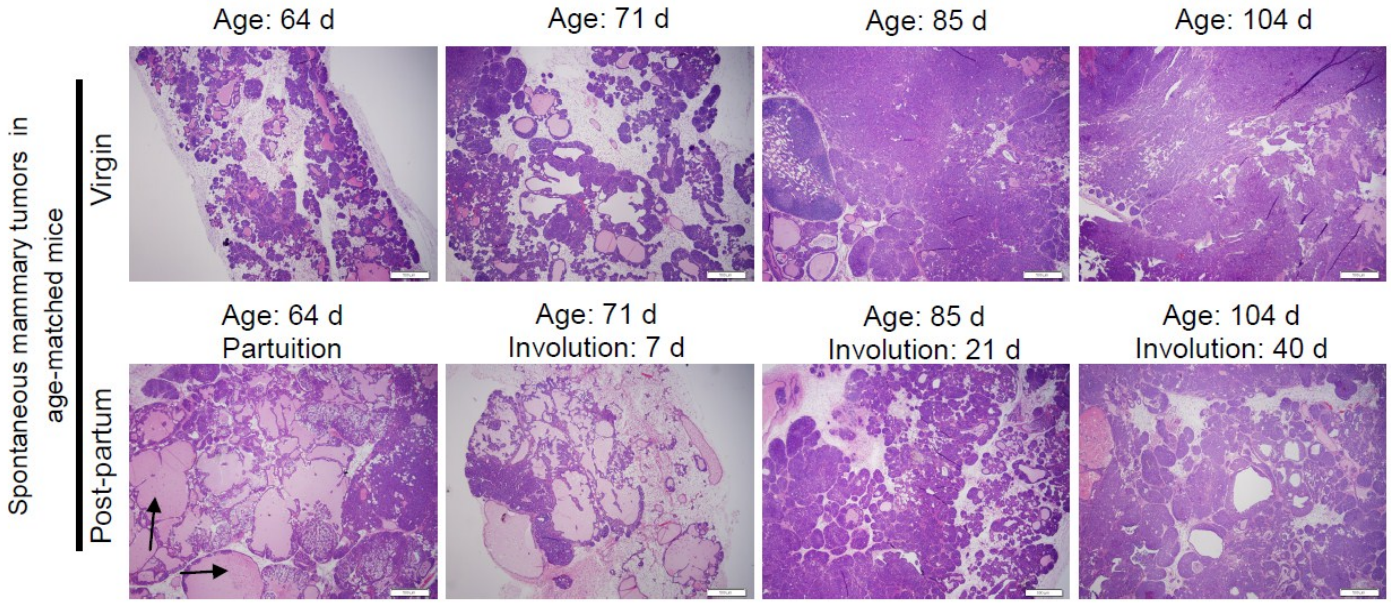

Supplemental Figure S4. Hematoxylin and eosin-stained sections of mammary tumors harvested from age-matched mice that were either nulliparous (top row) or parous (bottom row). Representative images are shown. N = 4-6 per group. Original magnification of images was taken at 100 X, using low power to demonstrate the widespread histological features of the mammary tumors.

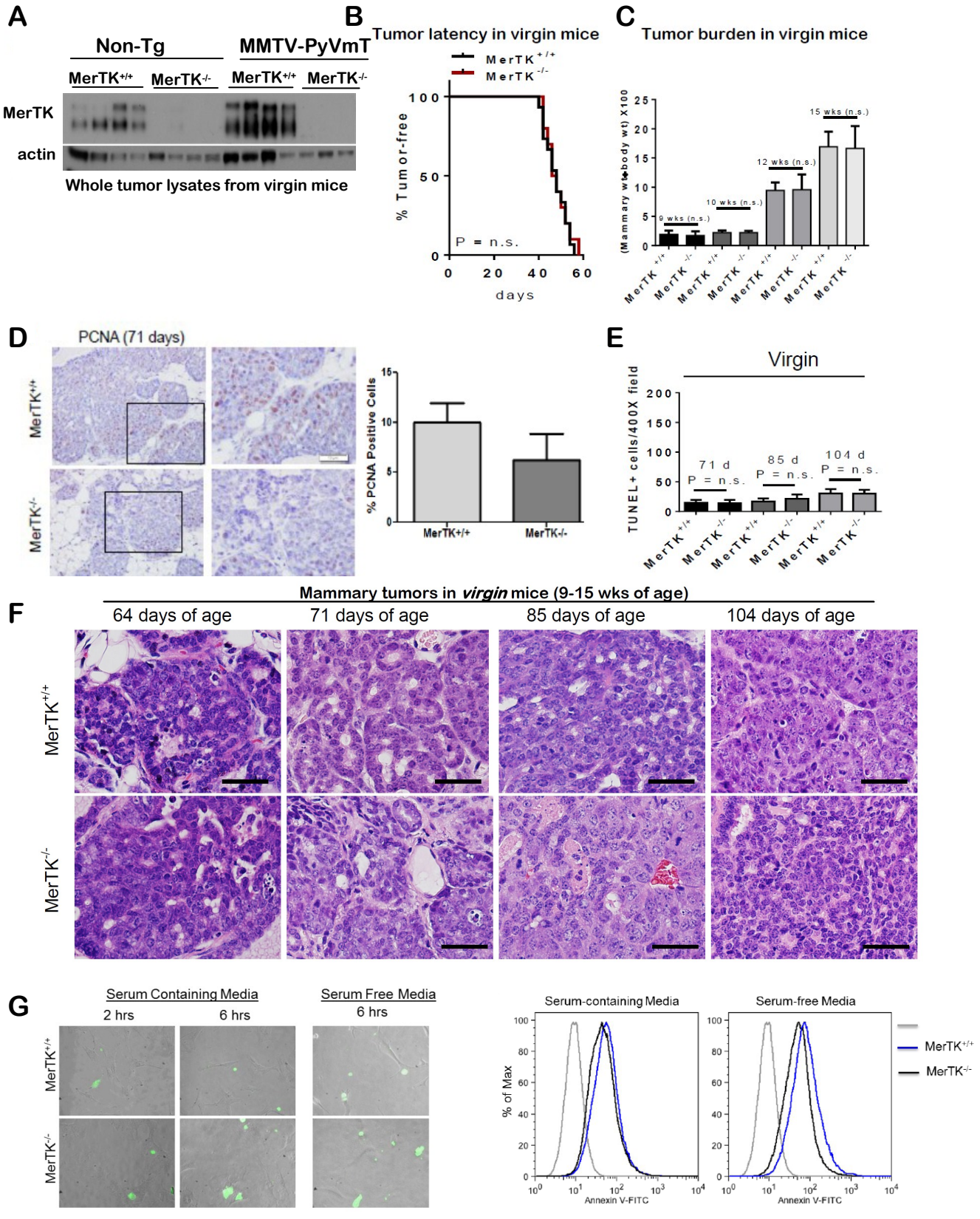

Supplemental Figure S5. A. Western analysis of tumors harvested at 71 d of age. **B**. Tumor latency in virgin *MerTK*$^{+/+}$ and *MerTK*$^{-/-}$ mice. **C.** Total tumor burden in virgin mice at 64, 71, 85, and 104 d of age, average ± S.D., N = 4. **D.** IHC for PCNA in tumors from 71 d old virgin mice. Qantitation shows the percentage of PCNA+ tumor cells (average, ± S.D., N = 6. Student's T-Test, P = n.s.). **E.** Quantitation of TUNEL analysis performed on tumor sections from virgin *MerTK*$^{+/+}$ and *MerTK*$^{-/-}$ mice at the ages indicated. Values shown are average ± S.D. n.s. = not significant. Student's T-test. **F.** Hematoxylin and eosin-stained sections of tumors harvested from virgin mice at ages indicated above each panel. **G.** PyVmT primary tumor cells harvested from *MerTK*$^{+/+}$ and *MerTK*$^{-/-}$ mice cultured in 10% serum or serum-free media (right panels) for 48 hours were cultured with Annexin V-FITC (5 µg/ml) for the final 3 h . Images were captured by live fluorescence microscopy at the end of the culture period. Cells were harvested and assessed by flow cytometry to detect FITC+ cells.

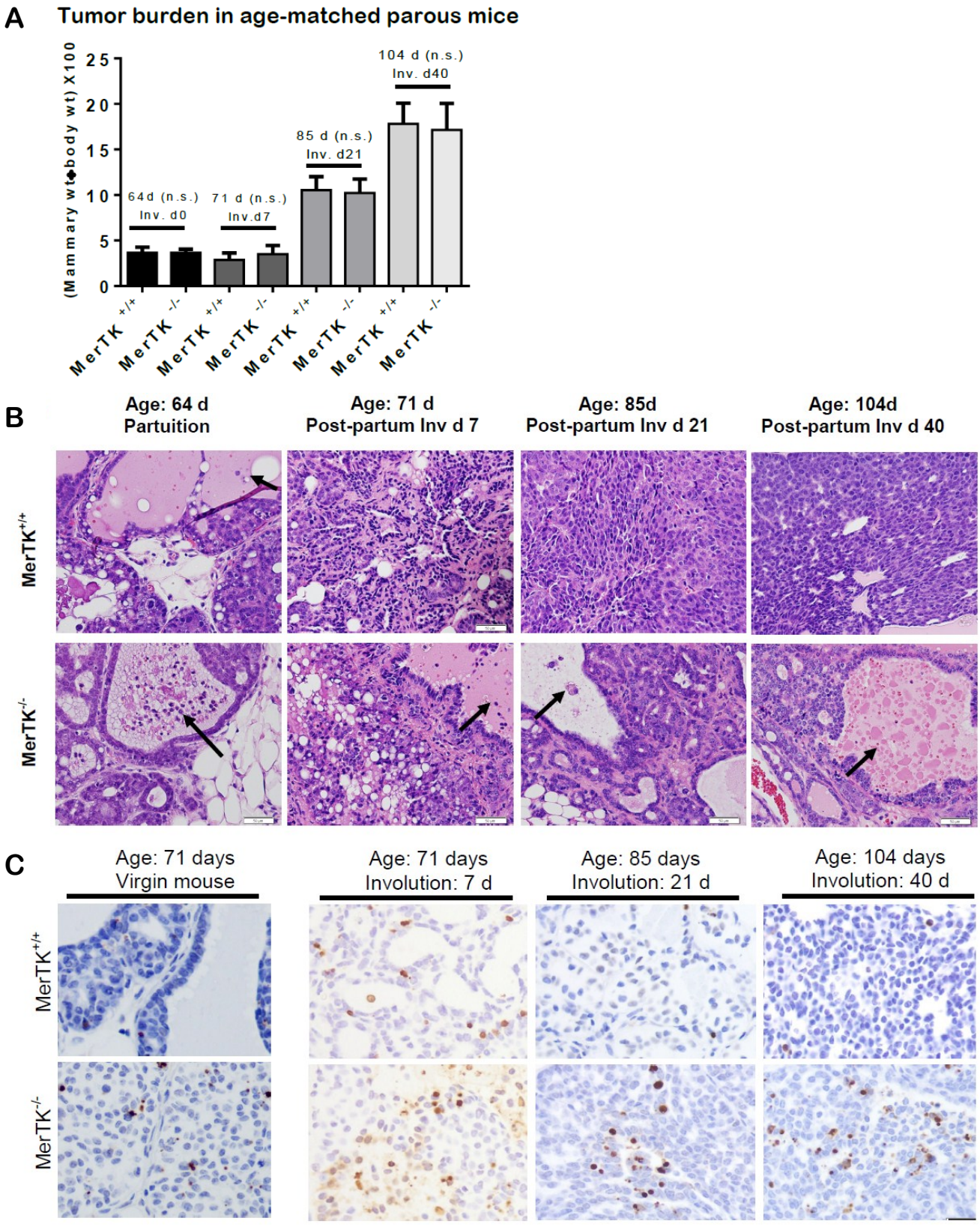

Supplemental Figure S6. A. Total tumor burden in parous mice at 64, 71, 85, and 104 d of age, average ± S.D., N = 4. **B.** Hematoxylin and eosin-stained sections of tumors harvested from parous mice at ages indicated above each panel. **C.** TUNEL analysis of tumor sections from parous mice harvested at ages indicated above each panel. Genotype for MerTK is indicated to the left.

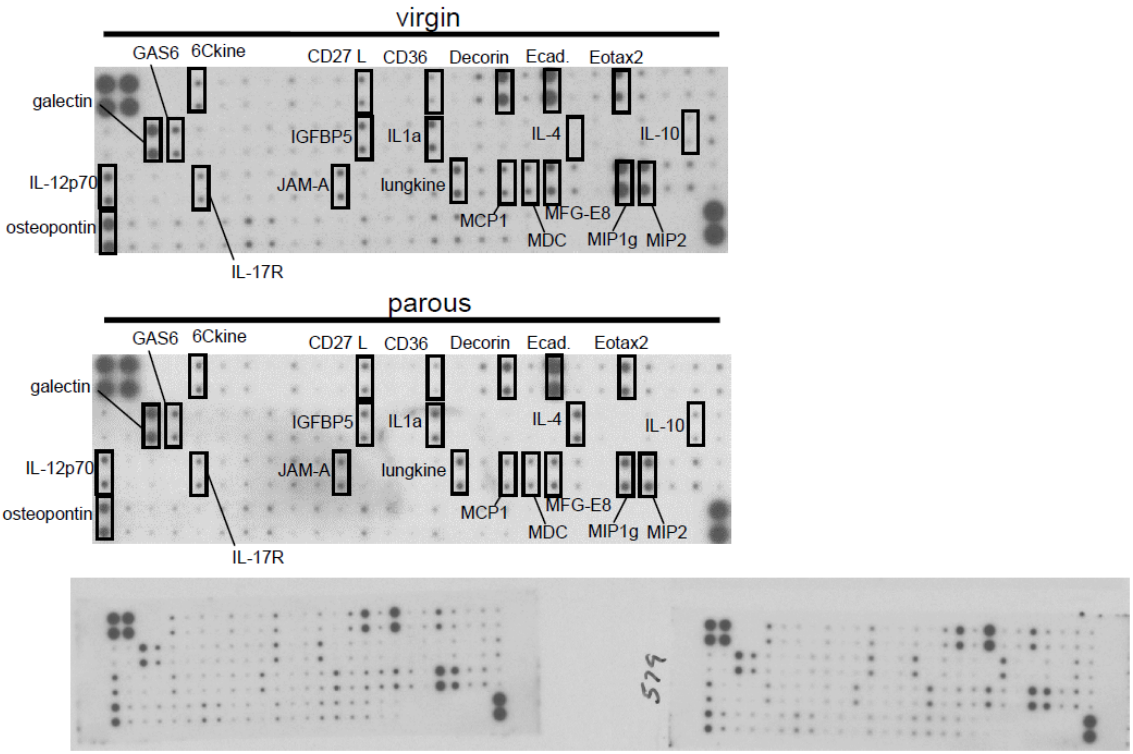

Supplemental Figure S7. Cytokine antibody array of whole tumor protein lysates harvested from age-matched virgin and post-partum (involution day 7) mice. Representative blots are shown. The upper panels show the names and locations of protein species of interest. The lower panel shows the original scan of the two antibody arrays, from the same film exposure.

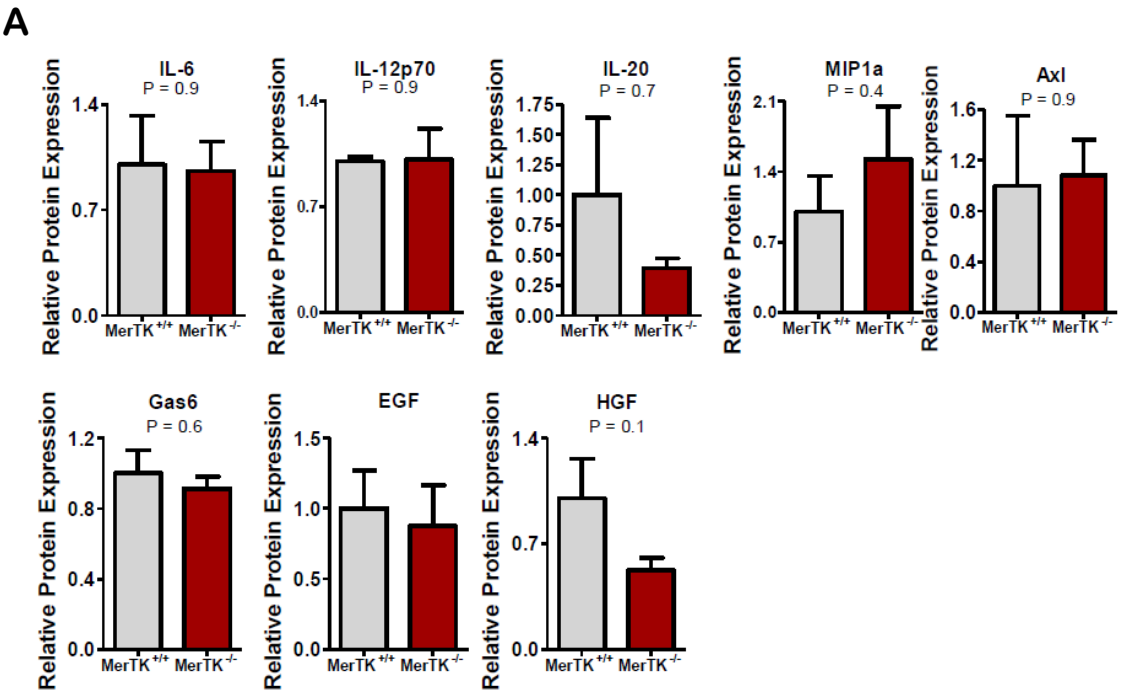

Supplemental Figure S8. A. Cytokine antibody array was performed using whole tumor lysates from 71 day old parous mice (involution day 7) (N = 4). Relative cytokine levels were quantified using Image J. **B.** Cytokine antibody array was performed using whole mammary lysates (from a normal, non-tumor-bearing mammary gland) from 71 day old parous mice (involution day 7) (N = 4). Relative cytokine levels were quantified using Image J.

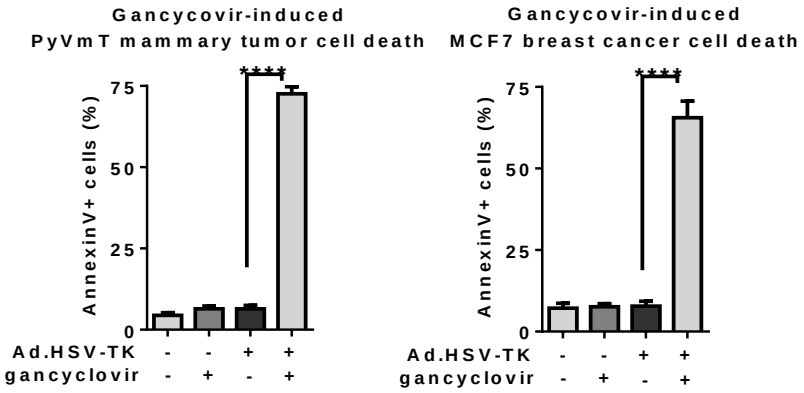

Supplemental Figure S9. Annexin V staining of MMTV-PyVmT primary mammary tumor cells (A) and MCF7 human breast cancer cells (B) cells treated with gancyclovir for 24 hours. Cells were infected with adenovirus expressing HSV-TK (Ad.HSV-TK) or adenovirus expressing led fluorescent protein (Ad.RFP). At 7 days post-infection, cells were treated with or without gancyclovir (0.5 µg/ml) for 0-36 hours. Live cells were cultured in the presence of Annexin V-FITC (5 µg/ml) for the final 1 hour of culture prior to photo washing, photo-documentation under live fluorescence, and quantitation of fluorescence.

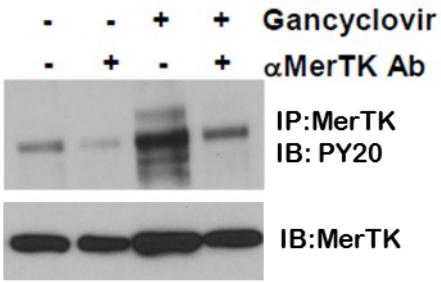

Supplemental Figure S10 Western analysis of Phospho-tyrosine immunoprecipitates from Raw264.7 macrophages treated 16 h with the goat anti-mouse MerTK antibody. Cells were acid-washed to remove residual goat anti-mouse MerTK , neutralized, then lysed. Whole cell lysates were used for immunoprecipitation with PT66 (mouse monoclonal anti-phosphotyrosine). Immune complexes were assessed by western analysis for MerTK using a goat anti-mouse MerTK antibody and anti-goat secondary antibody. Whole cell lysates used for input were assessed by western analysis for β-actin as an input control.

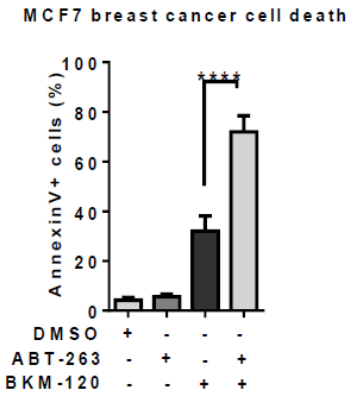

Supplemental Figure S11. Annexin V staining of MCF7 cells treated with BKM-120 (1 μM) ± ABT263 (2 μM) for 4 hours in suspension.

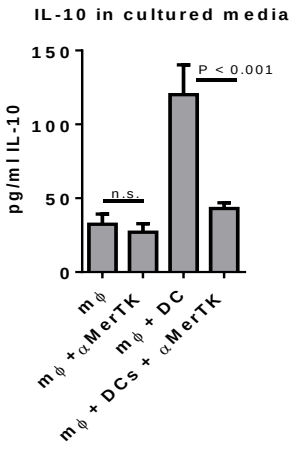

Supplemental Figure S12. Murine IL-10 was quantitated by ELISA in cultured media harvested from Raw264.7 murine macrophages cultured alone for 16 hours in the presence or absence of the goat anti-mouse MerTK neutralizing antibody, or co-cultured with dying MCF7 cells (DCs) for 16 hours in the presence and absence of the MerTK antibody. Cultured media was collected, passed through a 0.2 micron filter, and used neat for ELISA on pre-coated 96-well plates.

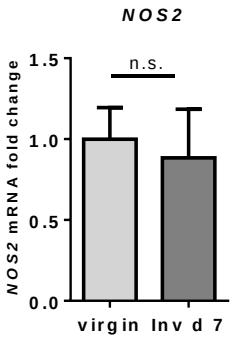

Supplemental Figure S13. qRT-PCR to detect *NOS2* transcripts in whole tumor RNA harvested from MMTV-PyVmT mice at 71 days of age. Mice were either virgin, or were at Inv d7. Values shown are the average of 4 tumor RNA samples, each analyzed in six replicates. P = not significant, Student's T-test.

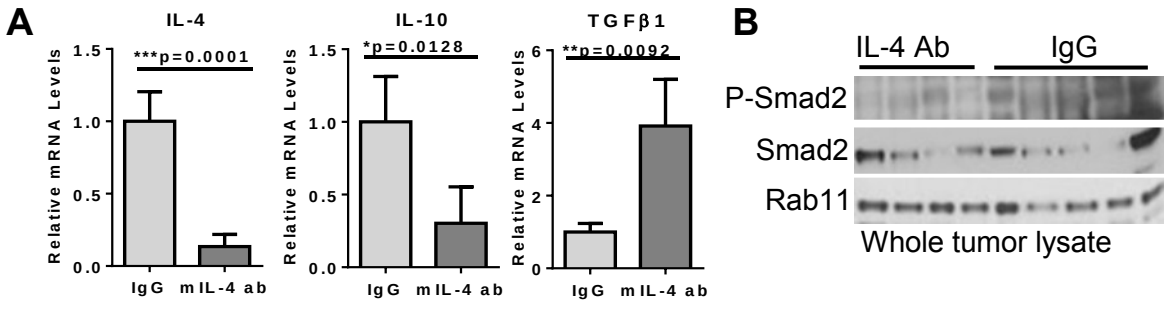

Supplemental Figure S14. A. qRT-PCR to detect *IL4, IL-10 and Tgfb1* transcripts in whole tumor RNA harvested from 71 d old MMTV-PyVmT mice at 71 days of age treated with 11B11 (anti-IL4 antibody) from Inv d1 through Inv d14. Values shown are the average of 4 tumor RNA samples, each analyzed in six replicates. P = values calculated using Student's T-test. **B.** Western analysis of whole tumor RNA harvested from mice treated with 11B11 (anti-IL4 antibody) from Inv d1 through Inv d14.

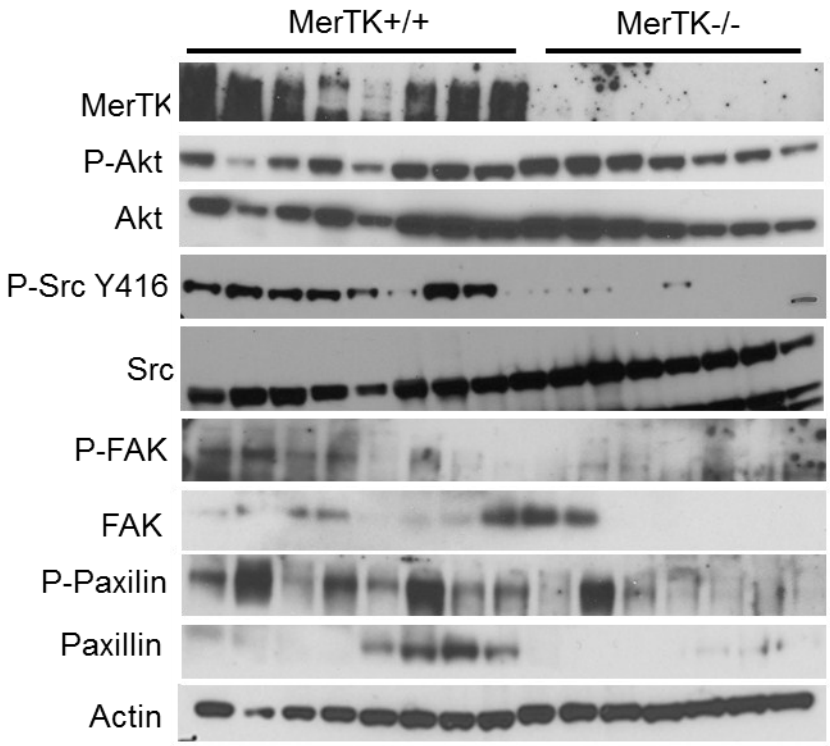

Supplemental Figure S15. Western analysis of whole tumor lysates harvested from mice at 71 d of age (Inv d7).

Appendix 3.
Clearance of dying cells accelerates malignancy.
Vaught DB and ***Cook RS***.
Oncotarget. 2015 Sept. 22; 6(28): 24590-24591. Pubmed PMID:26387138.

Editorial

Clearance of dying cells accelerates malignancy

David B. Vaught and Rebecca S. Cook

The breast endures vast changes during reproductive phases of a woman's life (puberty, pregnancy, lactation, post-partum involution, post-menopausal involution). Each phase uniquely shapes cancer susceptibility, formation, and progression. Although pregnancy at a young age decreases lifetime breast cancer risk, the first five years following pregnancy at any age are associated with increased breast cancer risk regardless of the woman's age, and with even greater risk with increasing age at the woman's first pregnancy [1]. Increasingly, women are postponing child-birth, which may increase the incidence of post-partum breast cancer (ppBC), defined as those breast cancers diagnosed 2-5 years after pregnancy. These ppBCs are distinguishable from those breast cancers that are diagnosed and treated during pregnancy, and which never are exposed to post-partum/post-lactational involution, and which correlate with a favorable prognosis. Currently, ppBC accounts for nearly 25% of all breast cancers in young (pre-menopausal) women. In contrast, ppBCs are highly aggressive, metastatic, and life-threatening, even when corrected for molecular breast cancer subtype and for the age of the woman at diagnosis [1].

Mouse models of ppBC that specifically compare mammary tumors from nulliparous (virgin) mice to those from age-matched parous (single pregnancy) mice confirm that post-partum involution increases metastasis by up to 10-fold [2,3]. The molecular mechanisms underlying the exaggerated lethality of post-partum breast cancers are related to an exaggerated abundance of M2-like tumor associated macrophages, which produce immune suppressive and wound healing cytokines and proteases that modify the post-partum mammary (and tumor) microenvironment [4], although the mechanisms that trigger this shift in macrophage behavior in the post-partum mammary gland remained obscure. It was recently demonstrated that widespread cell death, a hallmark of the mammary gland during post-partum involution when milk production ceases, triggers macrophage-mediated efferocytosis, M2 macrophage polarization and Th2 cytokine production in normal mammary glands during post-partum involution [5]. Remarkably, widespread cell death efferocytosis, macrophage M2 polarization, and Th2 cytokine-mediated wound healing in malignant post-partum breast cancers was similarly observed [3].

Under physiological conditions, dying cells are rapidly removed from the breast to prevent secondary necrosis of the dying cell, wherein intracellular antigens released from the necrotic cell might trigger inflammation, tissue damage, or autoimmunity [6]. To ensure suppression of inflammation or autoimmunity, efferocytosis is coupled with production of cytokines that dampen tissue-damaging immune responses, such as interleukin (IL)-10, IL-4, and Transforming Growth Factor (TGF)-β [7]. Macrophages use multiple cell surface protein to recognize and engulf dying cells. Among these, the receptor tyrosine kinase (RTK) MerTK is essential for post-partum efferocytosis and for subsequent induction of immunosuppressive and wound healing cytokines [6]. Genetically engineered mouse models lacking MerTK activity display impaired efferocytosis and limited expression of wound healing cytokines during post-partum involution, resulting in severe immune-mediated damage and scarring to the post-partum mammary gland that interferes with the success of lactogenesis upon future pregnancies [5].

We recently found that efferocytosis was a key driver of malignant progression in ppBCs, responsible for exaggerated M2-like polarization of tumor-infiltrating macrophages and production of IL-4, TGFβ, and IL-10 [3]. Genetic MerTK ablation inhibited efferocytosis in ppBCs, blocked macrophage M2-like polarization, impaired expression of efferocytosis-induced cytokines, and repressed formation of lung metastases. Pharmacologic inhibition of MerTK for the first 7 days of post-partum involution similarly blocked efferocytosis, and significantly decreased metastatic burden. Thus, a causal relationship exists between the tissue remodeling during physiological postpartum involution and the increased metastasis of postpartum mammary tumors. Both scenarios are characterized by transient and widespread programmed cell death, efferocytosis, and the abundant M2-like macrophages and wound-healing cytokines that associate with reduced breast cancer survival.

These observations highlight tumor cell death as a double-edged sword in the tumor microenvironment: although the chemotherapies, targeted therapies and radiation provide the benefit of widespread tumor cell death and tumor shrinkage, widespread efferocytosis in response to tumor cell death may enhance tumor wound healing, thus limiting the effectiveness of the targeted agent. In some cases, efferocytosis may even promote tumor metastasis. These issues require careful

consideration and experimental testing, as the role of efferocytosis in modulating the stromal response to therapeutically-induced tumor cell death is not fully understood. These recent findings support future endeavors to examine efferocytosis/MerTK targeting in combination with current treatment strategies to block unhealthy 'tumor healing' and improve tumor response to treatment.

Rebecca S. Cook: Department of Cancer Biology, Vanderbilt University and the Vanderbilt Ingram Cancer Center, Nashville, TN, USA

Correspondence to: *Rebecca S. Cook,* ***email*** *rebecca.cook@vanderbilt.edu*

Keywords: efferocytosis, MerTK, macrophages, post-partum breast cancer, tumor microenvironment

Received: *July 07, 2015*

Published: *September 15, 2015*

REFERENCES

1. Callihan E.B., et al. Breast Cancer Res Treat. 2013; 138: 549-559.
2. Lyons T.R., et al. Nat Med. 2011; 17: 1109-1115.
3. Stanford J.C., et al. J Clin Invest. 2014; 124: 4737-4752.
4. O'Brien J. et al. J Mammary Gland Biol Neoplasia. 2009; 1: 145-157.
5. Sandahl M., et al. BMC Dev Biol. 2010; 10: 122.
6. Zizzo G., et al. J Immunol. 2012; 189: 3508-3520.
7. Rothlin C.V. et al. Curr Opin Immunol. 2010; 22: 740-746.